Development of Novel Hydrogels for Application in Therapeutic Delivery

AUTHOR(S)

Robert D. Murphy

CITATION

Murphy, Robert D. (2018): Development of Novel Hydrogels for Application in Therapeutic Delivery. Royal College of Surgeons in Ireland. Thesis. https://doi.org/10.25419/rcsi.10803200.v1

DOI

10.25419/rcsi.10803200.v1

URL

https://repository.rcsi.com/articles/thesis/Development_of_Novel_Hydrogels_for_Application_in_Therapeutic_Delivery/10803200/1

1-7-2018

Development of Novel Hydrogels for Application in Therapeutic Delivery

Robert D. Murphy

— Use Licence —

RCSI

Development of Novel Hydrogels for Application in Therapeutic Delivery

Robert Murphy BSc

Department of Pharmaceutical and Medicinal Chemistry

RCSI

A thesis submitted to the School of Postgraduate Studies, Faculty of Medicine and Health Sciences, Royal College of Surgeons in Ireland, in fulfilment of the degree of

Doctor of Philosophy

Supervisor(s): Professor Andreas Heise

Professor Sally-Ann Cryan

July 2018

Declaration

I declare that this thesis, which I submit to RCSI for examination in consideration of the award of a higher degree Doctor of Philosophy is my own personal effort. Where any of the content presented is the result of input or data from a related collaborative research programme this is duly acknowledged in the text such that it is possible to ascertain how much of the work is my own. I have not already obtained a degree in RCSI or elsewhere on the basis of this work. Furthermore, I took reasonable care to ensure that the work is original, and, to the best of my knowledge, does not breach copyright law, and has not been taken from other sources except where such work has been cited and acknowledged within the text.

Signed _____

Student Number _____

Date _____

Acknowledgements

It's been an exciting road all the way and now, submitting my thesis and finishing up my PhD, feels so surreal. It honestly feels like it was just yesterday that I started my first day in the lab at DCU and 'nearly' spilled a triphosgene solution all over myself (I think that my hands are a bit steadier now). The experiences I have had over the last three and a half years have allowed me to grow not only on a scientific level but also on a personal level. In this time I have met some truly amazing people who I have been lucky to cross paths with on this journey.

First of all, none of it would have been possible without my supervisor, Prof. Andreas Heise. I would like to express my deepest gratitude to you for providing unwavering trust, support and guidance throughout my PhD. You motivated me with your excellent knowledge and ideas, and constantly encouraged me to grow as a scientist. Thank you for providing me with so many amazing opportunities (collaboration at UOW, Australia) and supporting me all the way through this journey (it is because of you that I have experienced Christmas on the beach). Thank you for also being so kind and approachable, it was always great to have a chat with you whether it was scientific or not. I sincerely appreciate everything that you provided me with as a supervisor and a friend, it was an absolute pleasure to work under your guidance.

To my co-supervisor Prof. Sally-Ann Cryan, thank you for your tremendous support during my PhD and your excellent ideas. You helped me settle in at RCSI and it was great working with you. Thanks to all of the people in the TREND group, in particular Dave, Joanne, Rachel, Joanne, Christina and Alice who made our lives easier on the bio and application side. It was a pleasure to work with all of you.

To all of the technical staff at School of Chemical Sciences at DCU, thank you for making my life easier during my time there. Veronica, Catherine, Ambrose, Nicola, Vinny, Damien, John and the rest of the team, you guys were constantly on hand and provided unbelievable support to our group. Thank you all for everything.

I would also like to thank Prof. Marc in het Panhuis for hosting me at UOW. Your expertise and guidance helped me immensely during my time in your research group. It was a pleasure to work with you and thank you for opening my eyes to the world of 3D printing. Also thank you to Charles, Alex, Holly, Reece, Mohammed, Khalid and Danielle, you guys helped me settle in and were fun to be around. Also thank you to all of the rest of the guys at IPRI notably Sepehr (you will be in the UFC one day), Malachy, Jeremy and Big Phil.

Thank you to everyone at RCSI for making our move over from DCU easier (even if I wasn't there at that time). Thanks to all of the guys at the Department of Chemistry and all of the technicians, notably Emmet, Graeme and Suzanne. You guys have been more than helpful during my time here and are an amazing support team.

I would also like to thank all of the past and present members of the Heise group (I don't think it's PRG anymore, is it?) for making my PhD journey so fun and memorable. Thanks to all of the people who were there at the start and for helping me feel comfortable in the group, Anton – we had fun times together and it was a pleasure working with you in the lab even though you always dreamt of the beach, Zeliha – it was a pleasure and I'll always remember how much fun it was working in Cambridge together and your banana bread, Jaco – thanks for all the help and banter in the lab and for saying English words that I never quite understood in a South African accent, Fernando – thank you for all the great times we had although I will never understand how you eat banana with every meal and Timo – it was fun to talk to you about all things football. Also a special thanks to Tushar, who was the man behind me joining the Heise lab and was so instrumental in the start of my PhD. You taught me the ropes of NCAs and were a great mentor and friend, thank you. To the current group, it was an absolute pleasure to work alongside you all. Saltuk – you're a character and I've had so much fun working with you and hearing your interesting stories, Elena – thanks for all the fun moments and banter we've had and I do hope that one day you conquer your fear of chicken and pasta on the same plate, Shona – thanks for all the fun times in the lab, the corny jokes and for organising everything-we'd be lost without you, Trish – it's been a pleasure working with you, Scott – thanks for all the 'craic' inside and outside the lab but I will always wonder how you

can drink 14 pints of Guinness and still be standing, Ruairi – it's been so much fun working with you, I will always cherish the stag do memory, Seamus – it's been fun working with you, thanks for all the laughs in the lab, Vivi – it's been a pleasure working with you even though you sometimes didn't understand my accent, Andre – you are a 'legend' thanks for all the fun we had together and Heliane – it was a pleasure to work with you. And to all the newer members, Mike, James and Anna, it's been great fun even though we've only worked together for a short time. It has been an unbelievable experience working with you all over the past years, thanks for all the fun times we shared together. I also would like to thank all of my friends with whom I have had the chance to enjoy some memorable times with outside of the lab.

I would also like to thank my family for their support throughout these past years. To my mother Bernie, you were always there to listen to any problems I had and always provided solutions. Thank you for your unconditional love and support. I would also like to express gratitude to my sisters Lyndsay and Leonie, thank you for always being there for me. Lastly, I would like to thank my amazing girlfriend Alice for sticking with me through this process. You gave me unbelievable support and expressed a positive attitude throughout my PhD. Even when I went to Australia for a year, you stuck through it and kept positive. Thank you for sharing this journey with me.

Thank you to everybody for the memories!

Table of Contents

Publications

M. Byrne, R. Murphy, A. Kapetanakis, J. Ramsey, S. A. Cryan, A. Heise; Star-Shaped Polypeptides: Synthesis and Opportunities for Delivery of Therapeutics, *Macromol. Rapid Commun.*, 2015, 36, 1862.

R. Murphy, T. Borase, C. Payne, J. O'Dwyer, S. A. Cryan, A. Heise; Hydrogels from Amphiphilic Star Block Copolypeptides, *RSC Adv.,* 2016, 6, 23370.

D. P. Walsh, R. Murphy, A. Panarella, R. M. Raftery, B. Cavanagh, J. Simpson, F. J. O'Brien, A. Heise, S. A. Cryan; Bioinspired Star-Shaped Poly(l-lysine) Polypeptides: Efficient Polymeric Nanocarriers for the Delivery of DNA to Mesenchymal Stem Cells, *Mol. Pharmaceutics*, 2018, 15, 1878.

R. Murphy, D. P. Walsh, C. A. Hamilton, S. A. Cryan, M. in het Panhuis, A. Heise; Degradable 3D-Printed Hydrogels Based on Star-Shaped Copolypeptides, *Biomacromolecules*, 2018, 19, 2691.

R. Murphy, M. in het Panhuis, S. A. Cryan, A. Heise; Disulphide Crosslinked Star Block Copolypeptide Hydrogels: Influence of Block Sequence Order on Hydrogel Properties, *Polym. Chem.,* 2018, 9, 3908.

Conference Presentations

R. Murphy, T. Borase, D. P. Walsh, J. Ramsey, C. Payne, S. A. Cryan, A. Heise; Star Polypeptides For Biomedical Therapeutics and Hydrogels, Polymer Precision Materials (P2M) Final Meeting, Lacanau, France, May 2015 (poster presentation).

R. Murphy, M. in het Panhuis, S. A. Cryan, A. Heise; Disulphide Crosslinked Star Block Copolypeptide Hydrogels: Influence of Block Sequence Order on Hydrogel Properties, Macro UK Young Researcher Meeting (YRM), Dublin, Ireland, July 2018 (poster presentation).

List of Abbreviations

AM	Additive manufacturing
AMPDA	2(aminomethyl)-2-methyl-1,3-propanediamine)
AMM	Activated monomer mechanism
ATR	Attenuated total reflection
ATRP	Atom transfer radical polymerisation
b	block
BLA	β-benzyl-L-aspartate
BLG	γ-benzyl-L-glutamate
BLL	ε-tertbutoxycarbonyl- L-lysine
BLT	Benzyl-L-tyrosine
BOC	Tert-butyloxycarbonyl
CAD	Computer-aided design
CCS	Core crosslinked star
CGC	Critical gelation concentration
CLSM	Confocal laser scanning microscopy
CNS	Central nervous system
CO_2	Carbon dioxide
DAPA	Diaminopimelic acid
DIW	Direct ink writing
DLS	Dynamic light scattering
DMF	Dimethylformamide
DOX	Doxorubicin
DP	Degree of polymerisation
DTT	Dithiothreitol
ECM	Extracellular matrix
EDC	1-Ethyl-3-(3-dimethylaminopropyl)carbodiimide
EG	Ethylene glycol
ESEM	Environmental scanning electron microscopy
FTIR	Fourier transform infrared
g	graft

GPC	Gel permeation chromatography
GSH	Glutathione
HBr	Hydrobromic acid
HCl	Hydrochloric acid
HFIP	Hexafluoroisopropanol
HMDS	Hexamethylenedisilazane
hMSC	Human mesenchymal stem cells
HOP	Hydrophobic oligopeptide
kDa	kilodalton
LCST	Lower critical solution temperature
MAPLE-DW	Matrix-assisted pulsed laser evaporation direct writing
MDR	Multidrug-resistant
MWCO	Molecular weight cut-off
NAM	Normal amine mechanism
NCA	N-carboxyanhydride
NHS	N-hydroxysuccinimide
NIRF	Near-infrared fluorescence
NMBAA	N, N'-methylenebisacrylamide
NMR	Nuclear magnetic resonance
PAMAM	Poly(amidoamine)
PBLG	Poly(γ-benzyl-L-glutamate)
PBLL	Poly(ε-tertbutoxycarbonyl- L-lysine)
PBLT	Poly(benzyl-L-tyrosine)
PEG	Poly(ethylene glycol)
PEI	Poly(ethylene imine)
PEO	Poly(ethylene oxide)
PGA	Poly(L-glutamic acid)
PI	Photoinitiator
PIP	Polyisoprene
PLA	Poly(L-alanine)
PLC	Poly(L-cysteine)
PLG	Poly(L-glutamate)

PLL	Poly(L-lysine)
PLP	Poly(L-phenylalanine)
PLT	Poly(L-tyrosine)
PLV	Poly(L-valine)
PPLG	Poly(γ-propargyl-L-glutamate)
PPI	Poly(propylene imine)
POSS	Polyhedral oligomeric silsesquioxane
PS	Polystyrene
PSar	Poly(sarcosine)
PZLL	Poly(ε-carbobenzyloxy-L-lysine)
RAFT	Reversible addition-fragmentation chain transfer
ROP	Ring opening polymerisation
OEG	Oligo(ethylene glycol)
OLC	Oligo(L-cysteine)
SEC	Size exclusion chromatography
SEM	Scanning electron microscope
SLA	Stereolithography
SNAPPs	Structurally nanoengineered antimicrobial peptide polymers'
TAD	Triazolinedione
TEM	Transmission electron microscope
TFA	Trifluoroacetic acid
THF	Tetrahydrofuran
UV	Ultroviolet
ZLL	ε-carbobenzyloxy-L-lysine
Z	Carbobenzyloxy

List of Figures

List of Schemes

List of Tables

Summary

This aim of this PhD was to develop new polypeptide hydrogels via the ring opening polymerisation (ROP) of *N*-carboxyanhydride (NCA) amino acid monomers. By incorporating a range of different amino acid building blocks and architectures, hydrogels with different properties could be obtained. Chapter 1 will cover the topics relating to the thesis including the use of NCA ROP for star shaped polypeptide formation and also its use in the generation of polymeric hydrogels. Chapter 2 will look at the effects of different amino acid side groups on the physical self-assembly behaviour and aqueous gelation of star shaped polypeptides. In chapter 3, the effect of switching the position of covalent disulphide crosslinks from core to shell mediated assembly and its impact on the mechanical properties of a range of star polypeptides will be discussed. In chapter 4, the fabrication of UV curable shear thinning star polypeptide hydrogels with 3D extrusion printing will be demonstrated. Finally in chapter 5, the use of a newly synthesised difunctional NCA monomer in the development of organogels and hydrogels is described.

CHAPTER 1

INTRODUCTION

Abstract

This chapter will detail the beginnings and current state of NCA derived synthetic polypeptides, the role of multifunctional initiators in the development of complex star shaped polypeptide architectures and their associated properties, the synthetic approaches undertaken for the design of hydrogelating materials from the NCA ring opening polymerisation; detailing the dependence on amino acid composition and architecture; followed by a brief introduction to 3D printing and its potential relevance in the fabrication of polypeptide hydrogels.

1.1 Polypeptides from the *N*-carboxyanhydride ring opening polymerisation

Polypeptides, sometimes referred to as poly(aminoacid)s, are an intriguing class of biomolecules which compose the building blocks of living biological systems. They possess a naturally occurring morphological characteristic with an intrinsic ability to self-assemble into higher order structures, rationalising their use as the basis for the design of functional materials.[1,2] Synthetic polypeptide mimics are well known with many experts in the field employing unique methodologies to control and predict self-ordering characteristics.[3,4] The inherent biocompatibility of the molecular framework has prompted the utilisation of these materials in areas such as tissue engineering[5,6] and drug delivery.[7,8] Many reports have outlined the versatility associated with modifying the composition of polypeptide materials, with many examples integrating orthogonal chemistries to enhance biological assimilation.[9-11] Polypeptides derived from the *N*-carboxyanhydride (NCA) ring opening polymerisation (ROP) represent a more practical yet rapid approach to producing sequence defined polypeptides with control over scalability, molecular weight and amino acid composition in comparison to both solution and solid phase peptide synthesis.[12] The side chain amino acid moieties provide point of interest for further chemical modification and thus a plethora of components can be introduced that may potentially possess stimuli triggered responsiveness. Additionally, the structure-property relationship can be modulated by tuning these side chain functionalities. The resulting self-assembly of polypeptide chains into conformations which include α-helix and β-sheet arrangements can bestow stability to the polypeptide system, much like that seen in biological proteins.[13]

1.1.1 Development of *N*-carboxyanhydride's

N-carboxyanhydride monomers derived from amino acids have been utilised in research for well over 100 years. In 1906, Hermann Leuchs reported the first instance of the preparation of amino acid NCAs.[14] The Leuchs method employs the halogenation of *N*-alkyloxycarbonyl substituted amino acids. Upon heating, the formed N-alkyloxycarbonyl amino acid halide is then cyclised forming the amino acid NCA and an alkyl halide. Alternatively, the Fuchs-Farthing method utilises the phosgenation of N-unsubstituted

amino acids.[15-17] The method employs the use of phosgene gas bubbled through an inert solvent containing the amino acid. Initially, the reaction proceeds with the formation of the N-chloroformyl intermediate, which then undergoes ring closure to generate the NCA and HCl (Scheme 1.1).

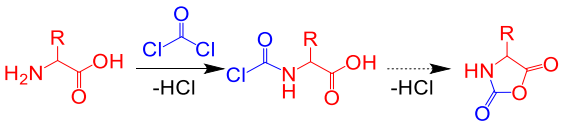

Scheme 1.1: Conventional route for synthesis of *N*-carboxyanhydrides using phosgenation strategies.

The limitations and safety concerns associated with phosgene, particularly its volatility and high toxicity, prompted the use of more stable phosgene derivatives in the form of liquid diphosgene and solid triphosgene, which are currently preferred for synthetic use. Both are safer alternatives to phosgene, while showing significant improvement over stoichiometric control.[18-21] To this day, both methods are still employed to develop amino acid precursors for the generation of polypeptide materials. However, controlled polymerisation of NCAs can be an issue post monomer synthesis due to the presence of impurities, which can be difficult to remove.

The drawbacks of both Leuchs and Fuchs-Farthing methods are the halide by-products generated during NCA formation. The presence of amino acid-HCl salts, 2-isocyanatoacyl chlorides, *N*-chloroformyl amino acids and/or alkyl halides as contaminates in NCAs may result in inhibition of chain propagation and thus premature chain termination.[22,23] Although recently, improved methods for NCA purification have been developed. Pure NCAs are mainly isolated by recrystallisation, but new methods have demonstrated qualitative removal of such by-products. The use of flash chromatography has been reported to yield pure amino acid NCAs of those with highly modified side groups or those that have proved difficult to crystallise.[24] Additionally, an interesting recent report disclosed the use of a celite filtration method as a purification of large scale NCAs.[25] A range of different amino acid NCAs were prepared using the phosgenation protocol, followed by precipitation and drying. The crude monomers were then re-dissolved and

passed through a bed of celite before being re-precipitated and stored without any subsequent recrystallisation. The pure NCAs were then polymerised yielding polypeptides devoid of any low molecular weight by-products as observed in GPC traces.

1.1.2 Mechanism of *N*-carboxyanhydride ring opening polymerisation

Synthetic polypeptides derived from the NCA ring opening polymerisation (ROP) have been explored since the 1940s, with advancements in chemical methodologies adding multiple preparatory protocols for control of the polypeptide polymerisation. The ROP of NCA monomers is widely known to proceed via the following mechanisms; the 'normal amine mechanism' (NAM) and the 'activated monomer mechanism' (AMM). The NAM promotes the ring opening polymerisation of NCAs through nonionic initiators, which are inherently more nucleophilic than basic and contain a mobile proton. Commonly used initiators are primary amines or secondary amines, while some reports have detailed the use of hydroxyl[26] and thiol based initiators.[27] The NCA ring is opened through nucleophilic attack of the carbonyl group (5-CO) resulting in the formation of a carbamic acid intermediate, which eventually undergoes decarboxylation to form a primary amine (Scheme 1.2, Path 1). Propagation of the polypeptide chain is through this terminal amine end group, which will subsequently ring open the next NCA monomer. This amine chain end is less nucleophilic than the initiator, meaning the chain propagation occurs far slower than the initiation step.

In the AMM, the initiator (usually a tertiary amine) is more basic than nucleophilic, and thus abstracts a proton from the NCA nitrogen (3-N) forming the conjugate anion. This NCA anion then acts as the initiating species by attacking the carbonyl group (5-CO) of another NCA monomer and proceeding to propagate the chain through formation of another NCA anion and the release of CO_2 (Scheme 1.2, Path 2). This mechanism usually yields high molecular polypeptides with poor control over poly dispersity due to the chain propagation rate being more rapid than the monomer initiation rate.

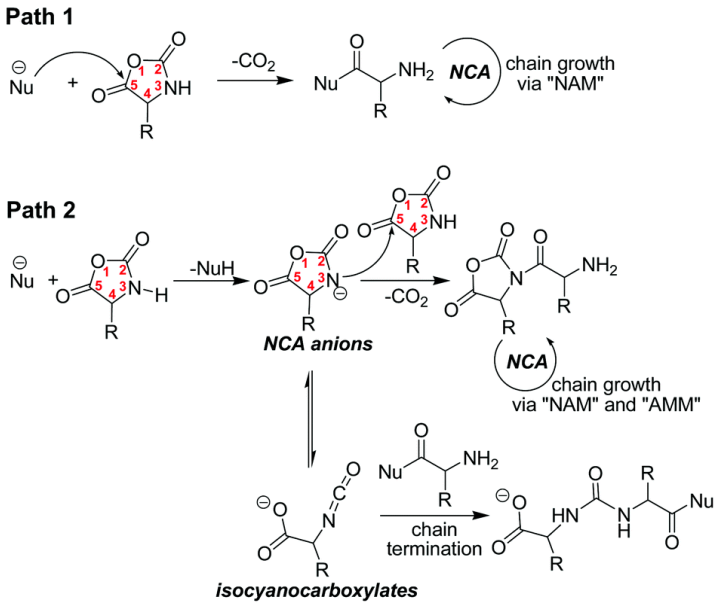

Scheme 1.2: ROP of α-amino acid NCAs by normal amine mechanism (NAM) and activated monomer mechanism (AMM).[33]

The coexistence of both competing mechanisms in the NCA ring opening polymerisation can prevent the production of well-defined polypeptides. Control over polypeptide sequence length and architecture is therefore difficult to achieve without optimising experimental conditions. Many research groups have made significant advances in preventing the occurrence of the AMM pathway in order to improve control over polypeptide sequence formation. Attempts in the form of continuous nitrogen purging of the NCA reaction solution[28] or reacting the NCAs at low temperature with application of constant vacuum have proven to make a substantial difference to resultant polypeptides homogeneity.[29] In addition, a multitude of different initiator systems have been successfully employed controlling propagating polypeptide chains in an attempt to prevent sequence termination reactions and proceed to yield well-defined polypeptides.[30-34]

1.2 Development of star polypeptides

Star shaped polypeptides are a class of structurally diverse branched architectures comprising multiple linear polypeptide sequences that are attached to a central core.[35] These linear sequences, quite often referred to as polypeptide 'arms', can be tailor made for particular applications by using the appropriate amino acid monomers. The star

shaped system allows for high control over polypeptide arm composition, polypeptide arm length, molecular weight and core composition, thus offering great versatility in terms of structural design and material properties. The synthetic strategy employed for the development of star shaped polypeptides is generally one of either; the grafting from method (core-first), the grafting to method or the arm-first method (Figure 1.1).

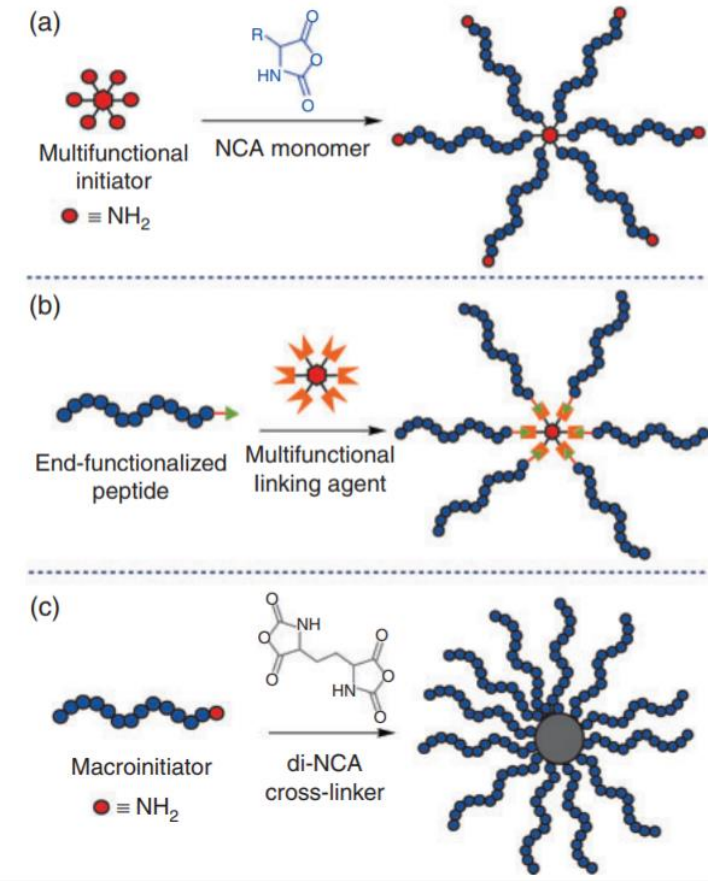

Figure 1.1: Design of polypeptide star polypeptides through (a) grafting from (core-first), (b) grafting-to and (c) arm first approaches.[35]

1.2.1 Grafting-from (core-first) approach

The grafting from approach is the most commonly used method for preparing these star shaped macromolecules. The grafting to principle is based around the development of individual polymer chains growing simultaneously from a multifunctional dendritic central core. The control of the polymerisation is governed by each grafting site on the macro-initiator possessing the same reactivity thus having greater control over the propagating chains and ideally maintaining homogeneity in the polymer arm length. This method can readily yield structurally diverse star shaped architectures with high

molecular weight. A multitude of different star polymers have been prepared using this approach in conjunction with a variety of monomers.

The difficulty associated with characterising the stars is a significant disadvantage of the preparation method. There are currently no direct analysis methods to correctly identify the globular structure, independent polymer arm length and molecular weight of the star polymers without first altering the macromolecule. In spite of this, much literature relates to the use of this method for producing star shaped polypeptides. The composition and structure of these initiators can vary significantly yielding star polypeptides with different functionalities within the core. Multifunctional molecules with amino functionalised surfaces have also been used.[36] For example, Inoue el al. have detailed the use of amine functionalised cyclotriphosphazenes as viable multifunctional initiators in NCA ROP.[37,38] In one report a hexakis(4-amino-phenoxy) cyclotriphosphazene was used in the ROP of β-benzyl-L-aspartate (BLA) NCA. They designed a library of 6-arm star polypeptides with different degrees of polymerisation (DP) of PBLA. While narrow dispersities were observed (1.2-1.3), some bimodal distributions were evident in the SEC traces.

Amine modified 4-armed perylene derivatives were used by Klok et al. to generate star polypeptides via the ROP of ZLL NCA. Removal of the Z protecting groups yielded water-soluble, fluorescent perylene-poly(L-lysine) derivative. However, the polypeptides were found to have very broad dispersities (1.2-4.6) and did not achieve targeted molecular weight. The limitation of the multifunctional chromophore was realised when a target DP of 400 did not meet theoretical values as determined by SEC, thus the development of elongated polypeptide chains (above 200 repeat units) was not viable due to the sterics associated with the perylene core.

The use of 3-arm initiators to develop star shaped homo and block copolymers has also been explored.[39,40] Barz et al. employed the tri-armed dendrimers for the generation of diblock stars consisting of sarcosine and protected lysine (TFA or Boc) sequences.[40] The star block copolypept(o)ide (PeptoStars) exhibit a well-controlled DP, have narrow dispersities and maintain uniform particle sizes (5 nm). Moreover, the introduction of a

disulfide core in the 3-arm structure provides redox responsive degradation of the star, with resulting cleaved copolymer arms equally possessing low dispersities. Another recent report described the use of poly(sarcosine) in the synthesis of a 3-armed star shaped hybrid block polypeptoide.[41] The trifunctional initiator tris-(2-aminoethyl)amine (TREN) was used in the ROP of *N*-methyl glycine (sarcosine) NCA to grow the hydrophilic inner blocks which were chain extended with poly(sarcosine)'s secondary amine terminus, growing a hydrophobic poly(ε-caprolactone) outer shell. The star diblock copolymers had controlled molecular weights, narrow molecular weight distributions (1.1), could assemble into nanoparticles (56-169 nm) in aqueous solution and showed good cell viability.

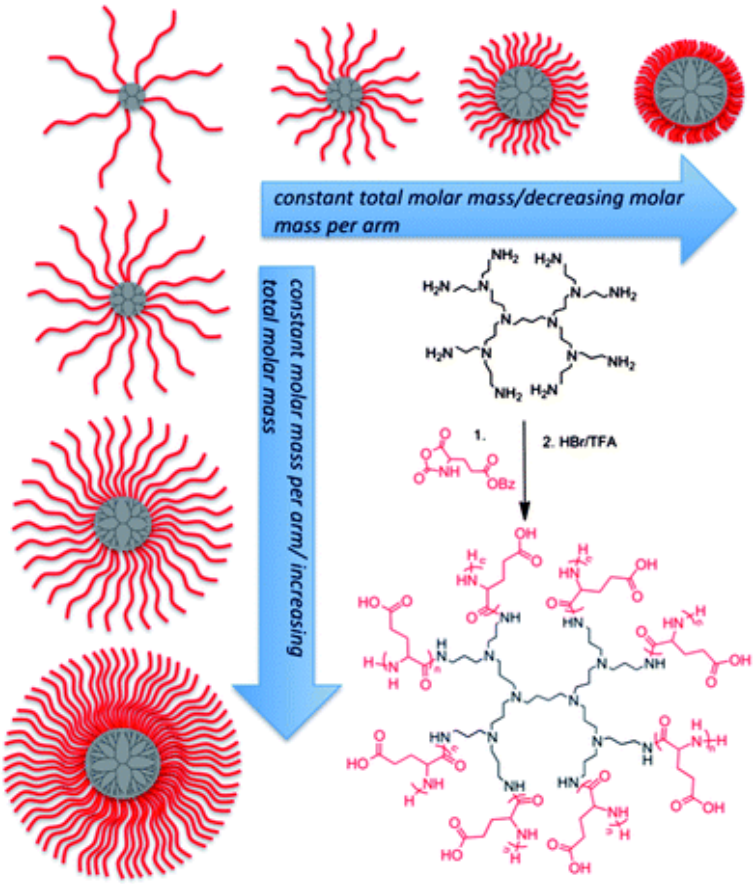

Figure 1.2: Star polypeptides prepared through NCA ROP of BLG NCA via poly(propylene)imine dendrimers.[43]

Structurally defined dendrimers such as PAMAM (poly(amidoamine)) and PPI (poly(propylene imine)) have also been used in the design of the architectures (Figure

1.2).[42-44] Okada et al. developed star shaped glycopolypeptides through the ROP of glycosylated NCA monomers using a 3rd generation PAMAM dendrimer.[45] The star polymers were found to have low dispersities as deduced from SEC while ^{13}C-NMR studies revealed that the ROP of the glyco-NCAs occurred through the terminal amino groups on the PAMAM dendrimer.

Although a drawback of using these dendritic amino macromolecules has been demonstrated by Mays and co-workers.[46] They studied three different amine terminated macroinitiators for the NCA ROP of ε-butyloxycarbonyl-L-lysine and γ-benzyl-L-glutamate monomers and compared their effects on molecular weight distribution. The purely primary amine based initiator, 2(aminomethyl)-2-methyl-1,3-propanediamine (AMPDA), produced monomodal star block copolypeptides with low dispersities. In contrast, with both the generation 0.0 PAMAM and generation 1.0 PPI dendrimers, they found that the tertiary amine groups located in the core can simultaneously initiate the ring opening polymerisation in tandem with the terminal primary amines, yielding bimodal star copolypeptides with higher dispersity.

An example of the translation of these dendrimer derived star polypeptide materials into viable biomaterials was recently provided by Lam et al.[47] They copolymerised Z-lysine and valine NCA monomers with 16 and 32 arm PAMAM dendrimers and subsequently deprotected them, affording water dispersible structurally nanoengineered antimicrobial peptide polymers' (SNAPPs) to combat multidrug-resistant (MDR) bacteria. The polymers were found to be active both *in vitro* and *in vivo* at sub-μM concentrations against Gram-negative bacteria, with no acquired resistance evident. They function by binding electrostatically with the negatively charged phospholipid headgroups of the bacterial outer membrane, resulting in cell membrane disruption and subsequent cell lysis.

Aside from dendrimers, other branched initiators have been used extensively in the development of star polypeptides. Similar to the PPI and PAMAM dendrimers, these branched polymers contain primary amine termini which possess the same capacity in

terms of NCA ROP initiation. Many cases have explored the growth of polypeptide shells from branched poly(ethylene imine) (PEI) cores.[48-50] One particular report detailed the design of a library of different poly(lysine) chain lengths tethered to a hyperbranched poly(ethylene imine) (PEI) core.[51] The star PLLs were found to be unimodal due to no existing tertiary amine initiation but had a larger molecular weight distribution than that of the dendrimer mediated NCA ROP. Liu et al. have published many reports on star polypeptides derived from PEI cores, including a recent report on branched block copolypeptides of poly(L-phenylalanine) chain extended with poly(L-lysine) or poly(L-glutamic acid) with a PEG shell as drug delivery vectors.[52] Another report from their group detailed the synthesis of a library of micelle forming amphiphilic star block copolymers from a PEI core.[53] The copolymers contained a hydrophobic oligopeptide (HOP) with either oligo(L-tryptophan), oligo(L-phenylalanine), oligo(L-leucine), oligo(γ-benzyl-L-glutamate) or oligo(ε-benzyloxycarbonyl-L-lysine) used as the inner shell sequence, and a hydrophilic PEG block as the outer shell. In those copolymers with short HOP blocks and elongated PEG peripheral blocks, unimolecular micelles were observed with DLS (dynamic light scattering). This micellisation enabled the copolymers to encapsulate hydrophobic drugs with relative loading capacity's ranging up to 10%. Chen et al. have also used polyalanine grafted to a PEI core as an efficient condensing agent for nucleic acids.[54] The star polymer series (DP 30, 60, 90) ranged in dispersities (1.1-1.4), were found assemble into smaller nanoparticles with larger alanine sequence length (~100nm) and were effective siRNA carriers in vitro.

Star polypeptides have also been generated through many other types of branched macroinitiators. Klok and co-workers were the first to report the synthesis of purely highly branched PLL by employing repetitive NCA ROP and strategic deprotection.[55,56] They simultaneously used a mix of Lys(TFA) and Lys(Z) monomers to synthesise a linear copolypeptide using a hexylamine initiator and then used selective deprotection steps to cleave the TFA protecting groups. Using the same monomer blend, they grew polypeptide branches from the pendent amino groups on the initial linear copolypeptide to produce the G0 branched PLL. Subsequent generations (G1, G2) were achieved using the same stepwise approach. Although the materials were not fully monodisperse as

indicated by SEC or uniform in terms of molecular structure, they represent a viable alternative as purely polypeptide based dendritic macromolecules.

1.2.2 Grafting-to approach

The 'grafting to' approach is another viable means of synthesising star shaped polymers. It involves the attachment of a multifunctional core to linear polymer sequence via a linking reaction. The efficiency of this approach is highlighted by the high degree of control associated with the design and synthesis of the polymeric arms, which allows for the production of structurally defined architectures after tethering said sequences to a dendritic core. Comprehensive characterisation of these synthetic linear arms can be completed using conventional methods, allowing for accurate determination of polymer arm density and arm length of the formed star polymers.[57] However, the amount of time necessary for quantitative conjugation and the purification steps associated with removing unreacted linear arms, which are generally used in excess, still present barriers to overcome. Nonetheless this straightforward albeit imprecise method has been studied extensively for the development of star polypeptides.

There is a plethora of specific conjugation reactions have been used for this method of star polymer development. One in particular is the copper catalysed azide-alkyne cycloaddition, which has been utlised in the design of a multitude of star polymers due to its facile, high yielding nature.[58] Many reports detail its use in the development of star polypeptide architectures. Lin et al. have also described the successful formation of diblock copolymers via the attachment of linear PBLG to a 3-armed azide terminated PS star polymer.[59] The 3-armed copolymers synthesised were shown to be quantitatively conjugated as confirmed using FTIR, NMR spectroscopies as well as GPC, with chromatographic traces showing the expected molecular weight shift. Similarly, star homopolypeptides were synthesised through alkyne terminated PBLG and multifunctional azide terminated polyhedral oligomeric silsesquioxane (POSS). Characterisation confirmed conjugation of POSS grafted with polypeptide arms.[60] Moreover, Alliferis and coworkers explored the use of urea linkages through the reaction of amine terminate block copolypeptides with a trifunctional isocyanate.[61] The linking

reaction successfully conjugated linear PBLG-b-PZLL arms to a 3-armed core with high control as deduced from the molecular weight shift which was in agreement with theoretical predictions.

1.2.3 Arm-first approach

A varied take on the grafting to method is the 'arm first' approach. It consists of the introduction of a multifunctional crosslinking monomer which reacts with the active terminal groups of the linear polymer. The linear polymeric arms are placed on to a densely packed core forming globular structure known as a core crosslinked star (CCS) polymer (Figure 1.3).[62,63] This approach holds the potential to introduce different functionalities within the core, enabling the control of multiple core functional groups depending on the choice of multifunctional crosslinker. However, a distinct disadvantage of this method is the long reaction times associated with the development of multi-arm star polymers (>50) and the limited control over the size of the core. Qiao et al. has also used this methodology to prepare core crosslinked star polymers consisting purely of polypeptides.[64]

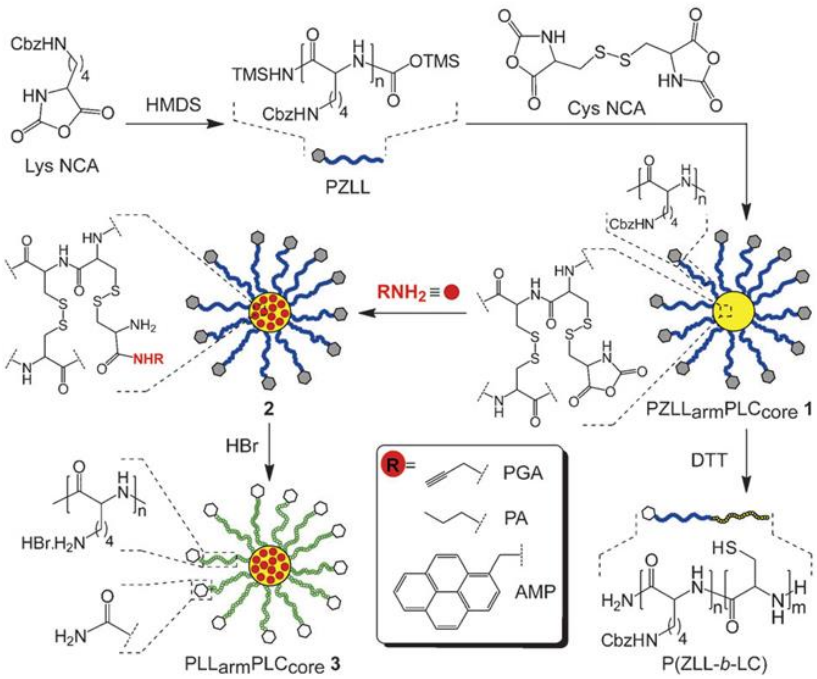

Figure 1.3: The generation of CCS polypeptides via an arm-first strategy using cystine NCA as a crosslinker.[64]

Linear PZLL or PBLG arms were prepared using hexamethylenedisilazane (HMDS) mediated ring opening polymerisation of respective NCAs, with core crosslinking achieved by macro-initiation of the difunctional L-cystine NCA monomer. Although the star polymers did have some linear molecular weight side products (PDI > 1.2), a library of star polymers with different properties owing to differing molecular weight (6–15 kDa) could be readily generated. The star copolypeptide contained a redox responsive core (disulphide) and was capable of encapsulating hydrophobic drugs.

Using a similar approach, Ding and coworkers prepared a series of nanogels from disulfide-core-cross-linked star copolymers.[65] The core crosslinked star copolymers were formed via one-step ring opening polymerisation of mixed L-phenylalanine and L-cystine NCA monomers with a monofunctional PEG-amine initiator. The formed nanogels were found to be biocompatible and exhibited enhanced intracellular release of doxorubicin (DOX) in GSH pretreated HeLa cells. CCS polymers have also been developed through hydrid system design. Audouin et al. synthesised a library of polymers via a combination of NCA ROP with FRP or RAFT.[66] An amino styrene initiated PBLG homopolypeptide was synthesised and subsequently crosslinked with a divinyl monomer generating CCS polymers with multiple different molecular weight distributions. Of the series of polymers generated, those synthesised using FRP led to polymers with higher yields than those synthesised with RAFT.

1.2.4 Miktoarm star polymers

In addition to symmetrically grafting homo, block or statistical polymers to a multifunctional core, asymmetric grafting is also possible creating what are referred to as 'miktoarm' polymers. The miktoarm star polymers are formed by integrating multiple different polymer chains composed of different chemical backbones on to a multi-arm macromolecule. A great example of the concept was published by Hadjichristidis et al., who formed an ABC type miktoarm with individual polystyrene (PS), polyisoprene (PIP) and poly(*tert*butoxycarbonyl-L-lysine) (PBLL) arms.[67] The mixed conformation of each respective sequence contributed to the formation of rod-coil like assemblies. In a similar fashion, click chemistry techniques have been used as synthetic route for the design of

AB miktoarm star polypeptides. Liu and coworkers used a 3-arm initiator with pendent reactive functional groups for both NCA ROP (primary amine) and click reactions (alkyne), both capable of growing polypeptide chains and attaching linear polypeptide arms respectively.[68] Alternatively, NCA ROP can be conducted on monofunctional initiators with clickable side groups and then tethered to star miktoarm polymers. For example, Pati et al. have recently reported the design of 3-armed miktoarm star copolymers composed of both glycopolypeptide and poly(ε-caprolactone) chains using NCA ROP and 'click chemistry'.[69] The linear glycopolypeptide was prepared via propargylamine mediated NCA ROP and then attached to the 3-armed star via azide-alkyne cycloaddition. The resulting miktoarm amphiphiles exhibited morphologies such as nanorods, polymersomes, and micelles in aqueous solution, with nanostructure formation easily modulated by tuning the chain length of the blocks. Another interesting example was detailed on the development of 4-armed mixed glycopolymer-polypeptide conjugate.[70] Two of the arms were functionalised with propionyl bromide, which were used as the reactive handles in the synthesis of a library of mannose, glucose, and galactose based glycopolymers via ATRP. The other 2 arms were azide functionalised, which were used to click on alkyne terminated PZLL. The subsequent deprotection afforded a 4-arm hydrophilic star miktoarm polymer, displaying a broad range of antimicrobial activity towards both Gram-positive and Gram-negative bacteria. The production of CCS polymers using miktoarm design principles has also been explored by Lu and coworkers.[71] Initially, they used a PEG macro-RAFT agent with an aldehyde-bearing divinyl monomer and a fluorescent aluminum tris(8-hydroxyquinoline) cross-linker to compose a CCS polymer. Aldehyde–aminooxy coupling with an aminooxy terminated PBLG yielded the fluorescently labeled polypeptide–PEG miktoarm conjugate. Subsequent β-hydroxyethylenediamine aminolysis of PBLG rendered functionalities that were used to form star miktoarm polyplexes with siRNA.

1.3 Polypeptide hydrogels

Hydrogels are a class of gelating materials comprising a water-soluble three-dimensional (3-D) crosslinked network. They are highly branched, porous and possess a similar water enveloped network to that of the extracellular matrix (ECM), which is an advantageous

characteristic when considering criteria for biomaterial design.[72,73] Historically, biomedical hydrogels have been prepared with natural occurring polymers such as gelatin or hyaluronic acid, with subsequent chemical augmentation affording material properties and functionalities that would be otherwise non-existent in their basic chemical form. However, there are still many disadvantages associated with the use of natural hydrogels mainly in terms of reproducibility. Prompting this, the emergence of hydrogelating materials from purely synthetic sources has helped to overcome some of these limitations. Similar to naturally occurring hydrogels, a synthetic hydrogel can be described as a hydrophilic polymer that is 'crosslinked' in solution by secondary forces that may be electrostatic, steric or covalent in nature.[74] In synthetic polymers, the option for pre and post polymerisation modification allows for the inclusion of functionalities that facilitate aqueous gelation and thus control the material properties. Resulting hydrogels may exhibit self-recovering, self-healing or shear thinning behaviour.[75,76] Of particular interest is their use as drug/gene delivery depot systems or tissue engineering scaffolds.[77] Of those materials available, synthetic polypeptide hydrogels comply with the criteria described.

1.3.1 Scope of polypeptide based hydrogels

Over the last decade, the use of peptide based hydrogels has been thoroughly explored.[78, 79] The aqueous gelation of these materials is highly sensitive to composition, which can be finely tuned using a range of synthetic strategies.[80] Their development can be tailored to predict secondary structural folding, creating polypeptide hydrogels with specific physical and mechanical properties such as stimuli responsiveness,[81] structural rigidity[82] and elasticity.[83] Comparable to natural hydrogels, biomimetic polypeptide hydrogels also display similar physicochemical properties to those compositions found in the ECM.[84] Multiple different side chain functionalities can also be imprinted into a polypeptide systems, providing diverse material properties. In addition, the polypeptide backbone is capable of both hydrolytic and proteolytic cleavage akin to the degradation profile of native proteins.[85,86] Their structural stabilisation stems from ordered arrangements of polypeptide strands via α-helical or β-sheet conformations.[87,88] These arrangements have been characterised using a number a qualitative methods including

circular dichroism (CD) and fourier-transform infrared (FTIR) spectroscopy. FTIR spectroscopy is a particularly valuable method for identification as it detects the bond vibrational modes of the amide carbonyl (amide I) and the amide secondary amine (amide II) in two characteristic regions of interest.[67] Small conformation changes in the peptide backbone can alter the structure, shifting the amide vibrational mode to a different wavenumber, allowing for observation of conformational change. Thus, synthetic polypeptides represent excellent candidates for applicable hydrogelating materials due to their highly desirable properties. Of those synthetic polypeptides, the design of hydrogels from the N-carboxyanhydride (NCA) ring opening polymerisation (ROP) has been of paramount interest in recent years.[89-91] Hydrogel production through the use of integrated orthogonal chemistries has helped to develop versatile fabrication systems in the design of advanced polypeptide structures.[92-94] The continuing emergence of these new synthetic 'tools' may provide a route to next generation hybrid polypeptide hydrogel systems which can be tailor-made to realise biomedical applications.[95,96]

1.3.2 Polypeptide hydrogels from physical crosslinking

Both chemical and physical interactions can result in the formation of crosslinking 'junctions' within aqueous solution and in some cases organic solvents.[97,98] In physical hydrogels, the crosslinks necessary for hydrogel network stabilisation are a consequence of independent hydrophobic segments which are directly attached to hydrophilic segments. Physical interactions in the form of hydrogen bonding and other non-covalent interactions such as electrostatic interactions, π-π stacking and hydrophobic interactions can stabilise supramolecular polypeptide assemblies.[99-101] The polypeptide chain aggregation occurring through the intermolecular/intramolecular assemblies of these physical moieties is the main driving force for the conformational orientation into either α-helixes and β-sheets, sometimes forming fibrillar hydrogels (Figure 1.4).[102,103]

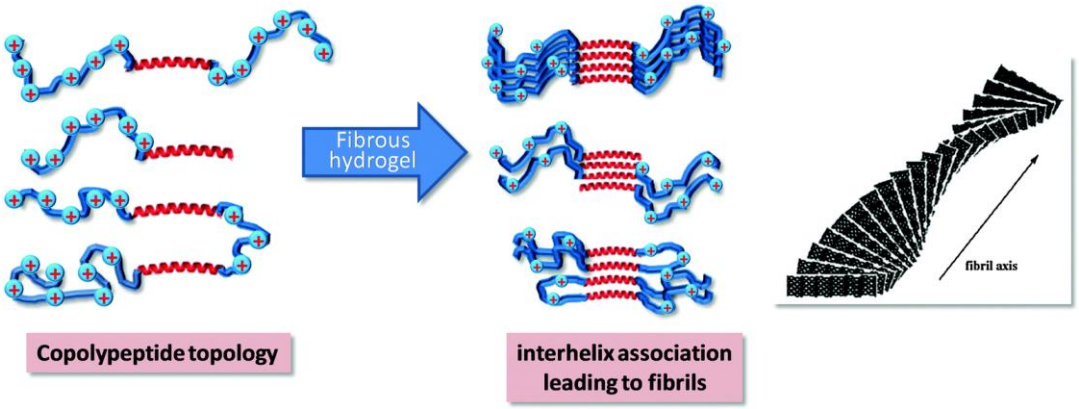

Figure 1.4: Fibrillar α-helical supramolecular hydrogel networks from hierarchical self-assembly of copolypeptides of different macromolecular topologies (diblock, triblock, pentablock).[80]

The role of secondary structure in polypeptide-based gelators is integral for their formation and stabilisation. In particular for multi-block copolypeptides, the presence or absence thereof plays a vital role in hydrogelation. Hydrogel mechanical properties can be finely tuned by controlling the secondary structure through structural modulation, such as changing the chain length of hydrophilic and hydrophobic blocks, modifying side groups with functionalities capable of supramolecular assemblies, and/or switching stereochemistry of polypeptide. Those polypeptides derived from *racemic* repeat units usually result in polymeric sequences devoid of any secondary structure, meaning hydrogelation relies primarily on the amphiphilic balance. Due to this inherent lack of hydrogen bonding, high polypeptide concentration is required for gelation.[104] As such amino acid L-isomers are primarily used in synthetic polypeptide amphiphiles. With these homo-isomeric peptide sequences, the assembly of one inherently α-helical or β-sheet forming hydrophobic block, together with a separate random coil forming hydrophilic block, can result in the supramolecular self-assembly in to a hydrogel matrix with an optimised hydrophile-hydrophobe ratio. Physically crosslinked hydrogels prepared from multi-block copolypeptides have been subject to extensive research from many groups, and are the basis of new age biomaterials for tissue engineering. Deming et al. have published many findings on their studies of copolypeptides, ranging from diblock to pentablock amphiphiles and employing a range of amino acid building blocks and different block lengths to finely tune gel strength.[105-108,] Interestingly extensive

biological studies were conducted on the diblock copolypeptide hydrogels (DCH) composed of tailored peptide sequence lengths of lysine and leucine.[109] The DCH could form 3D deposits *in vivo* and showed no toxicity after injection into the central nervous system (CNS).

1.3.3 Polypeptide hydrogels from chemical crosslinking

The introduction of reactive chemical crosslinkers to a solvated polypeptide can create dense three-dimensional gel networks capable of entrapping water. In the case of water soluble polymers, covalent bonding of pendent groups in hydrophilic polypeptide chains can lead to hydrogels with a chemically crosslinked network. In many cases, the chemical bonding of polypeptides in solution can result in hydrogels with definitive shapes as the chemical bonding is irreversible. Employing these principles, Hammond and co. have detailed the possibility of using reactive group grafted polypeptides as precursors to hydrogel networks.[82,90] They synthesised poly(γ-propargyl-L-glutamate) (PPLG) and then grafted mixtures of short PEG chains terminated with inert hydroxyl or reactive maleimide and/or norbornene groups via azide-alkyne cycloaddition. A series of macroscopic hydrogels were then formed through thiol-ene crosslinking of the PPLG macromers with a 4-arm star shaped PEG. The PPLG gels were far less dependent on swelling as a function of crosslink density in comparison to PEG only gels, mainly due to the retention of α-helical conformers. Bioconjugation reactions for specific amino acid residues has had a recent emergence for their potential use in the development of orthogonal crosslinkers for fabrication of polypeptide hydrogels. The triazolinedione (TAD) 'click-like' reaction has been used by Hanay and coworkers to covalently crosslink residues of tyrosine and tryptophan in segmented copolypeptides.[110,111] For instance, copolypeptides comprising tyrosine and lysine were reacted with a difunctional TAD molecule, which selectively formed a tyrosine-bisTAD conjugate in rapid time (60-70 s). The highly efficient crosslinking resulted in the formation of a stiff polypeptide hydrogel. Popescu et al. have explored the pH dependent self-assembly behavior of aqueous solution of poly(l-alanine)-block-poly(l-glutamic acid)-block-poly(l-alanine) amphiphiles and the effect of end-capping with benzaldehyde via a Schiff base reaction.[112] This dynamic bonding interaction lead to a sol-gel transition at

physiological pH (7.4) after heating and slow cooling, forming opaque stiff hydrogels due to assembly into twisted fibrillar β-sheets. The Schiff-base triggered gelation was reversible, with decoupling of the benzoic–imine dynamic covalent bonding evident when lowering pH (6.5). Other recent studies demonstrated the use of commonly employed chemical ligation amide coupling strategies which provided hydrogels with covalent crosslinks. Ma et al. exploited the side group chemistry of two separate poly-L-lysine and poly-L-glutamate polypeptides, crosslinking the pendant amine and carboxyl residues using EDC/NHS amidation.[113] The hydrogels formed exhibited low fouling of protein and were found to be non-cytotoxic. Gel properties changed with a different pH and ionic strength concentrations, while enzymatic triggered release of DOX and diclofenac was demonstrated. Similarly, Qiao and coworkers prepared cryogels through EDC/sulfo-NHS cross-linking of a random copolypeptide consisting of mixed poly(L-lysine) and poly(L-glutamate) using cryo conditions (Figure 1.5).[114]

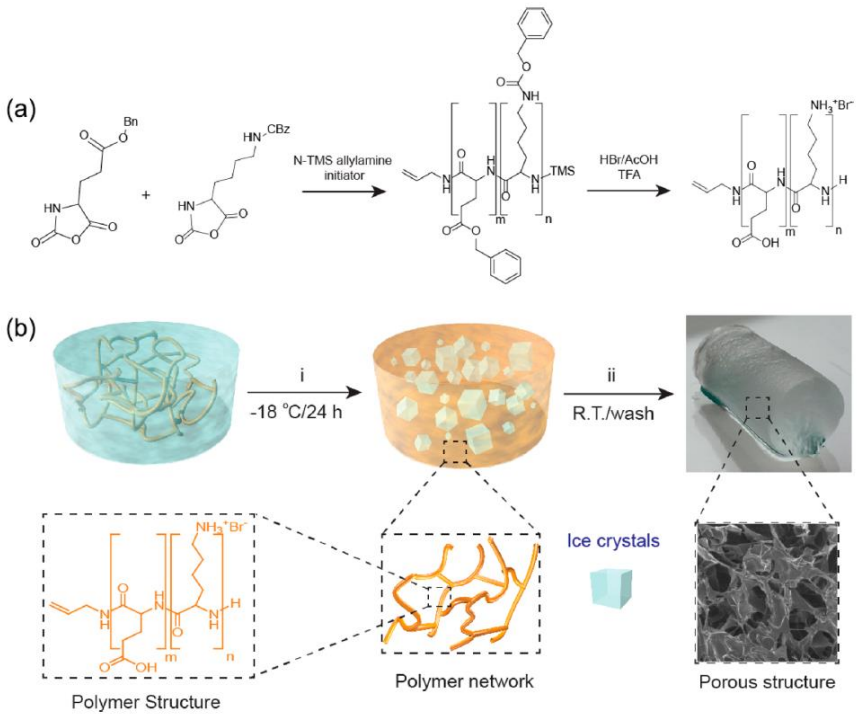

Figure 1.5: Development of macroporous hydrogels showing (a) scheme of polypeptide formation and (b) freeze thaw technique.[114]

Images from both environmental scanning electron microscopy (ESEM) and confocal laser scanning microscopy (CLSM) revealed large macroporous structures (≥100 µm). The

pore morphology could be readily changed (spongey or columnar-like) by tailoring the ratio of lysine to glutamic acid, which also had a large effect on the swelling and mechanical stiffness properties.

1.3.4 Polypeptide hydrogels with stimuli response

The inclusion of functional groups which are systemically triggered by stimuli such as temperature and light represent current design principles when requiring ''responsive'' hydrogels. For temperature mediated gel-to-sol or sol-to-gel transitions, conformational switches play a major role. A well-established example is the phase change of gelatin, whereby hydrogelation is anticipated to arise from the coil-helix interchange when subject to temperature reduction.[115] In synthetic approaches, many materials integrate the much used polymer PEG as a core building block, due to its ability to dehydrate and stimulate conformation changes in peptide blocks prompted by a change in temperature. Many reports detail the use of block copolymers of PEG and β-sheet forming peptides as thermoreversible hydrogelators with tunable LCST (lower critical solution temperature).

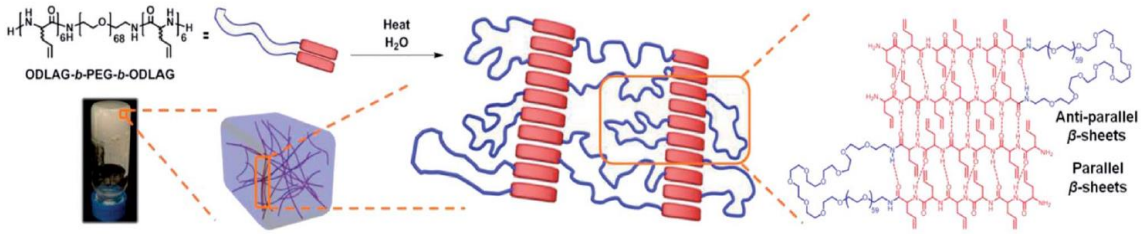

Figure 1.6: Nanofiber and hydrogel formation via temperature induced self-assembly of $ODLAG_6$-b-PEG_{68}-b-$ODLAG_6$.[120]

Jeong et al. have multiple reports detailing the incorporation of PEG into block copolypeptide amphiphiles and their thermoreversible sol-gel transition.[116-118] One particular report details the relationship between the orientation of polypeptide sequences composed of amphiphilic PEG-L-polyalanine and PEG-DL-polyalanine diblock copolymers.[104] Those polypeptide amphiphiles containing L-isomers switched from random coils to β-sheets and underwent a sol-gel transition (8.0 wt%) with an increase in temperature in the range of 20-40 °C. The DL-isomer remained as a random coil in

aqueous solution as it could not undergo secondary structural assembly. Similar to strategies used by the Jeong group, additional thermo-reversed gelators from PEG/β-sheet peptide copolymers (Figure 1.6) were reported by the Chen[119] and Wooley[120,121] groups. Huang and coworkers also used such design principles in the development of oligo-tyrosine PEG copolymers. They functioned as reverse thermal gelators at temperatures ranging between 22-50 °C, with CD suggesting more efficient β-sheet packing of the tyrosine segments at elevated temperatures.[122] The Li group have also published multiple reports on ethylene glycol (EG) modified glutamate as thermoresponsive functionalities within polypeptide sequences.[123-125] Similarly, Zhang et al. reported a non-ionic polypeptide hydrogel from copolymers of poly(g-[2-(2-methoxyethoxy)ethyl]-l-glutamate) and poly-L-leucine.[126] Thermoresponsive gelation was observed at elevated temperatures above 22 °C, while the hydrogel depots also maintained a controlled release of model protein cargos.

Photo induced crosslinking or polymerisation represents a convenient stimuli to manipulate for macroscopic control of hydrogelation. An early report from Ohkawa et al. described coumarin functionalised polymers of lysine and ornithine which underwent photodimerisation at low concentrations in aqueous media, forming enzymatically degradable transparent hydrogels.[127,128] A more recent example of photo-cylclisation for the production of hydrogels was provided by Chen and coworkers, who used PEG-b-poly(L-glutamic acid-graft-cinnamyl-L-glutamate) copolymers.[129] The presence of multiple cinnamyl moieties cause micellar assemblies in aqueous solution, which then convert to nanogels after photo-induced cyclodimerisation of residues. The drug release profile of the nanogels could be easily modulated by varying block composition. Photo-degradation also constitutes another promising aspect of the recent studies concerning polypeptide hydrogel networks. Deming et al. have prepared a photolabile NCA monomer based on L-lysine with an *o*-nitrobenzyloxycarbonyl (*o*NB) protecting group and used it in the design of block copolypeptide hydrogels (Figure 1.7).[130] The *o*NB-lysine residues functioned as a viable substitute for the commonplace hydrophobic residues used in block copolypeptide hydrogel design. After UV irradiation, full cleavage of the *o*NB groups was achieved, prompting a gel-sol transition. A photolysis assay allowed for the expedited released of a loaded dye into the surrounding aqueous media, showing

the capacity of the hydrogels as loading depots. Similarly, Li and coworkers reported a series of supramolecular photo/thermosensitive poly(*o*-nitrobenzyloxycarbonyl-L-lysine)-block-PEO (PNBL-b-PEO) hydrogels based on normal and reverse micellar assemblies after complexation with α-cyclodextrin (α-CD).[131] The hydrogels could switch orientation from reverse to normal micelles with pH gradient change and showed a rapid reduction in storage modulus from 11 to 1.8 kPa after 30 min of UV irradiation.

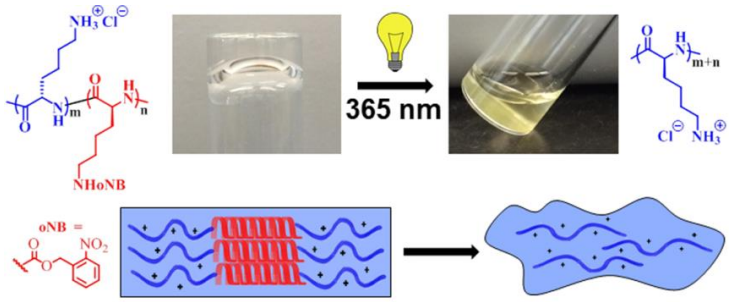

Figure 1.7: Photo-cleavage of poly(L-lysine)-block-poly(*o*NB-L-lysine) amphiphilic hydrogels resulting in polypeptide dissolution and complete hydrogel disruption.[130]

Enzymatic crosslinking provides another methodology for forming covalent linkers between peptide backbones, but is specific to the chemistry of certain side groups. Chen et al. have published multiple reports using the enzyme horseradish peroxidase (HRP) in combination with hydrogen peroxide (H_2O_2) on polypeptides with phenol functionalised residues.[132] Hydrogels of tyramine and poly(ethylene glycol) grafted poly(L-glutamic acid) were rapidly formed under physiological conditions in the presence HRP and H_2O_2.[133] The mechanical properties of the hydrogels could be readily modulated by changing the concentration of both HRP and H_2O_2. After subcutaneous injection into the back of rats, the hydrogels were maintained for 10 weeks and exhibited acceptable biocompatibility.

Physiologically, utilising disulfide bonding allows for swift selective cleavage under intracellular conditions (highly reductive) while it remains stable extracellularly due to the lower concentration of the reductant glutathione (GSH). Using this strategy, many redox responsive polypeptide hydrogels have been developed.[134] A reduction-sensitive disulphide polypeptide based nanocarrier with near-infrared fluorescence (NIRF) probe

was prepared by Yan et al.[135] GSH mediated DOX release *in vitro* was vastly accelerated in comparison to neutral conditions. Cell uptake studies showed that they the NIRF nanogel entered the cell via endocytosis. Using NIRF labeling, direct monitoring of drug release from the NIRF nanogel demonstrated that DOX molecules migrate to the nucleus while the NIRF nanogel localises in the cytoplasm. Alternative building blocks were used to develop dual thermal and redox responsive hydrogels (Figure 1.8) based on mPEG-poly-L-methionine, as reported by Chen et al.[136]

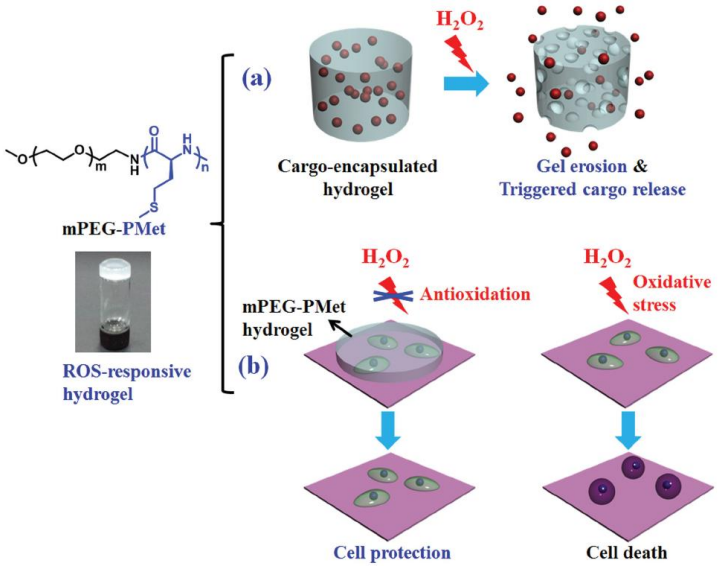

Figure 1.8: ROS-responsive mPEG-PMet hydrogels demonstrating (a) oxidation induced cargo release and (b) cytoprotective ability with oxidative stress.[136]

The hydrogels were quenched in the presence of a H_2O_2 rich environment, leading to oxidation of the methionine residues to sulphoxide/sulphones and destroying the β-sheet secondary structure necessary for gelation. The L-methionine residues functioned as antioxidants and showed cyto-protective properties against induced oxidative stress *in vitro* and *in vivo*. Hydrogels have also been made through incorporation of disulphides through alternative chemistry, For instance, poly-L-glutamic acid (PLG) grafted with disulfide bond forming phloretic acid has been reported.[137] The hydrogel was used as a cell-laden 3D matrix, releasing the cells via a GSH cue which disrupts the entangled hydrogel network. The cells released maintained high viability demonstrating the potential of this platform for cell encapsulation applications in tissue engineering. Moreover, faster degradation of the hydrogels (denoted PLG-g-CPA) was observed after

subcutaneous injection into rats, highlighting the advantage of using these disulphide containing hydrogels *in vivo*.

1.3.5 Polypeptide hydrogels from star architecture

In terms of materials, there have been few reports detailing star polypeptide hydrogelating materials from either CCS[64,65] or symmetrical stars. For symmetric star polypeptide hydrogels, Thornton et al. have previously demonstrated the synthesis of polyalanine decorated star polymers, tethered to a 4-arm poly(ethylene glycol) (PEG).[138] An accurate degree of polymerisation with the amount of alanine NCA in the monomer feed was deduced by ^{1}H-NMR spectroscopy. Both circular dichroism and FTIR spectroscopy revealed that the star polypeptide induces gelation through a predominant α-helical secondary structure with some β-sheet conformations evident. Increasing β-sheet conformation was noted for longer polyalanine chains. The hydrogels were also capable of loading albumin for prolonged periods, before stimulating its release by proteolytic degradation using the enzyme elastase. Dong et al. synthesised star polypeptides by ROP of diethylene glycol-L-glutamate NCA using a tetra(amine) with a disulfide core as the initiator (Figure 1.9).[139] The star polypeptide self-assembled into thermo/reduction responsive micelles, with a hydrogelation observed at 3.4-3.8 wt%. Their properties were tunable by controlling polypeptide segment length while the disulphide core allowed for reductive cleavage of the star polypeptide hydrogel. The chemotherapeutic drug DOX was loaded into the star polypeptide micelles which demonstrated a reduction-sensitive drug-release profile. Polypeptides with star architectures were also reported by Shen and coworkers.[140] Comprising of similar oligo(ethylene glycol) (OEG) functionalised poly(L-glutamate) (poly(L-EG_2Glu)) tethered to 8-arm and 32-arm dendrimer cores, the star polypeptides readily formed hydrogels in water. Critical gelation concentration (CGC) was highly dependent on the degree of arm branching. For an almost identical arm length, the 32-arm polypeptide (1.0 wt%) had lower CGC than the 8-arm polypeptide (2.0 wt%). TEM and AFM revealed entangled and branched fibrillar structures as a result of α-helical packing, which was attributed to the gelation. Rheological analysis showed that the hydrogels exhibit shear thinning and fast recovery properties.

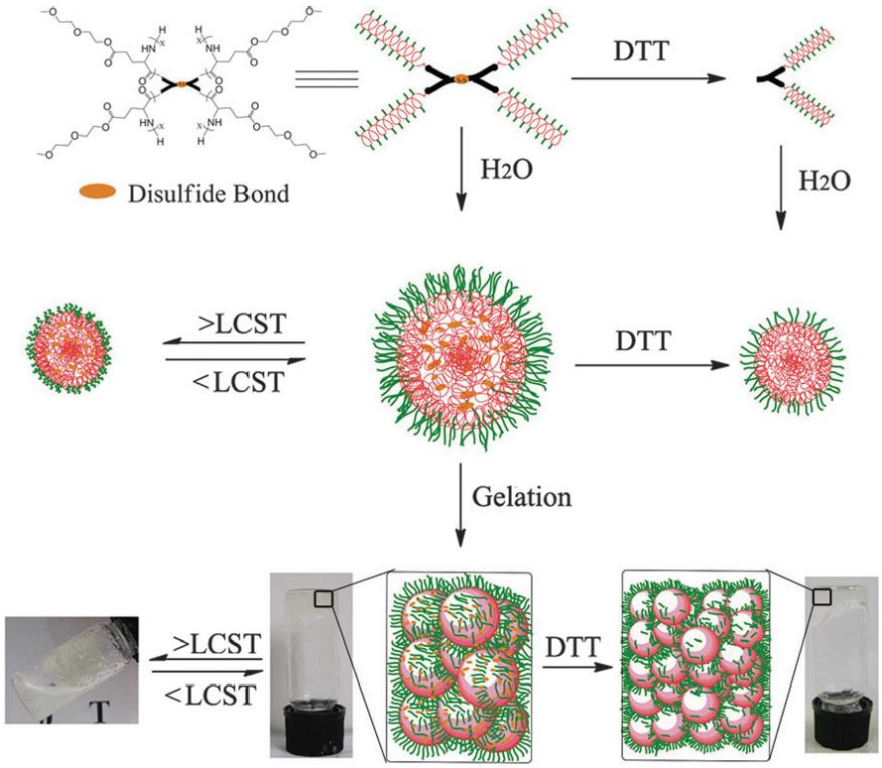

Figure 1.9: Scheme of redox/thermo responsive micellisation and hydrogelation of star polypeptides.[139]

1.4 3D Printing

Additive manufacturing (AM), or more commonly referred to as three dimensional (3D) printing is widely applied technique utilised in a multitude of object production fields.[141] The technology permits the development of objects with defined layer-by-layer construction through automated processing using computer aided design (CAD). Recently, it has emerged as an alternative to current technologies for the development of on-demand tissue engineering scaffolds as its precision and reproducibility make it one of the most straightforward fabrication methodologies.[142] A number of AM methods for the 3D fabrication of hydrogels have been explored (Figure 1.10), included laser assisted,[143,144] stereolithography,[145,146] inkjet[147,148] and extrusion based 3D printing.[149,150]

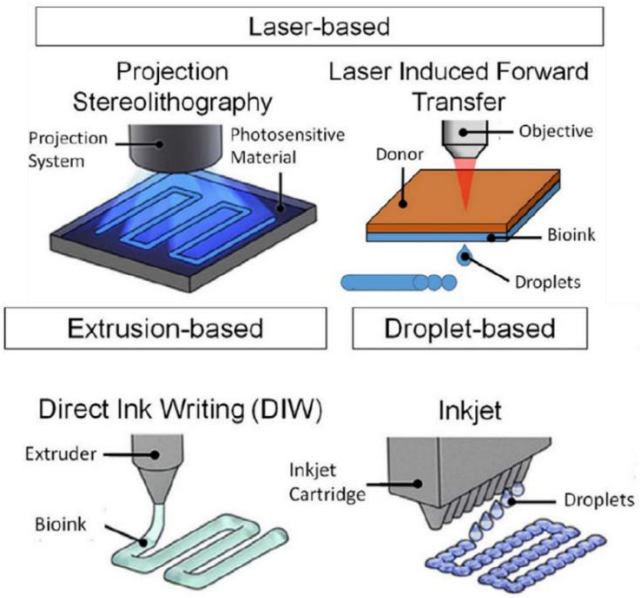

Figure 1.10: 3D printing techniques for hydrogels.[142]

1.4.1 Overview on 3D fabrication methods

Stereolithography (SLA) utilises an ultraviolet (UV) laser for the development of constructs with high accuracy.[151] Commonly used SLA methods function whereby the layers are built ''bottom up''. The first layer is attached to the build platform, which orientates above the resin reservoir. After this first layer is created, it is detached from the reservoir and continues to move with the rising build platform as each subsequent layer is created by the laser. The process is repeated until the final structure is generated. Either light reactive monomer resins or polymers containing photo-crosslinkable functionalities are used which are then processed through spatially limited photo-curing to design well-defined structures.

Inkjet printing generates structures through the continuous creation of droplets onto a substrate with a thin layer of powder.[152] Drop on drop creation can be achieved using thermal and piezoelectric printing heads. The thermal processing head vaporises the ink, forming a vapor bubble that expands and then ejects from the fluid reservoir. The piezoelectric processing head functions by introducing a voltage pulse to the fluid reservoir, which creates a pressure transition within the fluid reservoir resulting in droplet formation.

For 3D laser fabrication techniques, matrix-assisted pulsed laser evaporation direct writing (MAPLE-DW) is commonly utilsed.[153] It functions whereby a laser beam is passed through one side of a quartz support slide, with a layer of material to be printed coated on the other side. The beam is aimed at the interface of the quartz support slide resulting in rapid localised heating, which causes vaporisation of the material layer to occur. The resulting bubble expands from the bottom of the quartz slide depositing a jet of material.

For extrusion based 3D printing, sometimes termed direct ink writing (DIW); integrative computer software allows for the input of a scaffold blueprint, which is provided in the form of a CAD file, to enable the printer to recognise the construction directions for development of the desired shape. The extrusion proceeds as a continuous volume of hydrogel is projected from a nozzle creating layer-by-layer patterns which is governed by the movement of the printhead in the x-y-z axis.[150,154] Defined printing resolution is achieved by using smaller nozzle inner diameters (IDs) than those used for cannula injections. The rheological properties should be ascertained before attempting 3D printing, in order to identify the shear effects on the hydrogel inks' recovery post needle extrusion, as the reassembly of the ink should be rapid enough to ensure high shape fidelity of the deposited construct. However, there are some uncontrollable parameters that may affect the resolution of 3D deposited hydrogel layers such as gravity induced structure deformation, non-uniform extrusion through a change in printing speed or missing layers due to the presence of air bubbles. Therefore a consistent process is necessary when choosing the layering substrate, controlling the printing parameters and preparing the hydrogel inks.

The direction of 3D fabrication strategies towards applications of biological relevance resulted in a new age technology termed ''bioprinting'', which combines aspects of both additive manufacturing and cell culture. In bioprinting approaches, a computer-controlled 3D printer extrudes cell-laden hydrogel inks, also referred to as bio-inks, into preset biomimetic models. Similar to hydrogel inks, 3D patterning of bio-inks should result in the deposition of self-supporting, well defined geometric shapes. The difference here being that bio-inks are purposed for prompting the growth of new biological tissue

which has a particular cellular organisation and active biological function.[155] Initial screening of the rheological properties of the bio-ink should be determined as encapsulated cells can be sensitive to the shear rates associated with needle extrusion. The cue for proliferation and differentiation in said cells is usually achieved by incorporating biomolecules such as growth factors or other components into the bio-ink formulation in order to stimulate the desired cell response. Recently, bioprinting has been successfully used in the development of augments representing some of the anatomic geometries of the human body; such as skeletal muscle,[156] vascularised tissue,[157] bionic ears,[158] aortic valves[159] and bone tissue.[160] A particular advantage of these 3D deposited scaffolds is that the chances of immunorejection, so often seen in patient to patient organ transplants, is less likely. This is a consequence of using autologous primary stem cells, which are extracted directly from the patient.[161] The cells are seeded in the bio-ink and internal cues allow the tissues of choice to form over time. Theoretically the regenerated tissues formed in the 3D printed scaffold would then integrate accordingly into the target site of the patient after transplantation. Hence, there is a need for these bio-ink hydrogels to be designed appropriately in order to cope with the requirements necessary for the development of bio-engineered tissue.

1.4.2 Types of 3D printable hydrogel inks

The conventional feedstock material used for inks comes in the form of naturally occurring hydrogelating polymers. Collagen, hyaluronic acid, gelatin, agarose, alginate, fibrin, and chitosan have all been used in 3D printing technologies. These naturally derived hydrogels possess biomimetic function and a structural composition resembling the ECM. Sodium alginate (alginate) is one of the most commonly used hydrogels for inkjet and extrusion based printing.[144,149,150,158] It is a polysaccharide that can be isolated from seaweed. Alginate is densely populated with anionic functional groups, which permits the formation of ionic bridge domains when it interacts with divalent cations in solution. Normally it is 3D printed as a viscous solution into a bath containing divalent ions (usually $CaCl_2$) and thus crosslinked *in situ*, or it is 3D printed and then exposed to the same solution as a post-printing crosslinking strategy. As alginate does not contain any cell adhesive motifs, it is sometimes blended for bioactivity.[162] For example Butcher

et al. have used it in combination with gelatin to create aortic valve conduits that showed markedly improved mechanical properties and high cell viability over alginate alone.[163]

Gelatin, which is derived from animal tissues/skin/bone, is another primary source of gelating material for 3D printing.[157,160] It is a denatured form of the native protein collagen. Although collagen is a major component of the natural ECM and would ideally be suitable for 3D printing, it is limited in terms of formulations due to its poor water solubility and subpar mechanical properties. Owning better solubility, less tertiary structures than and consisting of cell adhesive RGD motifs, gelatin represents an ideal alternative for tissue engineering 3D fabrication methods. [164-166] Gelatin is generally functionalised with methacrylamide to obtain gelatin methacryloyl (GelMA), a commonly used photo-curable hydrogel ink. For 3D construct development, this provides a post processing strategy which functions to enhance mechanical stabilisation, prevent evaporation and entrap the matrix for cell proliferation.[167,168]

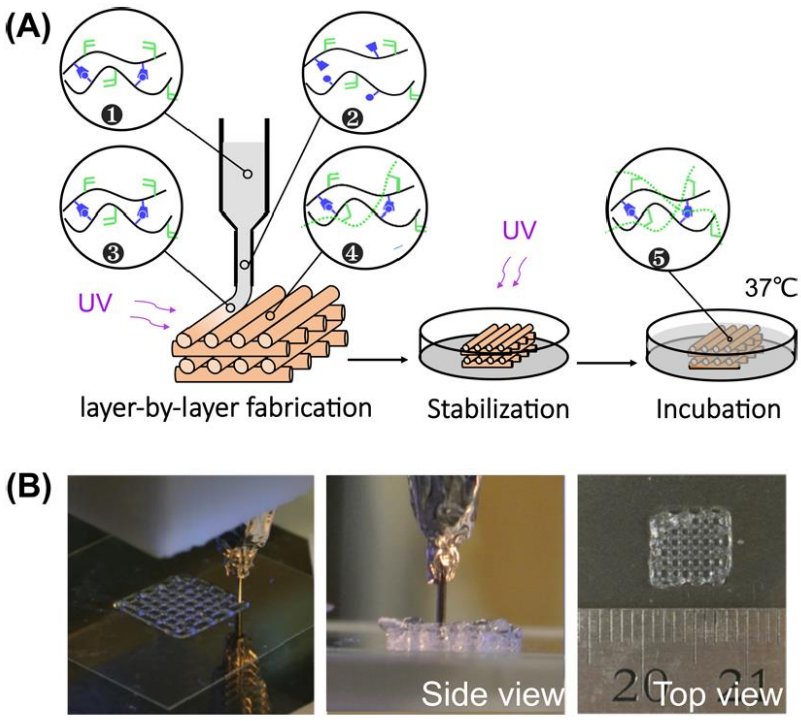

Figure 1.11: (A) Scheme of dual crosslinked hyaluronic acid hydrogels with their 3D extrusion and construct crosslinking techniques (B) Images of lattice constructs from the printing process.[172]

Similar to gelatin, hyaluronic acid (HA) has been as a basis for hydrogel inks. HA is a naturally occurring polysaccharide which is ubiquitous in both human and animal tissues. HA can be sourced from bacteria,[169] and it is both biodegradable and bioactive, making it a sustainable feedstock material for tissue engineering applications. However, it is highly hydrophilic and has low viscosity in highly aqueous media, limiting its application as a standalone hydrogel for 3D printing.[170] Burdick and coworkers have many reports on HA-based supramolecular hydrogel systems which are adapted for many applications in 3D printing (Figure 1.11).[171-173] Intricate constructs have also been generated using Me-HA containing hydrogel inks for bone tissue engineering.[174] Using similar modification strategies as those used for gelatin, hyaluronic acid has been functionalised to create viable cell-laden constructs. HA derivatives with hydrophobic functionalities have been used to introduce more control over the materials viscosity, with methacrylated hyaluronic acid (Me-HA) primarily used.

In purely synthetic hydrogels, many strides forward have been made towards developing materials capable of fulfilling the criteria demanded by cell-laden matrix 3D printing. Of those hydrogels, poly(ethylene glycol) (PEG) is commonly used for 3D printing owing to its hydrophilicity and cyto-compatibility.[145,146,175] In spite of this, PEG as a standalone hydrogel ink does not have the required mechanical properties for stable construct development and does not promote cellular function for encapsulated cells. As such it is normally blended with natural polymers or bioactive polymers in order to develop mechanically tunable hydrogel inks with biological functionality.[176-178] Functionalised PEG is generally used in the form of PEG-diacrylate (PEG-DA) or PEG-methacrylate (PEG-MA) which permits photo-curing post-extrusion. For example, Hockaday et al. used PEG-DA physically mixed with sodium alginate for 3D extrusion of aortic valves with vastly improved elastic moduli (~5-75 kPa).[158] Pluronic is another synthetic non-ionic copolymer consisting of a hydrophobic polypropylene oxide (PPO) sequence flanked by two hydrophilic polyethylene oxide (PEO) sequences. Wu and coworkers have used wholly diacrylate-functionalised pluronic hydrogels to design defined microvascular networks with diameters ranging from 200 to 600 μm via photo-curing.[179] Other than this it is commonly used as a supporting material in hydrogel inks as it requires high polymer concentration for gelation.[180]

There is a dearth of research completed on synthetic peptide based hydrogels as 3D printable inks. Of those known, ultrashort peptide amphiphiles have been explored. [181-184] These short amphiphilic peptides generally undergo self-assembly into fibrous hydrogels under physiological conditions. They are inherently biocompatible and have conformation stability in terms of structural folding arrangements,[185] which can facilitate extrusion based hydrogel recovery ensuring retention of printed construct fidelity. For instance, Hauser el al. reported stiff lysine containing hexapeptide hydrogels which were 3D printed into scaffolds that supported the differentiation of hMSCs into organotypic cell structures.[181] Other reports detailed the use of peptide hybrid systems as the basis in hydrogel inks used for 3D structural deposition. For synthetic polypeptide hydrogels derived from NCA ROP, only one such report currently exists.

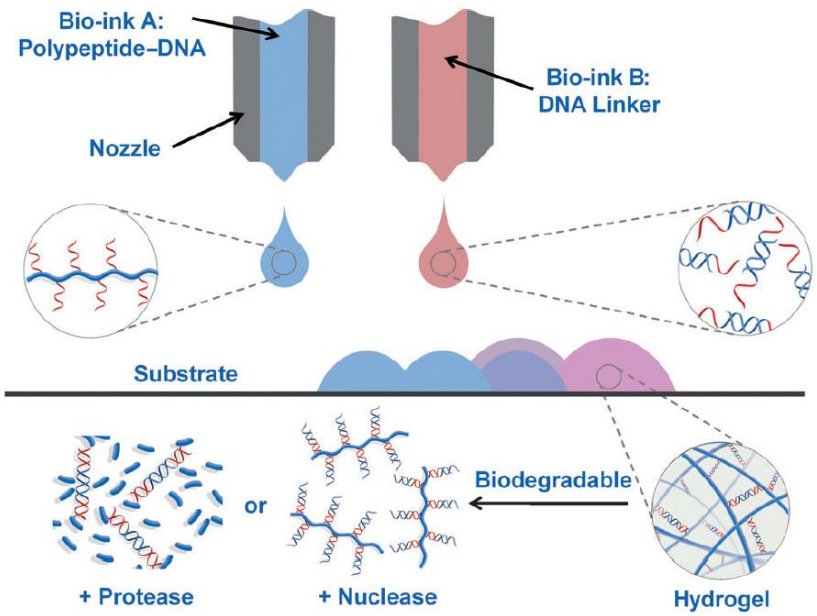

Figure 1.12: Ink-jet printing of the polypeptide-DNA hydrogel via DNA hybridisation forming hydrogel constructs which are responsive to enzymatic degradation.[186]

Duncan et al. developed a supramolecular polypeptide-DNA hybrid hydrogel for in situ 3D printing by designing two separate ink formulations (Figure 1.12).[186] Bioink A consisted of a polypeptide-DNA conjugate with a multitude of single stranded DNA (ssDNA) attached to a poly(L-glutamic $acid_{240}$-co-γ-propargyl-L-$glutamate_{20}$) peptide

backbone. Bioink B was formed from double stranded DNA (dsDNA) with “sticky ends”. Using ink-jet printing, both bio-inks were physically mixed rapidly forming hydrogels through DNA hybridised crosslinks, with deposited constructs having millimeter scale geometries and also demonstrating viability for cell encapsulation.

With this is mind, the use of established hydrogel systems within the field has discounted emerging synthetic hydrogels which have more control over the integration of mechanical behaviour and biochemical cues. While the majority of 3D printing using hyaluronic acid, alginate and gelatin as hydrogelating materials has realised some noteworthy success, a lack of more reproducible, straightforward polymeric hydrogel systems is a major shortcoming in the field of 3D printing.

1.5 Overview and Objectives

Significant progress in developing polymeric materials for their use in biomedical science has been accomplished in recent years. In particular the use of tailor made synthetic polypeptides, which have the ability to mimic the assembly and function of biological proteins, has expanded the field of material science in regenerative medicine with particular applicability in tissue engineering and drug/gene delivery. Hydrogelating materials from polypeptides are an emerging alternative to naturally occurring hydrogels due to their inherent biocompatibility and ease of design. Synthetically, they also represent more sophisticated, robust and tunable systems than the hydrogels obtained from natural sources. With this in mind, the purpose of this PhD project was to develop new hydrogel depots using amino acid building blocks and orthogonal chemistries via the *N*-carboxyanhydride (NCA) ring opening polymerisation (ROP) and then assess their potential for applicability in biomedical applications. The use of poly(propylene) imine (PPI) dendrimers as initiators in the development of star shaped copolypeptide hydrogels was the synthetic strategy employed in chapters 2 to 4, while chapter 5 applied a new difunctional NCA monomer (diaminopimelic acid) as an *in situ* crosslinker for hydrogel development.

Specifically, chapter 2 describes the effects of sequential corona blocks of different hydrophobic side groups and their hydrogelation ability for star shaped poly(L-lysine). By keeping the amphiphilic ratio constant, diblock sequences based on tyrosine, phenylalanine, valine and alanine were examined spectroscopically and rheologically. Pushability studies of the hydrogel materials was examined to determine their applicability as potential injectable drug/gene loading depots.

In chapter 3, star shaped diblock copolypeptide hydrogels that are crosslinked through both core and shell disulphides are examined. By maintaining the feed ratio of lysine and cysteine residues but switching the sequential addition of the NCA monomers for two separate star polymer systems, an in depth look at the architectural effects on both conformational and mechanical properties is described. The material were found to undergo spontaneous gelation within minutes of aqueous immersion with significantly low polymer content <0.5 wt%. The redox responsiveness of the disulphide bonds were also analysed through drug release profiles of the chemotherapeutic drug doxorubicin hydrochloride in the presence and absence of a reducing agent.

Chapter 4 looks at star copolypeptide hydrogels which were synthesised by employing an amphiphilic system using glutamate and valine residues. By introducing a UV crosslinkable group (allyl), the material was used as a hydrogel ink for 3D extrusion printing. Changing the sequence order from triblock with a block of allyl groups to a diblock where the allyl functionalities were grafted, 3D printed constructs with improved homogeneity and mechanical properties could be obtained. These constructs were examined for their degradation profile in different pH conditions and also probed for their potential to release molecular cargo in the form of a model drug. Moreover, the leachates of the 3D printed constructs were also examined for their toxicity towards 3T3 fibroblasts.

Chapter 5 describes the use of a newly synthesised difunctional NCA monomer which was subsequently evaluated as a crosslinker for both ionic polypeptide and non-ionic polypeptoide sequences. The use of the diaminopimelic acid (DAPA) NCA crosslinker for

the preparation of organogels and hydrogels was subsequently investigated after removal of the protecting groups. Spectroscopic and rheological analysis was also conducted to analyse the conformation and mechanical properties of the hydrogels.

1.6 References

1 X. Zhao, F. Pan, H. Xu, M. Yaseen, H. Shan, C. A. Hauser, S. Zhang, J. R. Lu, *Chem. Soc. Rev.*, 2010, 39, 3480.

2 R. V. Ulijn, A. M. Smith, *Chem. Soc. Rev*., 2008, 37, 664.

3 M. G. Ryadnov, A. Bella, S. Timson, D. N. Woolfson, *J. Am. Chem. Soc*., 2009, 131, 13240.

4 B. Ahn, W. Kwon, H. Kim, M. Ree, *Polym. Chem*., 2014, 5, 1912.

5 H. Peng, Y. Xiao, X. Mao, L. Chen, R. Crawford, A. K. Whittaker, *Biomacromolecules*, 2009, 10, 95.

6 E. H. Bromley, K. Channon, E. Moutevelis, D. N. Woolfson, *ACS Chem. Biol.,* 2008, 3, 38.

7 Y. B. Lim, E. Lee, M. Lee, *Angew. Chem. Int. Ed*. 2007, 46, 3475.

8 Y. Huang, Z. Tang, X. Zhang, H. Yu, H. Sun, X. Pang, X. Chen, *Biomacromolecules*, 2013, 14, 2023.

9 H. A. Klok, J. F. Langenwalter, S. Lecommandoux, *Macromolecules*, 2000, 33, 7819.

10 G. Floudas, P. Papadopoulos, H. A. Klok, G. W. M. Vandermeulen, J. Rodriguez-Hernandez, *Macromolecules*, 2003, 36, 3673.

11 Y. Huang, Y. Zeng, J. Yang, Z. Zeng, F. Zhu, X. Chen, *Chem. Commun*., 2011, 47, 7509.

12 N. Hadjichristidis, H. Iatrou, M. Pitsikalis, G. Sakellariou, *Chem. Rev*., 2009, 109, 5528.

13 S. Zhang, D. M. Marini, W. Hwang, S. Santoso, *Curr. Opin. Chem. Biol*., 2002, 6, 865.

14 H. Leuchs, *Ber.*, 1906, 39, 857.

15 F. Fuchs Ber. Dtsch. *Chem. Ges*, 1922, 55, 2943.

16 A. C. Farthing, *J. Chem Soc*., 1950, 627, 3213.

17 W. D. Fuller, M. S. Verlander, M. Goodman, *Biopolymers*, 1976, 15, 1869.

18 M. Oya, R. Katakai, H. Nakai, Y.Iwakara, *Chem. Lett*., 1973, 2, 1143.

19 R. Katakai, Y. Iizuka, *J. Org. Chem*., 1985, 50, 715.

20 W. H. Daly, D. Poche, *Tetrahedron Lett*., 1988, 29, 5859.

21 R. Wilder, S. Mobashery, *J. Org. Chem.*, 1992, 57, 2755.

22 L. C. Dorman, W. R. Shiang, P. A. Meyers, *Synth. Commun*., 1992, 22, 3257.

23 T. J. Deming, *J. Polym. Sci. Part A: Polym. Chem*., 2000, 38, 3011.

24 J. R. Kramer, T. J. Deming, *Biomacromolecules*, 2010, 11, 3668.

25 J. E. Semple, B. Sullivan, K. N. Sill, *Synth. Commun*., 2017, 47, 53.

26 Š. Gradišar, E. Žagar, D. Pahovnik *ACS Macro Lett.,* 2017, 6, 637.

27 X. Zhang, M. Oddon, O. Giani, S. Monge, J. J. Robin, *Macromolecules*, 2010, 43, 2654.

28 J. Zou, J. Fan, X. He, S. Zhang, H. Wang, K. L. Wooley, *Macromolecules*, 2013, 46, 4223.

29 G. J. M. Habraken, M. Peeters, C. H. J. T. Dietz, C. E. Koning, A. Heise, *Polym. Chem*., 2010, 1, 514.

30 T. J. Deming, *J. Am. Chem. Soc*., 1998, 120, 4240.

31 T. J. Deming, *Macromolecules*, 1999, 32, 4500.

32 H. Lu, J. Cheng, *J. Am. Chem. Soc.*, 2007, 129, 14114.

33 W. Zhao, Y. Gnanoub, N. Hadjichristidis, *Polym. Chem*., 2015, 6, 6193.

34 C. D. Vacogne, H. Schlaad, *Polymer*, 2017, 124, 203.

35 A. Sulistio, P. A. Gurr, A. Blencowe, G. G. Qiao, *Aust. J. Chem*., 2012, 65, 978.

36 D. Yonga, Y. Luoa, F. Dua, J. Huanga, W. Lua, Z. Daic, J. Yua, S. Liu, *Colloids Surf. B Biointerfaces*, 2013, 105, 31.

37 K. Inoue, H. Sakai, S. Ochi, T. Itaya, T. Tanigaki, *J. Am. Chem. Soc*., 1994, 116, 10783.

38 K. Inoue, S. Horibe, M. Fukae, T. Muraki, E. Ihara, H. Kayama, *Macromol. Biosci*., 2003, 3, 26.

39 A. Duro-Castano, R. M. England, D. Razola, E. Romero, M. Oteo-Vives, M. A. Morcillo, M. J. Vicent, *Mol. Pharm*., 2015, 12, 3639.

40 R. Holm, B. Weber, P. Heller, K. Klinker, D. Westmeier, D. Docter, R. H. Stauber, M. Barz, *Macromol. Biosci*., 2017, 17, 1600514.

41 S. Cui, X. Pan, H. Gebru, X. Wang, J. Liu, J. Liu, Z. Li, K. Guo, *J. Mater. Chem. B*, 2017, 5, 679.

42 H. M. Wu, S. R. Pan, M. W. Chen, Y. Wub, C. Wang, Y. T. Wen, X. Zeng, C. B. Wu, *Biomaterials*, 2011, 32, 1619.

43 M. Byrne, P. D. Thornton, S. A. Cryan, A. Heise, *Polym. Chem*., 2012, 3, 2825.

44 M. Byrne, D. Victory, A. Hibbitts, M. Lanigan, A. Heise, S. A. Cryan, *Biomater. Sci*., 2013, 1, 1223.

45 K. Aoi, K. Tsutsumiuchi, A. Yamamoto, M. Okada, *Tetrahedron*, 1997, 53, 15425.

46 T. Aliferis, H. Iatrou, N. Hadjichristidis, J. Messman, J. Mays, *Macromol. Symp*., 2006, 240, 12.

47 S. J. Lam, N. M. O'Brien-Simpson, N. Pantarat, A. Sulistio, E. H. H. Wong, Y. Y. Chen, J. C. Lenzo, J. A. Holden, A. Blencowe, E. C. Reynolds, G. G. Qiao, *Nat. Microbiol.*, 2017, 1, 16162.

48 H. Y. Tian, C. Deng, H. Lin, J Sun, M. Deng, X. Chen, X. Jing, *Biomaterials*, 2005, 26, 4209.

49 H. Tian, W. Xiong, J. Wei, Y. Wang, X. Chen, X. Jing, Q. Zhu, *Biomaterials*, 2007, 28, 2899.

50 Y. Yan, D. Wei, J. Li, J. Zheng, G. Shi, W. Luo, Y. Pan, J. Wang, L. Zhang, X. He, D. Liu, *Acta Biomater.*, 2012, 8, 2113.

51 Y. Yan, J. Li, J. Zheng, Y. Pan, J. Wang, X. He, L. Zhang, D. Liu, *Colloids Surf. B Biointerfaces*, 2012, 95, 137.

52 J. Li, S. Xu, J. Zheng, Y. Pan, J. Wang, L. Zhang, X. He, D. Liu, *Eur Polym. J.*, 2012, 48, 1696.

53 J. Li, J. Li, S. Xu, D. Zhang, D. Liu, *Colloids Surf. B Biointerfaces*, 2013 110, 183.

54 Z. Guo, H. Tian, L. Lin, J. Chen, C. He, Z. Tang, X. Chen, *Macromol. Biosci.*, 2014, 14, 1406.

55 H. A. Klok, J. Rodrıguez-Hernandez, *Macromolecules*, 2002, 35, 8718.

56 J. Rodrıguez-Hernandez, M. Gatti, H. A. Klok, *Biomacromolecules*, 2003, 4, 249.

57 S. Park, H. Y. Cho, K. B. Wegner, J. Burdynska, A. J. D. Magenau, H. J. Paik, S. Jurga, K. Matyjaszewski, *J. Am. Chem. Soc.*, 2013, 46, 5856.

58 M. Malke, H. Barqawi, W. H. Binder, *ACS Macro Lett.*, 2014, 3, 393.

59 J. Lin, Q. H. Zhou, L. D. Li, Z. N. Li, *Colloid Polym. Sci.*, 2014, 292, 3177.

60 S. W. Kuo, H. T. Tsai, *Polymer*, 2010, 51, 5695.

61 T. Aliferis , H. Iatrou , N. Hadjichristidis , *J. Polym. Sci., Part A: Polym. Chem.*, 2005 , 43, 4670 .

62 W. Wang, L. Zhang, M. Liu, Y. Le, S. Lv, J. Wanga, J. F. Chen, *RSC Adv.*, 2016, 6, 6368.

63 D. Kafouris, M. Gradzielski, C. S. Patrickios, *Macromol. Chem. Phys.*, 2009, 210, 367.

64 A. Sulistio, A. Widjaya, A. Blencowe, X. Zhang, G. G. Qiao, *Chem. Commun.*, 2011, 47, 1151.

65 J. Ding, F. Shi, C. Xiao, L Lin, L. Chen, C. He, X. Zhuang, X. Chen, *Polym. Chem.*, 2011, 2, 2857.

66 F. Audouin, R. J. I. Knoop, J. Huang, A. Heise, *J. Polym. Sci. A Polym. Chem*., 2010, 48, 4602.

67 S. Junnila, N. Houbenov, S. Hanski, H. Iatrou, A. Hirao, N. Hadjichristidis, O. Ikkala, *Macromolecules*, 2010, 43, 9071.

68 J. Rao, Y. Zhang, J. Zhang, S. Liu, *Biomacromolecules*, 2008, 9, 2586.

69 D. Pati, S. Das, N. G. Patil, N. Parekh, D. H. Anjum, V. Dhaware, A. V. Ambade, S. Sen Gupta, *Biomacromolecules*, 2016, 17, 466.

70 D. Pranantyo, L. Q. Xu, Z. Hou, E. T. Kang, M. B. Chan-Park, *Polym. Chem*., 2017, 8, 3364.

71 J. Huang, H. Liang, D. Cheng, J. Lu, *Polym. Chem*., 2016, 7, 1792.

72 M. Guvendiren, H. D. Lu, J. A. Burdick, *Soft Matter*., 2012, 8, 260.

73 H. Tan, C. M. Ramirez, N. Miljkovic, H Li, J. P. Rubin, K. G. Marra, *Biomaterials*, 2009, 30, 6844.

74 M. R. Matanovi , J. Kristl, P. A. Grabnar, *Int. J. Pharm*., 2014, 472, 262.

75 M. Nakahata, Y. Takashima, H. Yamaguchi, A. Harada, *Nat. Commun*., 2011, 2, 511.

76 A. B. South, L. A. Lyon, *Angew. Chem*., 2010, 122, 779.

77 D. Seliktar, *Science*, 2012, 336, 1124.

78 D. M. Ryan, B. L. Nilsson, *Polym. Chem*., 2012, 3, 18.

79 C. J. Bowerman, B. L. Nilsson, *J. Am. Chem. Soc*., 2010, 132, 9526.

80 C. Chassenieux, C. Tsitsilianis, *Soft Matter*, 2016, 12, 1344.

81 J. P. Schneider, D. J. Pochan, B. Ozbas, K. Rajagopal, L. Pakstis, J. Kretsinger, *J. Am. Chem. Soc*, 2002, 124, 15030.

82 A. M. Oelker, S. M. Morey, L. G. Griffith, P. T. Hammond, *Soft Matter*, 2012, 8, 10887.

83 K. Trabbic-Carlson, L. A. Setton, A. Chilkoti, *Biomacromolecules,* 2003, 4, 572.

84 L. E. R. O'Leary, J. A. Fallas, E. L. Bakota, M. K. Kang, J. D. Hartgerink, *Nat. Chem*., 2011, 3, 821.

85 S. Zhang, M. Altman, *React. Funct. Polym*., 1999, 41, 91.

86 B. S. Berlett, E. R. Stadtman, *J. Biol. Chem*., 1997, 272, 20313.

87 L. D. D'Andrea, L. Regan, *Trends Biochem. Sci*., 2003, 28, 655.

88 P. T. Lansbury Jr, P. R. Costa, J. M. Griffiths, E. J. Simon, M. Auger, K. J. Halverson, D. A. Kocisk, Z. S. Hendsch, T. T. Ashburn, R. G. S. Spencer, B. Tidor, R. G. Griffin, *Nature Struct. Biol.*, 1995, 2, 990.

89 M. Patel, T. Kanekob, K. Matsumura, *J. Mater. Chem. B*, 2017, 5, 3488.

90 C. C. Ahrens, M. E. Welch, L. G. Griffith, P. T. Hammond, *Biomacromolecules,* 2015, 16, 3774.

91 H. Cui, X. Zhuang, C. He, Y. Wei, X. Chen, *Acta Biomater.,* 2015, 11, 183.

92 T. Stukenkemper, J. F. G. A. Jansen, C. Lavilla, A. A. Dias, D. F. Brougham, A. Heise, *Polym. Chem.*, 2017, 8, 828.

93 T. Borase, A. Heise, *Adv. Mater.*, 2016, 28, 5725.

94 J. Yuan, Y. Sun, J. Wang, H. Lu, *Biomacromolecules,* 2016, 17, 891.

95 K. Ren, C. He, C. Xiao, G. Li, X. Chen, *Biomaterials*, 2015, 51, 238.

96 L. Yin, Z. Song, K. H. Kim, N. Zheng, H. Tang, H. Lu, N. Gabrielson, J. Cheng, *Biomaterials*, 2013, 34 2340.

97 F. Hermes, K. Otte, J. Brandt, M. Gräwert, H. G. Börner, H. Schlaad, *Macromolecules*, 2011, 44, 7489

98 C. D. Vacogne, M. Schopferer, H. Schlaad*, Biomacromolecules*, 2016, 17, 2384.

99 D. J. Adams, P. D. Topham, *Soft Matter*, 2010, 6, 3707.

100 F. J. Hoeben, P. Jonkheijm, E. W. Meijer, A. P. Schenning, *Chem. Rev*. 2005, 105, 1491.

101 D. J. Adams, *Macromol. Biosci.*, 2011, 11, 160.

102 E. F. Banwell, E. S. Abelardo, D. J. Adams, M. A. Birchall, A. Corrigan, A. M. Donald, M. Kirkland, L. C. Serpell, M. F. Butler, D. N. Woolfson, *Nat. Mater*. 2009, 8, 596.

103 M. C. Giano, D. J. Pochan, J. P. Schneider, *Biomaterials*, 2011, 32, 6471.

104 Y. Y. Choi, M. K. Joo, Y. S. Sohn, B. Jeong, *Soft Matter*, 2008, 4, 2383.

105 A. P. Nowak, V. Breedveld, L. Pakstis, B. Ozbas, D. J. Pine, D. Pochan, T. J. Deming, *Nature*, 2002, 417, 424.

106 A. P. Nowak, V. Breedveld, D. J. Pine, T. J. Deming, *J. Am. Chem. Soc.*, 2003, 125, 15666.

107 L. M. Pakstis, B. Ozbas, K. D. Hales, A. P. Nowak, T. J. Deming, D. Pochan, *Biomacromolecules*, 2004, 5, 312.

108 Z. Li, T. J. Deming, *Soft Matter*, 2010, 6, 2546.

109 C. Y. Yang, B. Song, Y. Ao, A. P. Nowak, R. B. Abelowitz, R. A. Korsak, L. A. Havton, T. J. Deming, M. V. Sofroniew, *Biomaterials*, 2009, 30, 2881.

110 S. B. Hanay, B. Ritzen, D. F. Brougham, A. A. Dias, A. Heise, *Macromol. Biosci.*, 2017, 17, 1700016.

111 S. B. Hanay, D. F. Brougham, A. A. Dias, A. Heise, *Polym. Chem*., 2017, 8, 6594.

112 M. T. Popescu, G. Liontos, A. Avgeropoulos, E. Voulgari, K. Avgoustakis, C. Tsitsilianis, *ACS Appl. Mater. Interfaces*, 2016, 8, 17539.

113 G. Ma, W. Lin, Z. Yuan, J. Wu, H. Qian, L. Xu, S. Chen, *J. Mater. Chem. B*, 2017, 5, 935.

114 S. J. Shirbin, F. Karimi, N. Jun-An Chan, D. E. Heath, G. G. Qiao *Biomacromolecules*, 2016, 17, 2981.

115 M. Djabourov, J. Leblond, P. Papon, *J. Phys*., 1988, 49, 319.

116 Y. Jeong, M. K. Joo, K. H. Bahk, Y. Y. Choi, H. T. Kim, W. K. Kim, H. J. Lee, Y, S. Sohn, B. Jeong, *J. Control. Release*, 2009, 137, 25.

117 U. P. Shinde, M K. Joo, H. J. Moon, B. Jeong, *J. Mater. Chem*., 2012, 22, 6072.

118 D. Y. Ko, H. J. Moon, B. Jeong, *J. Mater. Chem. B*, 2015, 3, 3525.

119 Y. Cheng, C. He, C. Xiao, J. Ding, H. Cui, X. Zhuang, X. Chen, *Biomacromolecules*, 2013, 14, 468.

120 X. He, J. Fan, F. Zhang, R. Li, K. A. Pollack, J. E. Raymond, J. Zou, K. L. Wooley, *J. Mater. Chem. B*, 2014, 2, 8123.

121 J. Fan, R. Li, H. Wang, X. He, T. P. Nguyen, R. A. Letteri, J. Zou, K. L. Wooley, *Org. Biomol. Chem.*, 2017, 15, 5145.

122 J. Huang, C. L. Hastings, G. P. Duffy, H. M. Kelly, J. Raeburn, D. J. Adams, A. Heise, *Biomacromolecules*, 2013 14, 200-206

123 C. Chen, Z. Wang, Z. Li, *Biomacromolecules*, 2011, 12, 2859.

124 C. Chen, D. Wu, W.Fu, Z. Li, *Biomacromolecules,* 2013, 14, 2494−2498

125 S. Zhang, W. Fu, Z. Li, *Polym. Chem*., 2014, 5, 3346.

126 S. Zhang, D. J. Alvarez, M. V. Sofroniew, T. J. Deming, *Biomacromolecules*, 2015, 16, 1331.

127 H. Yamamoto, T. Kitsuki, A. Nishida, K. Asada, K. Ohkawa, *Macromolecules* 1999, 32, 1055.

128 K. Ohkawa, K. Shoumura, M. Yamada, A. Nishida, H. Shirai, H. Yamamoto. *Macromol. Biosci.*, 2001, 1, 149.

129 J. Ding, X. Zhuang, C. Xiao, Y. Cheng, L. Zhao, C. He, Z. Tanga, X. Chen. *J. Mater. Chem.,* 2011, 21, 11383.

130 G. E. Negri, T. J. Deming, *ACS Macro Lett*. 2016, 5, 1253.

131 P. Li, J. Zhang, C. M. Dong, *Polym. Chem*., 2017, 8, 7033.

132 K. Ren, C. He, C. Xiao, G. Li, X. Chen, *Biomaterials,* 2015, 51, 238-249

133 K. Ren, C. He, Y. Cheng, G. Li, X. Chen, *Polym. Chem*., 2014, 5, 5069.

134 Y. X. Zhang, Y. F. Chen, X. Y. Shen, J. J. Hu, J. S. Jan, *Polymer*, 2016, 86, 32.

135 T. Xing, C. Mao, B. Lai, L. Yan. *ACS Appl. Mater. Interfaces,* 2012, 4, 5662.

136 Q. Xu, C. He, K. Ren, C. Xiao, X. Chen. *Adv. Healthcare Mater*., 2016, 5, 1979.

137 Q. Xu, C. He, Z. Zhang, K. Ren, X. Chen, *ACS Appl. Mater. Interfaces,* 2016, 8, 30692.

138 P. D. Thornton, S. M. Reduwan Billah, N. R. Cameron, *Macromol. Rapid Commun.,* 2013, 34, 257.

139 D. L. Liu, X. Chang, C. M. Dong. *Chem. Commun*., 2013, 49, 1229.

140 Y. Shen, S. Zhang, Y. Wan, W. Fu, Z. Li, *Soft Matter*, 2015, 11, 2945.

141 H. Lipson, M. Kurman, Fabricated: the new world of 3D printing, John Wiley & Sons: 2013.

142 S. Ji, M. Guvendiren, *Front. Bioeng. Biotechnol*., 2017, 5, 23.

143 S. J. Bryant, J. L. Cuy, K. D. Hauch, B. D. Ratner, *Biomaterials*, 2007, 28, 19, 2978,

144 Z. Zhang, R. Xiong, R. Mei, Y. Huang, D. B. Chrisey, *Langmuir,* 2015, 31, 6447.

145 B. Dhariwala, E. Hunt, T. Boland, *Tissue Eng*. 2004, 10, 1316.

146 K. Arcaute, B. Mann, R. Wicker, *Acta. Biomater*. 2010, 6, 1047.

147 C. J. Ferris, K. J. Gilmore, S. Beirne, D. McCallum, G. G. Wallace, *Biomater. Sci*., 2013, 1, 224.

148 J. A. Inzana, D. Olvera, S. M. Fuller, J. P. Kelly, O. A. Graeve, E. M. Schwarz, S. L. Kates, H. A. Awad, *Biomaterials*, 2014, 35, 4026.

149 S. E. Bakarich, R. Gorkin III, M. in het Panhuis, G. M. Spinks, *ACS Appl. Mater. Interfaces*, 2014, 6, 15998.

150 J. M. Grolman, D. Zhang, A. M. Smith, J. S. Moore, K. A. Kilian, *Adv. Mater.,* 2015, 27, 5512.

151 F. P. Melchels, J. Feijen, D. W. Grijpma, *Biomaterials*, 2010, 31, 6121.

152 M. Singh, H. M. Haverinen, P. Dhagat, G. E. Jabbour, *Adv. Mater*. 2010, 22, 673.

153 Y. Lin, Y. Huang, D. B. Chrisey, *J. Appl. Phys*., 2009, 105, 093111.

154 S. E. Bakarich, M. in het Panhuis, S. Beirne, G. G. Wallace, G. M. Spinks, *J. Mater. Chem. B*, 2013, 1, 4939.

155 V. Mironov, N. Reis, B. Derby, *Tissue Eng*., 2006, 12, 631.

156 Y. J. Choi, T. G. Kim, J. Jeong, H. G. Yi, J. W. Park, W. Hwang, D. Cho, *Adv. Healthcare Mater.,* 2016, 5, 2636.

157 V. K. Lee, D. Y. Kim, H. Ngo, Y. Lee, L. Seo, S. S. Yoo, P. A. Vincent, G. Dai, *Biomaterials*, 2014, 35, 8092.

158 M. S. Mannoor, Z. Jiang, T. James, Y. L. Kong, K. A. Malatesta, W. O. Soboyejo, N. Verma, D. H. Gracias, M. C. McAlpine, *Nano Lett.*, 2013, 6, 2634.

159 L. A. Hockaday, K. H. Kang, N. W. Colangelo, P. Y. C. Cheung, B. Duan, E. Malone, J. Wu, L. N. Girardi, L. J. Bonassar, H. Lipson, C. C. Chu, J. T. Butcher, *Biofabrication*, 2012, 4, 035005.

160 B. Byambaa, N. Annabi, K. Yue, G. Trujillo-de Santiago, M. M. Alvarez, W. Jia, M. Kazemzadeh-Narbat, S. R. Shin, A. Tamayol, A. Khademhosseini, *Adv. Healthcare Mater*., 2017, 6, 1700015.

161 S. V. Murphy, A. Atala, *Nature Biotechnol*., 2014, 32, 773.

162 T. Pan, W. Song, X. Cao, Y. Wang, *J. Mater. Sci. Technol*., 2016, 32, 889.

163 B. Duan, L. A. Hockaday, K. H. Kang, J. T Butcher, *J. Biomed. Mater. Res. Part A*, 2013, 101, 1255.

164 W. Jia, P. S. Gungor-Ozkerim, Y. S. Zhang, K. Yue, K. Zhu, W. Liu, Q. Pi, B. Byambaa, M. R. Dokmeci, S. R. Shin, A. Khademhosseini, *Biomaterials*, 2016, 106, 58.

165 A. A. Bocquier, J. R. Potts, A. R. Pickford, I. D. Campbell, *Structure*, 1999, 7, 1451.

166 N. Sawatjui T. Damrongrungruang, W. Leeanansaksiri, P. Jearanaikoon, S. Hongeng, T. Limpaiboon, *Mater. Sci. Eng. C*, 2015, 52, 90.

167 J. W. Nichol, S. Koshy, H. Bae, C. M. Hwang, S. Yamanlar, A. Khademhosseini, *Biomaterials*, 2010, 31, 5536.

168 T. Billiet, E. Gevaert, T. De Schryver, M. Cornelissen, P. Dubruel, *Biomaterials,* 2014, 35, 49.

169 B. Widner, R. Behr, S. Von Dollen, M. Tang, T. Heu, A. Sloma, D. Sternberg, P. L. DeAngelis, P. H. Weigel, S. Brown, *Appl. Environ. Microbiol.*, 2005, 71, 3747.

170 L. Pescosolido, W. Schuurman, J. Malda, P. Matricardi, F. Alhaique, T. Coviello, P. R. van Weeren, W. J. A. Dhert, W. E. Hennink, T. Vermonden, *Biomacromolecules*, 2011, 12, 1831.

171 C. B. Highley, C. B. Rodell, J. A. Burdick, *Adv. Mater.*, 2015, 27, 5075.

172 L. Ouyang, C. B. Highley, C. B. Rodell, W. Sun, J. A. Burdick, *ACS Biomater. Sci. Eng.*, 2016, 2, 1743.

173 L. Ouyang, C. B. Highley, W. Sun, J. A. Burdick, *Adv. Mater.* 2017, 29, 1604983.

174 M. T. Poldervaart, B. Goversen, M. de Ruijter, A. Abbadessa, F. P. W. Melchels, F. C. Oner, W. J. A. Dhert, T. Vermonden, J. Alblas, *PLoS One*, 2017, 12, e0177628.

175 G. Gao, T. Yonezawa, K. Hubbell, G. Dai, X. Cui, *Biotechnology J.*, 2015, 10, 10, 1568.

176 A. L. Rutz, K. E. Hyland, A. E. Jakus, W. R. Burghardt, R. N. Shah, 2015, *Adv. Mater.*, 27, 1607.

177 G. Gao, A.F. Schilling, K. Hubbell, T. Yonezawa, D. Truong, Y. Hong, G. Dai, X. Cui, *Biotechnol. Lett.*, 2015, 37, 2349.

178 A. Skardal, J. Zhang, G. D. Prestwich, *Biomaterials*, 2010, 31, 6173.

179 W. Wu, A. DeConinck, J. A. Lewis, *Adv. Mater.* 2011, 23, 178.

180 H. W. Kang, S. J. Lee, K. I. Ko, C. Kengla, J. J. Yoo, A. Atala, *Nat. Biotechnol.*, 2016, 34, 312.

181 Y. Loo, A. Lakshmanan, M. Ni, L. L. Toh, S. Wang, C. A. E. Hauser, *Nano Lett.*, 2015, 15, 10, 6919.

182 Q. Wei, M. Xu, C. Liao, Q. Wu, M. Liu, Y. Zhang, C. Wu, L. Chenge, Q. Wang, *Chem. Sci.*, 2016, 7, 2748.

183 C. Echalier, R. Levato, M. A. Mateos-Timoneda, O. Castaño, S. Déjean, X. Garric, C. Pinese, D. Noël, E. Engel, J. Martinez, A. Mehdi, G. Subra, *RSC Adv.*, 2017, 7, 12231.

184 B. Raphael, T. Khalil, V. L. Workman, A. Smith, C. P. Brown, Charles Streuli, A. Saiani, M. Domingos, *Mater. Lett.*, 2017, 190, 103.

185 A. Lakshmanan, C. A. E. Hauser, *Int. J. Mol. Sci.*, 2011, 12, 9, 5736.

186 C. Li, A. Faulkner-Jones, A. R. Dun, J. Jin, P. Chen, Y. Xing, Z. Yang, Z. Li, W. Shu, D. Liu, R. R. Duncan, *Angew. Chem., Int. Ed.*, 2015, 54, 3957.

CHAPTER 2

PHYSICALLY CROSSLINKED STAR POLYPEPTIDE HYDROGELS

This chapter was published in; *RSC Adv.*, 2016, 6, 23370.

Abstract

A range of 8-arm star shaped diblock copolypeptides were developed to investigate their potential as self-assembling amphiphiles in aqueous media. These star shaped block copolypeptides were synthesised by sequential N-carboxyanhydride (NCA) polymerisation from a polypropylene imine (PPI) dendrimer core to comprise a poly(L-lysine) core and poly(L-tyrosine), poly(L-phenylalanine), poly(L-valine) and poly(L-alanine) outer blocks. All star block copolypeptides except the poly(alanine) copolypeptide spontaneously self-assemble into hydrogels at low polymer concentration ≤ 2.0 wt%. Investigation of the secondary structure by FTIR and Circular Dichroism (CD) spectroscopy confirm a largely random coil conformation. The hydrogels were further investigated for their viscoelastic properties revealing a correlation between structural chemistry of pendant side groups and hydrogel strength. The highest gel strength was achieved with the star block copolypeptide consisting of poly(L-phenylalanine) outer blocks. The versatility of the hydrophilic/hydrophobic system allows for a straightforward modification of the hydrophobic shell sequence which can be utilised to modulate the mechanical strength for various applications.

Christina Payne conducted the rheology at RCSI.

Joanne O' Dwyer conducted the injectability assay at RCSI.

Fernando Salles de Oliveira assisted with the SEM imaging at DCU.

2.1 Introduction

Hydrogels are highly versatile materials in biomedical science. Based on their high water content and permeability as well as their structural integrity similar to the extracellular matrix, hydrogels are ideal building blocks in regenerative medicine and as therapeutic delivery systems.[1-4] Continued development of more efficient synthetic methodologies has enabled the design of a class of potentially biocompatible hydrogelators in the form of structurally well-defined oligopeptide amphiphiles.[5] Supramolecular self-assembly of oligopeptide amphiphiles into interconnected hydrogel networks is known to be stabilised via hydrogen bonding and other non-covalent interactions such as electrostatic interactions, π-π stacking and hydrophobic interactions.[6-9]

Polypeptide structures readily obtained by the polymerisation of amino acid N-carboxyanhydrides (NCA) have also been explored for hydrogel formation. For example, Deming presented the design of hydrogels from linear amphiphilic co-polypeptides.[10-13] One such report details the hierarchical self-assembly of these materials composed of a hydrophobic poly(L-leucine) segment grafted to a cationic poly(L-lysine) block. Self-assembly was attributed to the specific peptide secondary conformation, whereby adjacent lysine sequences form long fibrous networks while poly(L-leucine) residues adopt a rigid α-helical arrangement driving spontaneous hydrogel formation in an aqueous environment. Subsequent *in vivo* studies have demonstrated the suitability of these block copolypeptides as potential scaffolds or delivery matrixes in CNS tissue.[14] Our group recently disclosed an NCA-derived PEG2000-Tyr_5 amphiphilic block copolymer that can undergo thermoresponsive hydrogelation at a low concentration range of 0.25-3.0 wt% within a temperature range of 25 to 50°C. [15] While this material displays a desirable inverse thermoresponse (i.e. it hydrogelates upon temperature increase), it is extremely sensitive to structural variation, which limits the scalability and applicability of the material. We hypothesize that a pre-organisation of the polypeptide amphiphiles might overcome these disadvantages while maintaining a low solid content in the hydrogel. Pre-organisation was first utilised by Jeong who reported a series of amphiphilic hybrid PEG block copolymers obtained by ring-opening polymerisation of alanine or phenylalanine NCAs.[16-21] These materials self-assemble into nanostructures

such as micelles in aqueous solutions and further transition into hydrogels at high polymer concentration in the range of 3.0-14 wt% through intermicellar aggregation when the temperature increases. However, the initial step of micelle formation is a dynamic process and strongly dependents on the conditions and concentration of the amphiphiles.

Here we propose amphiphilic star polypeptides as hydrogelators in which the individual amphiphiles are "fixed" to a central core thus providing a covalent core-shell nanoparticle similar to micelles. Star polypeptide synthesis by NCA polymerisation has significantly advanced recently[22-25] and several groups have evaluated these higher order polypeptide structures for the delivery of therapeutics.[26-28] Only few examples of star polypeptide hydrogels have been reported thus far. Li prepared a series of poly(L-diethylene glycol glutamate) (L-EG_2Glu) sequences grafted from 8-arm and 32-arm dendritic molecules.[29] Highly dependent on arm and sequence composition, the star polymers underwent transformation into hydrogel networks at low critical gelation concentration (CGC) ranging from 1-3 wt% The lower CGC threshold could only be observed using the 32-arm polypeptides, which recorded a notably higher polydispersity index (PDI) than the 8-arm analogues. Thornton has also reported the generation of polypeptide hydrogels comprising of a star shaped architecture.[30] Synthesised via the polymerisation of alanine NCA from a 4-armed star shaped poly(ethylene glycol) (PEG) initiator, the hydrogel could form at about 10.0 wt% and was found to be enzymatically degradable.

Herein we present the synthesis of a series of novel star shaped diblock copolypeptide amphiphiles, affording materials which are spontaneously forming hydrogels. The use of the highly branched star architectures allows for superior intermolecular physical interactions between the adjacent hydrophobic moieties when compared with their linear counterparts. Close examination of the conformation via spectroscopic analysis revealed that the gelation of the star macromolecular architecture appears to be governed by the influence of a range of hydrophobic residues, i.e. methyl (L-alanine), isopropyl (L-valine), phenyl (L-phenylalanine) and phenol (L-tyrosine) groups. The disparate chemistry attached to the individual moieties promotes contrasting self-

assembling properties in the series of star polypeptide amphiphiles. This enables a seamless modification of hydrogel strength by alternating the hydrophobic side chain.

2.2 Experimental

2.2.1 Materials

All chemical were obtained from Sigma Aldrich unless other wise noted. ε-carbobenzyloxy-L-lysine, L-phenylalanine, O-benzyl-L-tyrosine, L-alanine and L-valine were purchased from Bachem. Second generation (G2) poly-propylene imine (PPI) dendrimer was obtained from SyMO-Chem BV (The Netherlands). The NCAs of ε-carbobenzyloxy-L-lysine, L-phenylalanine, O-benzyl-L-tyrosine, L-alanine and L-valine were synthesised following literature procedures.[15,32]

2.2.2 Methods

Nuclear Magnetic Resonance (NMR) analysis was completed using a Bruker Avance 400 (400 MHz) spectrometer at room temperature with *d*-DMSO, D_2O, $CDCl_3$ and *d*-TFA as solvents. Attenuated total reflection (ATR) FTIR spectra were recorded using a Perkin-Elmer Spectrum 100 in the region of 4000-650cm^{-1}. Four scans were completed with a resolution of 2 cm^{-1}. A background measurement was performed prior to loading the sample onto the ATR for measurement. Size Exclusion Chromatography (SEC) was performed on an Agilent 1200 system in combination with two PSS GRAM analytical (8 × 300 and 8 × 100, 10 μ) columns, a Wyatt Dawn Heleos 8 multi angle light scattering detector (MALS) and a Wyatt Optilab rEX differential refractive index detector (DRI) with a 658 nm light source. The eluent was DMF containing 0.1 M LiBr at a flow rate of 1 mL min^{-1}. The column temperature was set to 40 °C with the MALS detector at 35 °C and the DRI detector at 40 °C. Molar masses and polydispersities (dispersity, Đ = Mw/Mn) were calculated from the MALS signal by the Astra software (Wyatt) using the refractive index increment (dn/dc) of 0.101 for ply-ε-carbobenzyloxy-L-lysine (PZLL). All GPC samples were prepared using a concentration of 2 mg/mL and were filtered through a 0.45 μm millipore filter, prior to injection. Circular dichroism (CD) spectra were recorded on an Aviv CD Spectrophotometer 410 (Aviv Biomedical, Inc. New Jersey, USA). The star copolypeptides were prepared at a concentration of 0.3 mg mL^{-1} in deionised water. Each

solution was placed into a quartz cell with a path length of 0.1cm and analysed in the UV region (180 to 280 nm). Deionised water was used as a reference for baseline correction before sample measurement. The mean residue ellipticity was calculated using the following equation:

$$[\Theta]_{MRW} / (10 \times l \times c) \quad (1)$$

With experimentally determined (Θ) in mdeg, mean residue weight (MRW) in g/mol, path length (l) in cm and sample concentration (c) in mg/mL. The existence of α-helical conformation can be calculated from the following equation:

$$\% \text{ α-helix} = (-[\Theta_{222}] + 3{,}000)/39{,}000 \quad (2)$$

Where $[\Theta_{222}]$ is the ellipticity measured at 222nm.[31] Rheological measurements were performed on a TA Instruments AR 1000 Rheometer. All measurements were conducted at room temperature using 40 mm diameter cone plane geometry and 4° cone angle. Push-ability testing was performed to evaluate the suitability of hydrogels as injectable candidates. The assay was carried out using a Zwick Roell Z050 mechanical testing machine (Germany) fitted with a 5 N load cell. Samples were gelled in 97% deionised water prior to the assay and injected through a 25G needle. Scanning Electron Microscopy (SEM) was carried out on a Hitachi S3400n Scanning Electron Microscope equipped with a tungsten thermionic emitter. All samples were initially freeze dried and then sputter-coated with gold before imaging. Pore sizes were determined using a fixed scale bar, measuring the width of three equivalent fibres. The mean width was then used. The salt assaying of the materials was conducted in triplicate. Sample sizes used (~20 mg) were incubated at 3.0 wt% in a range of NaCl concentrations until they were visibly transparent. Vials were weighed empty and that weight was used as a reference. The swollen weight of the hydrogels was determined after subtracting the reference. The weight swelling ratio of the star diblock copolypeptide hydrogels was determined using the following equation:

$$Q = (m_s - m_r)/m_r \quad (3)$$

Where m_r is the hydrogel mass in dry state and m_s is the hydrogel mass in the swollen state.

2.2.3 Synthesis of ε-carbobenzyloxy-L-lysine NCA

ε-carbobenzyloxy-L-lysine (10.00 g, 35.7 mmol), α-pinene (12.50 g, 91.7 mmol) and 100 mL ethyl acetate were placed in a three-neck round bottom flask and heated under reflux. Triphosgene (8.30 g, 27.9 mmol) was dissolved in 40 ml ethyl acetate and 2/3 was added drop-wise during the first hour. The remaining solution was added and reflux was maintained until all solids disappeared and the solution became clear (4 h). Distillation was performed to remove 2/3 of ethyl acetate followed by addition of 120ml n-heptane; the solution was then heated to recrystallise. The NCA was recrystallised thrice and subsequently washed with n-heptane to remove any trace impurities. It was dried under vacuum to afford a colourless fluffy solid (yield 85%).

^{1}H NMR: (*d*-DMSO): δ [ppm] = 9.10 (1H, s, -**NH**-COO-CO-), 7.39–7.27 (6H, m, -**C$_6$H$_5$** & -**NH**-CH$_2$), 5.00 (2H, s, -**OCH$_2$**-C$_6$H$_5$), 4.42 (1H, t, -CO-**CH**-CH$_2$-), 2.99 (2H, q, -CH$_2$-NH-), 1.73–1.30 (6H, m, -**CH$_2$**-**CH$_2$**-**CH$_2$**-NH-). *similar procedures were performed for O-benzyl-L-tyrosine (recrystallised thrice), L-phenylalanine (recrystallised twice), L-valine (redissolved and precipitated once and recrystallised once) and L-alanine (redissolved and precipitated once and recrystallised once).

2.2.4 Synthesis of 8-arm diblock copolypeptides

The NCA of ε-carbobenzyloxy-L-lysine (2.37 g, 7.74 mmol) was added to a Schlenk flask. Under a N_2 atmosphere, 35 mL of anhydrous $CHCl_3$ was added until the NCA was dissolved. The flask was placed in a temperature controlled oil/water bath at 0°C. G2 PPI dendrimer (18 mg, 2.42×10^{-2} mmol) was prepared in 2 mL of dry $CHCl_3$, and quickly added to the Schlenk flask via syringe. The solution was allowed to stir for 24 hours at 0°C. FTIR spectroscopic analysis was utilised to confirm total consumption of NCA monomer. A sample was taken directly via syringe to monitor the molecular mass using GPC. The NCA of O-benzyl-L-tyrosine (288 mg, 9.68×10^{-1} mmol) was dissolved in 5 mL anhydrous $CHCl_3$

and charged to the Schlenk flask via syringe. The solution was allowed to stir at 0°C until all of the NCA monomer was consumed as confirmed by FTIR. The polymer was precipitated into excess diethyl ether and dried under vacuum in a dessicator (yield 89%). *****Other star block copolymers were prepared accordingly replacing the O-benzyl-L-tyrosine NCA with L-phenylalanine NCA, L-alanine NCA and L-valine NCA.

2.2.5 Deprotection of 8-arm diblock copolypeptides

1 g of star poly(ε-carbobenzyloxy-L-lysine)-block-poly(O-benzy-L-tyrosine) was dissolved in 11 mL of trifluoroacetic acid (TFA) and allowed to stir for 1 h. 5mL of HBr 33 wt% in acetic acid was added drop wise to the solution in a six-fold excess with respect to ε-carbobenzyloxy-L-lysine and O-benzyl-L-tyrosine and allowed to stir for 15 h. The polymer was precipitated twice into diethyl ether (40 mL) and centrifuged. The TFA/diethyl ether waste was decanted and the precipitate was washed once more with diethyl ether. The polymer was dried under vacuum and then subsequently dissolved in deionised water. Dialysis was performed against deionised water for 4 days using a 3.5kDa MWCO membrane, with frequent water replacement. The polymer was then lyophilised (yield 65%). *Deprotection of the other block copolymers was carried out with a reduced quantity of HBr as PZLL was the only sequence present bearing cleavable protecting groups.

2.3 Results and Discussion

2.3.1 Preparation of star diblock copolypeptides

The general design of the 8-arm star polypeptide hydrogelators comprises a core region of hydrophilic poly(L-lysine) (PLL) blocks extended with hydrophobic oligopeptide blocks. The latter were selected from a range of amino acids capable of exhibiting differed modes of interaction and hydrophobicities to elucidate the structural effect on the hydrogel formation. Elaborating on previous work from our group,[24] an 8-arm primary amine terminated PPI dendrimer was used as an initiator in the ring opening polymerisation of ε-carbobenzyloxy-L-lysine (ZLL or cbz-L-lysine) NCA at a constant PPI to ZLL-NCA ratio of 1:320 (i.e. targeting 40 units per arm) using high vacuum techniques at 0°C.[32]

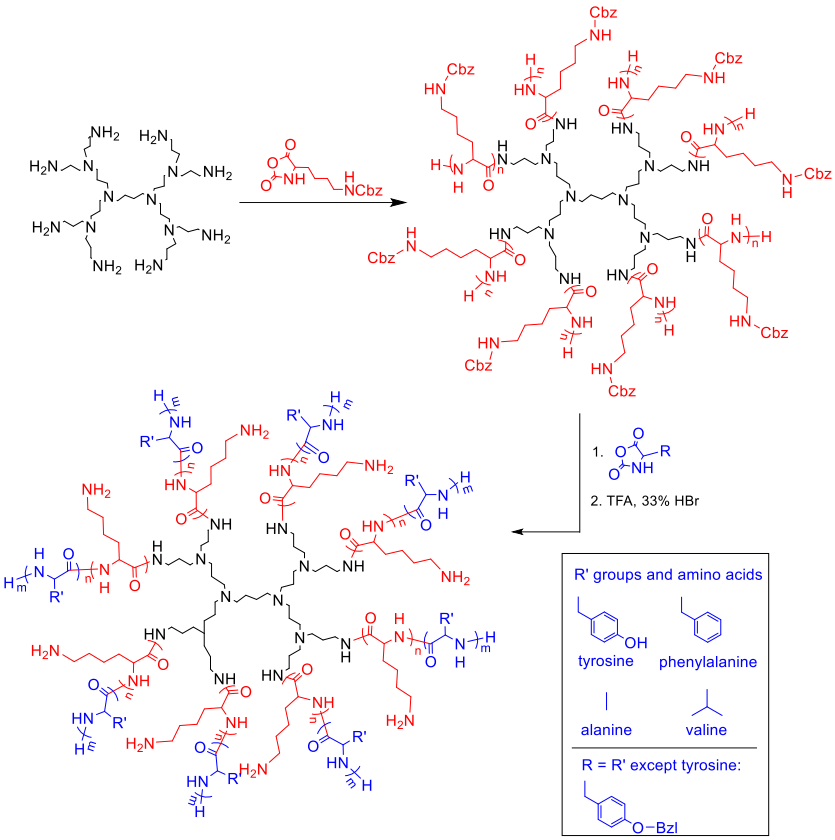

Scheme 2.1: Synthesis of diblock copolypeptides from 8-arm polypropylene imine (PPI) dendrimer core using sequential NCA monomers.

Subsequent macroinitiation of hydrophobic amino acid NCAs of O-benzyl-L-tyrosine (BLT), L-phenylalanine (LPA), L-alanine (LA) and L-valine (LV) was accomplished after full ZLL NCA conversion (confirmed by FTIR by disappearance of NCA anhydride bands) without intermediate work-up targeting an average block length of 5 units per arm (Scheme 2.1, Table 2.1). The choice of amino acids is rationalised by the fact that the poly(LPA) block bearing phenyl functionalities in comparison to the poly(LT)'s phenol moieties.

Table 2.1: Molecular weights and polydispersities of amphiphilic diblock copolypeptides.

Polymer[(a)]	M_n (g/mol) theor.	M_n (g/mol) SEC	*Đ*
8-$PZLL_{40}$	83,800	82,300	1.04
8-$PZLL_{40}$-*b*-$PBLT_5$	94,000	93,400	1.07
8-$PZLL_{40}$	83,800	70,900	1.05
8-$PZLL_{40}$-*b*-$PLPA_5$	89,600	79,400	1.09
8-$PZLL_{40}$	83,800	67,900	1.03
8-$PZLL_{40}$-*b*-PLV_5	87,900	77,500	1.05
8-$PZLL_{40}$	83,800	60,600	1.03
8-$PZLL_{40}$-*b*-PLA_5	86,600	63,600	1.04
1-$PZLL_{32}$	10,400	8,300	1.04
1-$PZLL_{32}$-*b*-$PBLT_5$	11,200	9,500	1.11
1-$PZLL_{148}$[(b)]	83,800	38,700	1.02
1-$PZLL_{148}$-*b*-$PBLT_{30}$	94,000	46,600	1.20

(a) indices denote the theoretical composition (NCA/R-NH_2 ratio). (b) The indices for this sample denote the degree of polymerisation from SEC analysis as full monomer conversion was not achieved. *linear denoted by 1 and star (8-arm) denoted by 8.

Moreover, both poly(LA) and poly(LV) peripheral sequences bear aliphatic methyl and isopropyl groups, respectively, without the possibility of aromatic π-π interaction. Successful grafting of PZLL from the PPI core was confirmed by ^{1}H-NMR spectroscopy (Figure 2.1A, 2.1B). After addition of the second block, size excluison chromatography (SEC) confirmed the anticipated increase in molecular weight for all star diblock copolypeptides (Figure 2.2, Table 2.1, Figure A1-3).

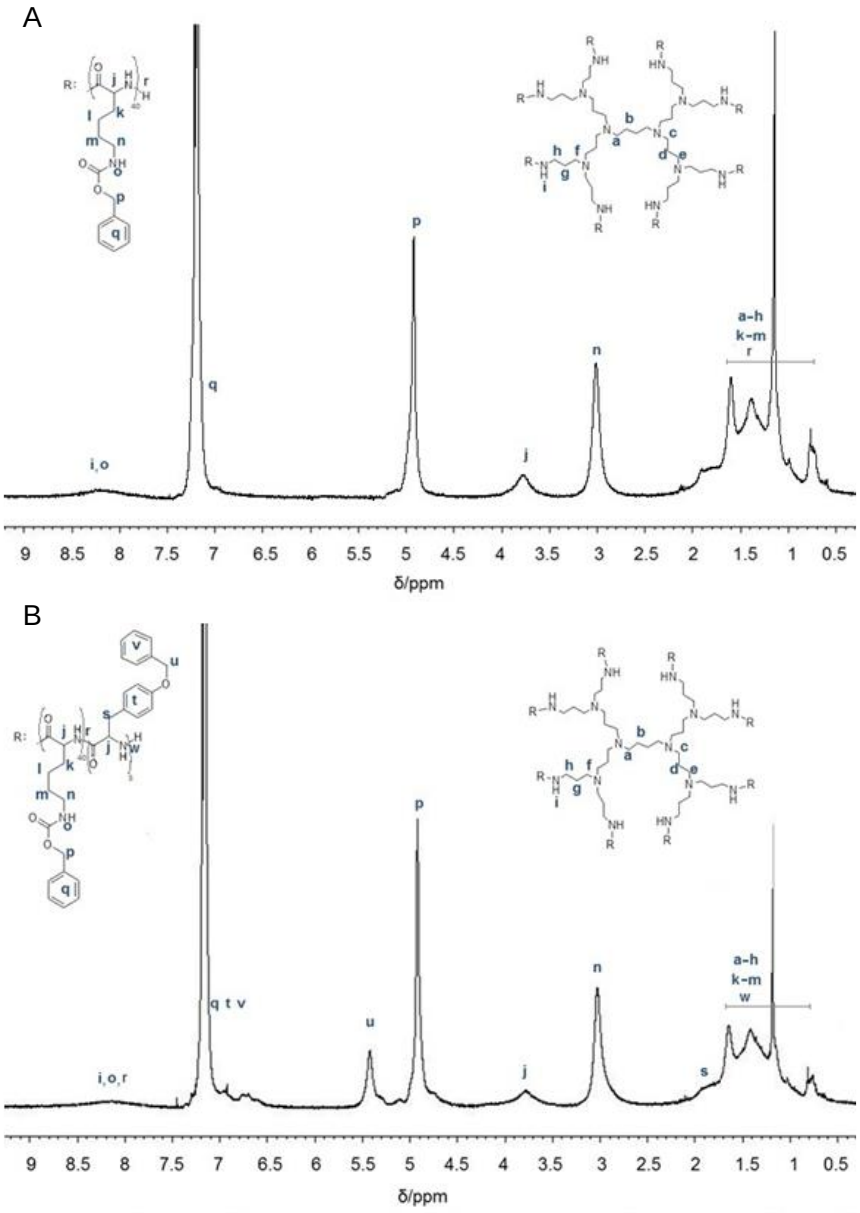

Figure 2.1: [1] H-NMR spectra of (A) 8-PZLL$_{40}$ and (B) 8-PZLL$_{40}$-*b*-PBLT$_5$ in $CDCl_3$.

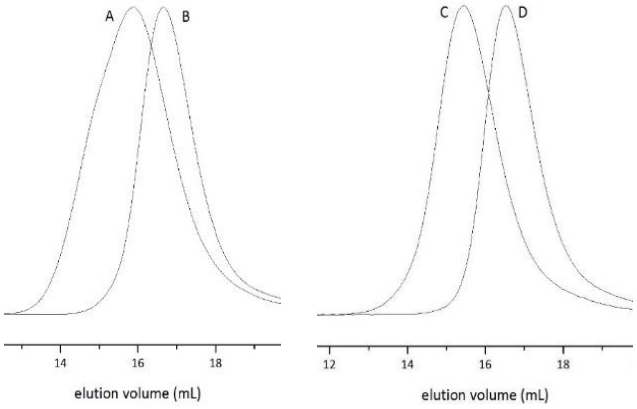

Figure 2.2: SEC traces of A) 8-PZLL$_{40}$-*b*-PLPA$_5$, B) 8-PZLL$_{40}$, C) 8-PZLL$_{40}$-*b*-PLV$_5$ and D) 8-PZLL$_{40}$.

Quantitative deprotection of the PZLL inner block was achieved with TFA and HBr 33 wt% in acetic acid, which in the case of PBLT simultaneously deprotected the tyrosine benzyl ether, which was evident from the quantitative disappearance of the aromatic peak at 7.2 ppm in the ^{1}H-NMR spectra (Figure 2.3) yielding amphiphilic star block copolymers 8-PZLL$_{40}$-*b*-PBLT$_5$, 8-PLL$_{40}$-*b*-PLT$_5$, 8-PLL$_{40}$-*b*-PLV$_5$ and 8-PLL$_{40}$-*b*-PLPA$_5$.

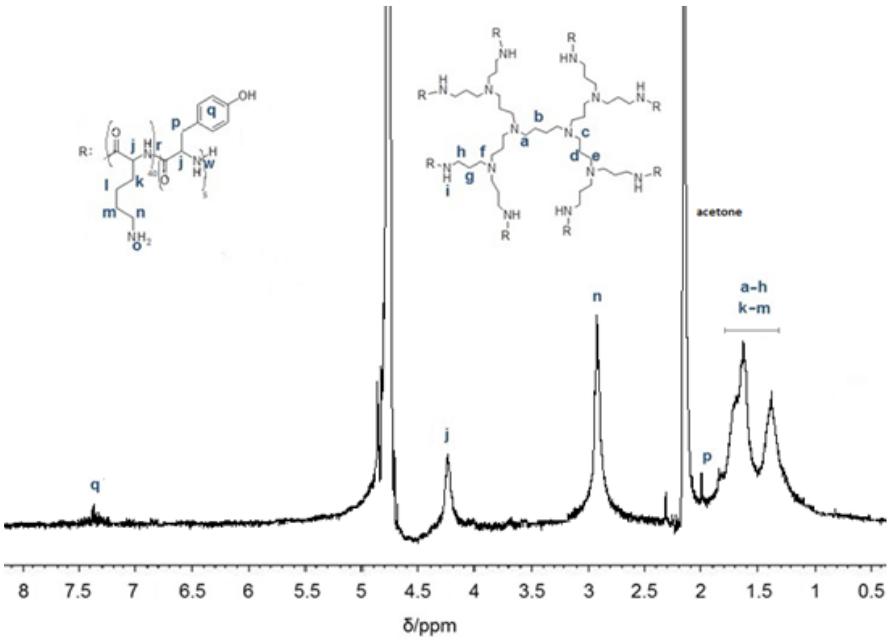

Figure 2.3: ^{1}H-NMR spectra of 8-PLL$_{40}$-*b*-PLT$_5$ in D_2O.

2.3.2 Polypeptide hydrogelation and morphology

The hydrogelation capacity became immediately apparent for each of the library of star copolypeptides. Deprotected 8-arm PLL (8-PLL_{40}) alone did not form hydrogels in water, while the tyrosine extended star block copolymer 8-PLL_{40}-*b*-PLT_5 formed transparent hydrogels at concentrations as low as 2.0 wt%. Both 8-PLL_{40}-*b*-$PLPA_5$ and 8-PLL_{40}-*b*-PLV_5 also spontaneously formed hydrogels in contrast to 8-PLL_{40}-*b*-PLA_5, which did not form hydrogels at any concentration (Figure 2.4). Upon observation, 8-PLL_{40}-*b*-PLT_5 was visibly more transparent than the other samples, which appear slightly opaque. In an attempt to investigate the influence of the star shaped architecture on the hydrogel formation the synthesis of a linear analogue 1-PLL_{320}-*b*-PLT_{40} with exactly the same overall molecular weight and 1-PLL_{40}-*b*-PLT_5 representative of a single arm was attempted. While the latter could be synthesised, limitations of the amine initiation in realizing high molecular weights only permitted the synthesis of a linear equivalent L-$PZLL_{148}$-*b*-$PBLT_{30}$. Notably, neither linear analogue underwent hydrogelation highlighting the importance of the star architecture in this process.

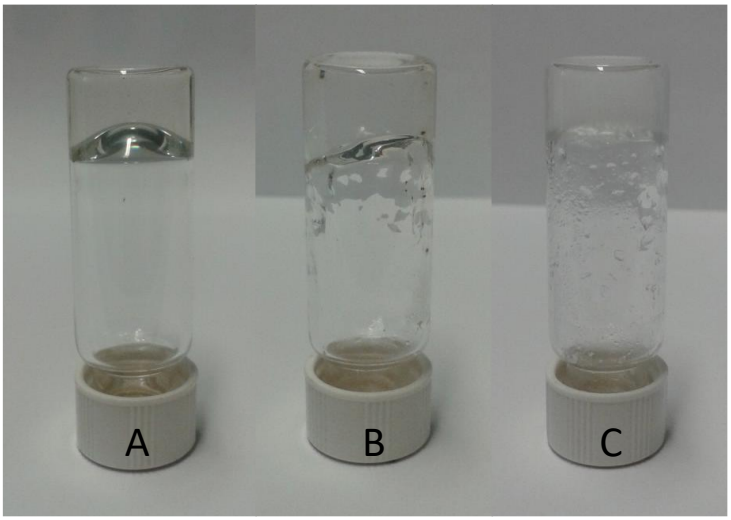

Figure 2.4: Hydrogels obtained from 8-PLL_{40}-*b*-PLT_5 (A), 8-PLL_{40}-*b*-PLV_5 (B) and 8-PLL_{40}-*b*-$PLPA_5$ (C) at a polymer concentration of 3.0 wt%.

In order to elucidate the morphology of the star diblock copolypeptide hydrogels, samples were freeze dried in the gelled state and visualised using Scanning Electron Microscopy (SEM) (Figure 2.5). Condensed fibers are observed in lyophilised 8-PLL_{40}-*b*-PLT_5, revealing a highly porous structure with fibers ~25.7 µm apart. While 8-PLL_{40}-*b*-

$PLPA_5$ exhibits a ribbon-like network with twisting layers developing into a small porous structure characteristic of β-sheet conformation.[33] Observed in 8-PLL_{40}-*b*-PLV_5 is an elongated network with pore sizes as large as 37.3 µm and supermolecular fibers stacking along a single axis.

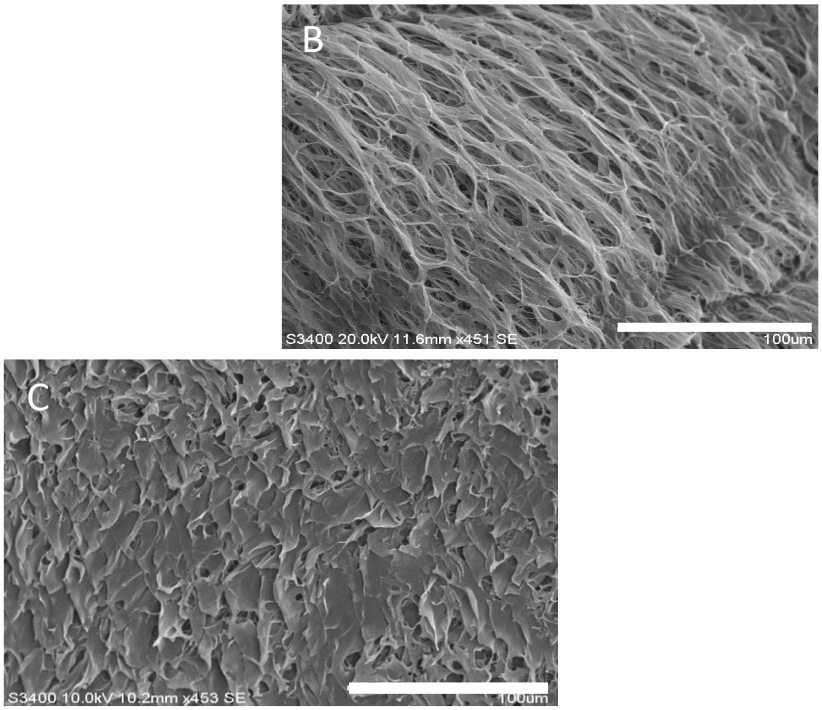

Figure 2.5: SEM images of lyophilised hydrogels obtained from A) 8-PLL_{40}-*b*-PLT_5,B) 8-PLL_{40}-*b*-PLV_5 and C) 8-PLL_{40}-*b*-$PLPA_5$. Scale bar = 100 µm.

2.3.3 Secondary structure analysis

The conformational analysis of each star diblock polypeptide was done using ATR-FTIR in the dry state after lyophilisation and Circular Dichroism (CD) in the gel state. In the dry state all star polypeptides display an intense amide I band around 1647 cm^{-1}, characteristic of a dominant random coil conformation. In addition, small differences in the band structure around the amide I and amide II bands are apparent, which suggests the coexistence of β-motifs (Figure 2.6).

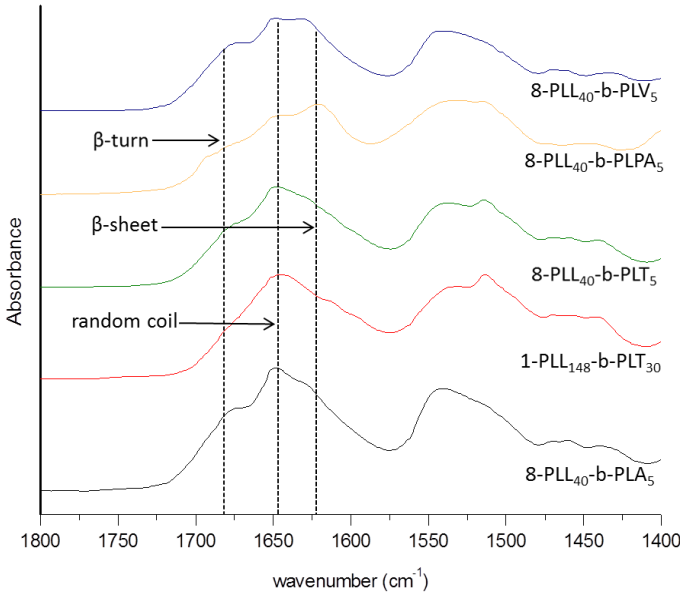

Figure 2.6: FTIR spectra with assigned amide bands.

For example, in the 8-PLL_{40}-*b*-PLT_5 spectrum an additional amide I shoulder peak is visible at 1677cm^{-1}, suggestive of β-turn. The other gel forming polypeptides 8-PLL_{40}-*b*-$PLPA_5$ and 8-PLL_{40}-*b*-PLT_5 also exhibited a split amide I band (1628cm^{-1} and 1648cm^{-1}). The 1648 cm^{-1} C=O vibration can be assigned to random coil structures, while the presence of β-sheets is suggested by the band at 1628 cm^{-1}. Also in this case a shoulder peak at 1674cm^{-1} could be assigned to the presence of β-turn conformation. The co-occurrence of random coil, β-sheet and β-turn configurations seems conceivable considering the complex star shaped polypeptide architecture. Hierarchal stacking of the hydrophobic moieties can occur through intermolecular and intramolecular interactions. Evident β-sheet structures here can be attributed to intermolecular stacking of residues akin to the parallel or twisting patterns.[34,35] The β-turn motif is plausible since oligopeptide sequences may fold 'back on themselves' through hydrogen bonding 3-4 residues apart.[36,37] Both stacking configurations are comparable to patterns observed in micelle formation considering the architecture of the star polypeptide.[38-40] Notably, there is an absence of β-sheet bands in non-hydrogelling 8-PLL_{40}-*b*-PLA_5. Observed are vibrational modes located at 1649 cm^{-1} and 1543 cm^{-1}, representative of a random coil population. In the absence of β-sheet structure no intramolecular network can be formed. The

importance of the coexistence of two conformations for hydrogel formation was highlighted in the literature albeit for linear PLL block copolymers adopting β-sheets and α-helices. [31]

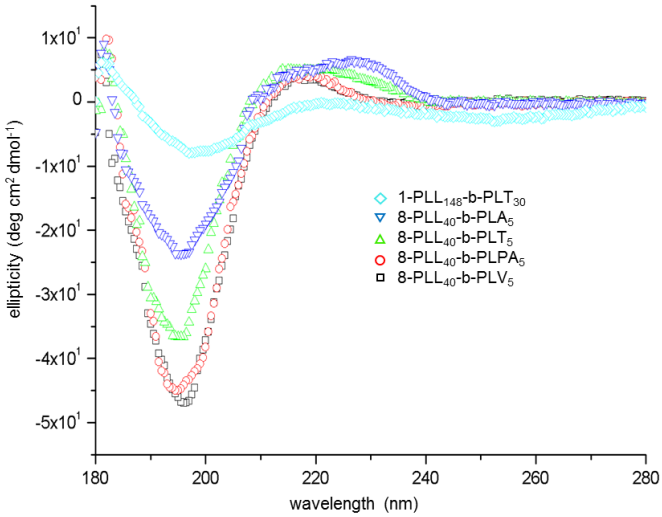

Figure 2.7: Circular dichroism (CD) spectra of amphiphilic block copolymers in water.

CD spectroscopy was utilised to gather information about the asymmetric arrangement of the peptide backbone in the hydrogel state. The CD spectra of all polypeptides are collated in Figure 2.7. All of the star architectures exhibited a broad negative trough below 200 nm and an intense positive peak above 215 nm in agreement with the FTIR results of a random coil configuration. The highest random coil content was observed for 8-PLL_{40}-*b*-PLV_5 and 8-PLL_{40}-*b*-$PLPA_5$. The decreasing band intensity of the 8-PLL_{40}-*b*-PLT_5 minima at 195 nm suggest that the random coil content is affected by the hydroxyl substituent on the phenyl ring. The random coil contribution is further reduced in the non-gelling 8-PLL_{40}-*b*-PLA_5 as well as in the linear reference polypeptide. Notably, the degree of unordered conformation in 8-PLL_{40}-*b*-PLV_5 is sufficient enough to promote hydrogelation. However, the same conformational abundance is deficient in 8-PLL_{40}-*b*-PLA_5, explaining the absence of self-assembly. The CD spectra are devoid of any characteristic β-sheet or β-turn peaks, which would be evident by maxima at ~200nm and ~220 nm and minima at ~206nm.[41] The common feature of coil conformation observed from the spectroscopic analysis indicates that PLL regulates the folding pattern (Figure A4) due to its excess with respect to the hydrophobic sequence.

2.3.4 Hydrogel properties

The extent of gelation of the star shaped polypeptides was determined from comparison of dry and swollen samples. The critical gelation concentration (CGC) was determined from incremental increase in water concentration which was followed by time equilibrated gelation (Table 2.2). The transition from sol to gel for 8-PLL_{40}-*b*-PLT_5 was noted at 2.0 wt% polymer content using the vial inversion method. In contrast 8-PLL_{40}-*b*-$PLPA_5$ still maintained its crosslinked network at a higher water concentration (98.75%). A low MGC was also observed in the 8-PLL_{40}-*b*-PLV_5 sample (1.5 wt%). The degree of swelling of the star block copolypeptides measured with a solid content of 3.0 wt% did not reveal significant differences in the equilibrium weight swelling ratios (~50-55 %; Table 2.2.2).

Table 2.2: Hydrogel swelling and mechanical properties (EGT: equilibrium gelation time; CGC: critical gelation concentration; Q: swelling ratio).

polypeptide	EGT (s)[(a)]	CGC (wt%)	Q[(b)]	G' (Pa)	Injection force (N)
8-PLL_{40}-*b*-PLT_5	1200	2.00	50.76	180.7	5.88
8-PLL_{40}-*b*-$PLPA_5$	600	1.25	55.69	2210.1	7.29
8-PLL_{40}-*b*-PLV_5	350	1.50	49.88	220.5	7.22

(a) time from initial dispersion in aqueous media until complete dissolution with gelation confirmed using the vial inversion method. (b) 3.0 wt% in deionised water*; Q* = (m_s–m_r)/m_r, where m_r is the hydrogel mass in dry state and m_s is the hydrogel mass in the swollen state.

An interesting feature of these materials is their stability in salt solution. For reference, only Deming has previously demonstrated the stability of cationic polypeptide hydrogels in both high and low ionic strength media.[11] Although alternative secondary structural configuration contributes to self-assembly here, the hydrogels exhibit similar properties over a small range of ionic concentrations (Figure 2.8). The swollen gel networks appear unhindered over this range, although a rheological assay may provide a better insight into the true 'masking effect' of NaCl on the PLL electrolyte segments. A reduction in the

degree of swelling is prompted after incubation in saturated 10^{-2} M NaCl solution and was noted in accordance with increasing visual turbidity. Thus, the deterioration of the gel network of all star polypeptide samples became apparent. Media began to separate from the gel and collapse of the network ensued after equilibrium incubation.

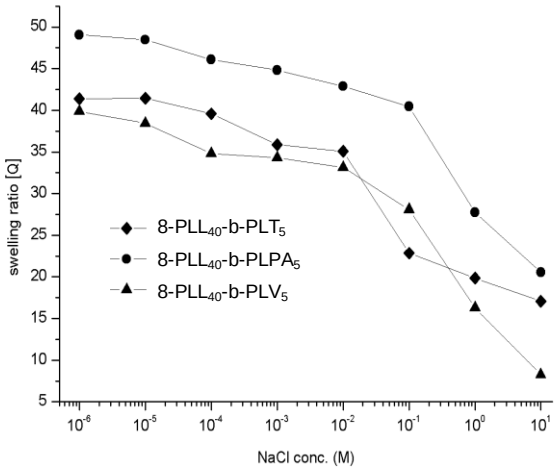

Figure 2.8: Swelling ratio of star diblock copolypeptides (3.0 wt%) as a function of increasing ionic concentration.

The rheological properties of all star block copolypeptides hydrogels were measured at the same polymer concentration (3.0 wt%) in water in order to determine the viscoelasticity of the samples. Initially, the linear viscoelastic regime was assessed by a strain sweep experiment to determine the storage (G') and loss modulus (G'') (Figure 2.9). The 8-PLL_{40}-*b*-PLT_5 hydrogel exhibited a storage modulus of 168 Pa, which was found to be the weakest polypeptide hydrogel. Altering the chemistry of the side group by removing the hydroxyl group had a significant effect on the mechanical properties. To illustrate the sizeable gap in gel strength, the storage modulus increased to 2040 Pa for 8-PLL_{40}-*b*-$PLPA_5$ hydrogel. The difference of ~1870 Pa between its L-tyrosine analogue illustrates the highly sensitive nature of physical crosslinking sites within these star shaped hydrogel networks.

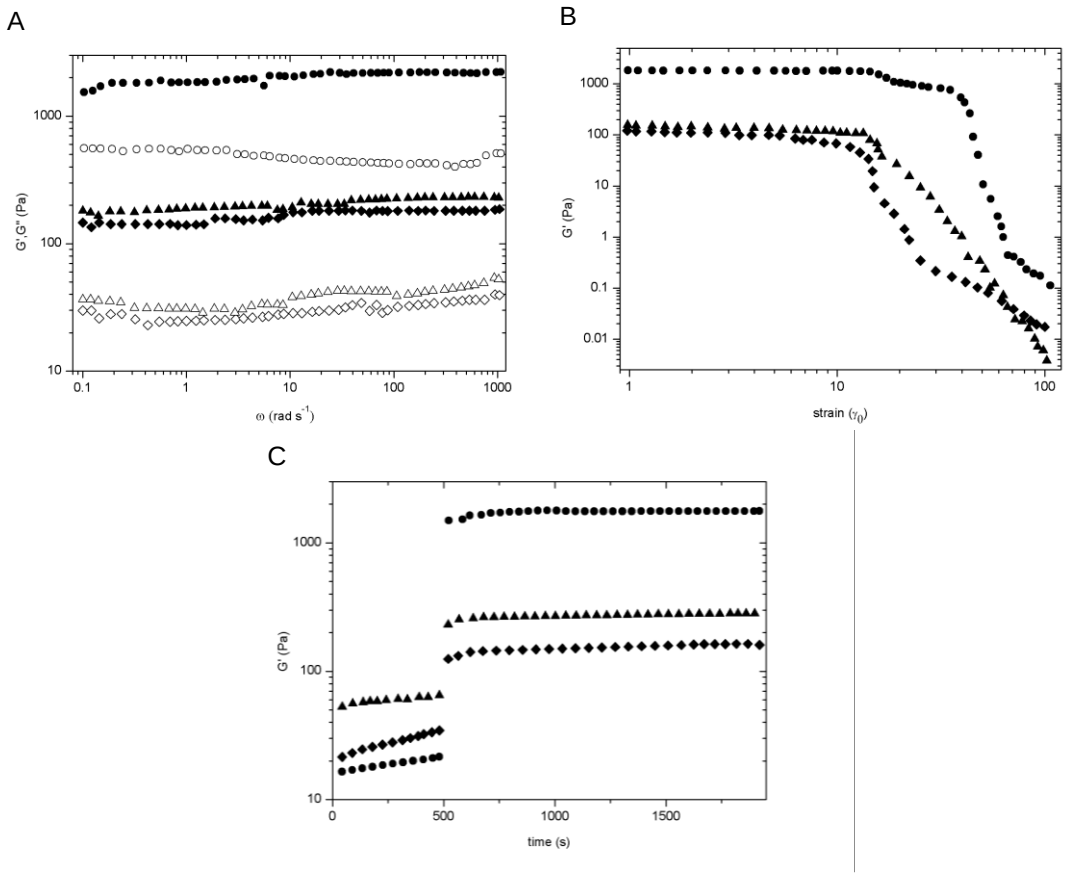

Figure 2.9: Rheological properties of star diblock copolypeptides, 8-PLL_{40}-*b*-$PLPA_5$ (●), 8-PLL_{40}-*b*-PLV_5 (▲), 8-PLL_{40}-*b*-PLT_5 (◆). Frequency sweep (A) of hydrogels over linear frequency (sheared at γ = 0.1, ω = 1-1000 rad s^{-1}); closed symbols - storage modulus; open symbols - loss modulus. Amplitude sweep (B) of hydrogels over increasing strain (sheared at γ = 1-100, ω = 1 rad s^{-1}). Strain based recovery (C) of hydrogels (sheared at γ = 1, ω = 6 rad s^{-1} for 8 mins before switching to γ = 0.1, ω = 6 rad s^{-1} for 24 mins).

It could be hypothesised that incorporation of the hydroxyl group provides a partially solubilising functionality via the acidic proton, which would allow water to penetrate. The relationship between storage modulus and strain is depicted in Figure 2.9B. Upon incremental increase in the strain amplitude (γ = 1 Ð 00), shear thinning of each of the hydrogels samples became apparent. However, all star diblock copolypeptide hydrogels demonstrated rapid recovery properties after application of a large strain (Figure 10C). Initially, the gel structure was broken down under large oscillatory amplitude (γ = 1). The storage modulus *G'* of both 8-PLL_{40}-*b*-PLT_5 and 8-PLL_{40}-*b*-PLV_5 underwent a reduction just over one order of magnitude while the *G'* of 8-PLL_{40}-*b*-$PLPA_5$ dropped by two orders of

magnitude. After a return to a lower amplitude strain (γ = 0.1) all polypeptide hydrogels recovered to their original gel strength within 5-20 seconds. In particular, 8-PLL_{40}-*b*-$PLPA_5$ underwent network re-assembly almost instantaneously. These properties validate the hydrogels as suitable candidates for applications through a syringe/needle. Indeed, when the gels were loaded into a syringe only a moderate force of 5.9-7.3 N was required to push them though the attached needle and subsequently recover their gel state. (Table 2.2). The force applied is acceptable when considering compression forces up to 10 N were required for therapeutic pramlintide injections, albeit with slightly smaller needles (29G and 31G).[42] The data implies an advantageous feature of these materials, which is that hydrogel strength can be easily modulated for application purposes. The comparative storage and loss moduli of both 8-PLL_{40}-*b*-PLT_5 and 8-PLL_{40}-*b*-PLV_5 hydrogels would be suitable for a drug delivery matrix.[43] The high strength associated with the 8-PLL_{40}-*b*-$PLPA_5$ hydrogel (3.0 wt%, 2.2kPa) regards it compatible in applications ranging from wound healing scaffolds to vascular tissue scaffolds.[44,45] The polymer 8-PLL_{40}-*b*-$PLPA_5$ demonstrated superiority in physical crosslinking due to the densely packed aromatic residues. It can be concluded that the inclusion of a hydroxyl substituent on the aromatic ring or the replacement with an aliphatic residue proved to be detrimental to hydrogel strength as the storage modulus decreased almost tenfold in each case.

2.4 Conclusions

A series of star shaped amphiphilic diblock copolypeptides with a poly(L-lysine) core and alternating hydrophobic outer peptide blocks were prepared from the 8-arm PPI dendrimer mediated ring opening polymerisation of amino acid NCA monomers. Spontaneous aqueous self-assembly was observed for copolymers composed of L-tyrosine, L-phenylalanine and L-valine outer blocks but was absent in those with L-alanine outer blocks or linear polymers modelling a single star copolypeptide arm. Sol-gel transitions were observed at particularly lower polymer concentration (1.25 wt%) for star copolymers containing the phenyl functionality. This presence of this moiety also appears to contribute to a stronger gel network as seen in the rheological measurements. The unique self-assembly associated with amphiphilic star polypeptides

afforded hydrogel materials with multiple properties. They maintain structure with high water content, can be injected with minimal force and are potentially enzymatically degradable, and such may be utilised for various applications.

2.5 References

1 T. Vermonden, R. Censi, W. E. Hennink, *Chem. Rev.*, **2012**, 112, 2853.

2 A. Altunbas, D. J. Pochan, *Top Curr. Chem.,* **2012**, 310, 135.

3 N. A. Peppas, J. Z. Hilt, A. Khademhosseini, R. Langer, *Adv. Mater.,* **2006**, 18, 1345.

4 Y. Li, J. Rodrigues, H. Tomás, *Chem. Soc. Rev.,* **2012**, 41, 2193.

5 M. C. Branco, J. P. Schneider, *Acta Biomater.,* **2009**, **5**, 817.

6 D. J. Adams, P. D. Topham, *Soft Matter,* **2010**, 6, 3707.

7 J. B. Matson, S. I. Stupp, *Chem. Commun.,* **2012**, 48, 26.

8 F. J. Hoeben, P. Jonkheijm, E. W. Meijer, A. P. Schenning, *Chem. Rev.*, **2005**, 105, 1491.

9 D. J. Adams, *Macromol. Biosci*., **2011**, 11, 160.

10 A. P. Nowak, V. Breedveld, L. Pakstis, B. Ozbas, D. J. Pine, D. Pochan, T. J. Deming, *Nature*, **2002**, 417, 424.

11 A. P. Nowak, V. Breedveld, D. J. Pine, T. J. Deming, *J. Am. Chem. Soc.,* **2003**, 125, 15666.

12 A. P. Nowak, V. Breedveld, T. J. Deming, *Supramol. Chem.*, **2006**, 18, 423.

13 Z. Li, T. J. Deming, *Soft Matter*, **2010**, 6, 2546.

14 C. Y. Yang, B. Song, Y. Ao, A. P. Nowak, R. B. Abelowitz, R. A. Korsak, L. A. Havton, T. J. Deming, M. V. Sofroniew, *Biomaterials*, **2009**, 30, 2881.

15 J. Huang, C. L. Hastings, G. P. Duffy, H. M. Kelly, J. Raeburn, D. J. Adams, A. Heise, *Biomacromolecules*, **2013**, 14, 200.

16 Y. Y. Choi, J. H. Jang, M. H. Park, B. G. Choi, B. Chi, B. Jeong, *J. Mater. Chem.,* **2010**, 20, 3416.

17 H. J. Oh, M. K. Joo, Y. S. Sohn, B. Jeong, *Macromolecules,* 2008, **41**, 8204.

18 Y. Jeong, M. K. Joo, K. H. Bahk, Y. Y. Choi, H. T. Kim, W. K. Kim, H. J. Lee, Y. S. Sohn, B. Jeong, *J. Control. Release,* **2009**, 137, 25.

19 E. Y. Kang, B. Yeon, H. J. Moon, B Jeong, *Macromolecules,* **2012**, 45, 2007.

20 U. P. Shinde, M. K. Joo, H. J. Moon, B. Jeong, *J. Mater. Chem.,* **2012**, 22, 6072.

21 M. H. Park, M. K. Joo, B. G. Choi, B. Jeong, *Acc. Chem. Res.,* **2012**, 45, 423.

22 A. Sulistio, A. Blencowe, A. Widjaya, X. Zhang, G. Qiao, *Polym. Chem.*, **2012**, 3, 224.

23 S. Junnila, N. Houbenov, S. Hanski, H. Iatrou, A. Hirao, N. Hadjichristidis, O. Ikkala, *Macromolecules.*, 2010, 43, 9071.

24 M. Byrne, D. Victory, A. Hibbitts, M. Lanigan, A. Heise, S. A. Cryan, *Biomater. Sci.*, 2013, 1, 1223.

25 S. Abraham, C. S. Ha, I. Kim, *J. Polym. Sci. Part A: Polym. Chem.*, 2006, 44, 2774.

26 K. Wang, H. Q. Dong, H. Y. Wen, M. Xu, C. Li, Y. Y. Li, H. N. Jones, D. L. Shi, X. Z. Zhang, *Macromol. Biosci.*, 2011, 11, 65.

27 M. Byrne, P. D. Thornton, S. A. Cryan, A. Heise, *Polym. Chem.*, 2012, 3, 2825.

28 H. M. Wu, S. R. Pan, M. W. Chen, Y. Wub, C. Wang, Y. T. Wen, X. Zeng, C. B. Wu, *Biomaterials*, 2011, 32, 1619.

29 Y. Shen, S. Zhang, Y. Wan, W. Fu, Z. Li, *Soft Matter,* 2015, 15, 2945.

30 P. D. Thornton, S. M. Reduwan Billah, N. R. Cameron, *Macromol. Rapid Commun.,* 2013, 34, 257.

31 T. J. Deming , *Soft Matter*, 2005, 1, 28.

32 G. J. Habraken, M. Peeters, C. H. Dietz, C. E. Koning, A. Heise, *Polym. Chem.*, 2010, 1, 514.

33 M. A. Poirier, H. Jiang, C. A. Ross, *Hum. Mol. Genet.,* 2005, 14, 765.

34 E. G. Bellomo, M. D. Wyrsta, L. Pakstis, D. J. Pochan, T. J. Deming, *Nature Materials*, 2004, 3, 244.

35 V. Moretto, M. Crisma, G. M. Bonora, C. Toniolo, *Macromolecules*, 1989, 22, 2939.

36 K. Rajagopal, B. Ozbas, D. J. Pochan J. P. Schneider, *Eur. Biophys. J.*, 2006, 35, 162.

37 E. G. Hutchinson, J. M. Thornton, *Protein Sci.,* 1994, 3, 2207.

38 S. E. Paramonov, H. W. Jun, J. D. Hartgerink, *J. Am. Chem. Soc.*, 2006, 128, 7291.

39 S. Mann, *Nat. Mater.*, 2009, 8, 781.

40 J. D. Hartgerink, E. Beniash, S. I. Stupp, *Science,* 2001, 294, 1684.

41 M. W. Werten, A. P. Moers, T. Vong, H. Zuilhof, J. C. van Hest, F. A. de Wolff, *Biomacromolecules*, 2008, 9, 1705.

42 D. Merritt, B. Schreiner, S. Harris, M. B. DeYoung, S. Strobel, J. Lauinger, *J. Diabetes Sci. Technol.*, 2010, 4, 1438.

43 F. Rehfeldt, A.J. Engler, A. Eckhardt, F. Ahmed, D. E. Discher, *Adv. Drug Deliv. Rev.*, 2007, 59, 1329.

44 A. Song, A. A. Rane, K. L. Christman, *Biomaterials*, 2007, 28, 567.

45 A. C. Jiminez-Vergara, V. Guiza-Arguello, S. Becerra-Bayona, D. J. Munoz-Pinto, R E. McMahon, A. Morales, L. Cubero-Ponce, M. S. Hahn, *Annals of Biomed. Engineer.*, 2010, 38, 2885.

CHAPTER 3

DISULPHIDE CROSSLINKED COPOLYPEPTIDE HYDROGELS

This chapter was published in; *Polym. Chem*., **2018**, 9, 3908.

Abstract

A series of 32- and 64-arm star shaped diblock copolypeptides containing opposite block sequences of oligo(cysteine) and poly(lysine) resulting in hydrogels comprising core and shell mediated disulfide crosslinking. Spontaneous gelation was observed within minutes of aqueous immersion, without any necessary pretreatment at concentrations as low as 0.05 wt%. The secondary structure underwent a change in agreement with the gel-sol transition as evidenced by a combination of FTIR and CD spectroscopy. Changing the sequence on the 32-arm from core crosslinking to shell crosslinking had a significant effect on hydrogel storage modulus as it changed from 820 Pa to 4530 Pa. Notably, changing the polypeptide block sequence order had a direct effect on mechanical properties (including self-recovery behaviour). While the core crosslinked hydrogel underwent shear induced recovery almost instantaneously after passing through a standard syringe needle, the shell crosslinked hydrogel expelled water when subject to the same shear. The responsiveness of the molecular system to redox stimuli provides further desirable attributes that could allow for controlled, targeted delivery of therapeutic payloads.

3.1 Introduction

Polymeric hydrogels, which are a class of gelating materials comprised of a three-dimensional (3-D) crosslinked network, have received considerable attention in recent times for their applicability in biomedical science. Of particular interest is their use as drug/gene delivery systems and vectors, tissue engineering scaffolds or bio-devices such as sensors.[1] Hydrogels have been prepared from a variety of biocompatible natural and synthetic polymers including polysaccharides and vinyl polymers.[2,3] In synthetic polymers, pre- and post polymerisation modifications can be readily achieved allowing for inclusion of functional groups that can facilitate gelation. Hydrogels produced can exhibit self-recovering, self-healing or shear thinning behaviour.[4-6]

Polypeptides represent excellent candidates for hydrogelating materials as they possess a number of desirable properties. They bear a variety of different side chain functionalities, can orientate into ordered conformations stabilising their structures and can also hydrolyse in the presence of enzymes similar to protein degradation.[7,8] Hydrogel networks prepared from biomimetic polypeptides also display similar physicochemical properties to those compositions found in the extracellular matrix (ECM).[9] Ordered conformation of parallel peptide strands results in self-assembly through secondary interactions such as α-helical or β-sheet assemblies,[10,11] akin to that of native proteins.[12] As a result, much recent literature surrounds the use of synthetic polypeptides as hydrogelators due to their likeness to biomolecules.[13-15]

The facile nature of the N-carboxyanhydride (NCA) ring opening polymerisation (ROP) for polypeptide production as well as the use of orthogonal chemistries has helped to develop versatile fabrication system in order to design advanced structures.[16-19] The versatility of the synthesis allows for development of hybrid polypeptide hydrogel systems which can be tailor-made to realise biomedical applications.[20,21] The crosslinks necessary for network formation are induced by independent hydrophobic physical or chemical interactions linked to a water soluble domain.[22] Chain aggregation can occur through micellar or fibril assembly due to adjacent crosslinks arising from α-helical and β-sheet conformations, resulting in alternative self-assembly patterns.[23,24]

In hydrogel design, the incorporation of molecular crosslinks and/or polymer backbones that are hydrolytically labile is beneficial for degradation. Polypeptides represent an ideal platform for such owing to the cleavable functionalities in their structure. Enzymolysis is an additional trigger for peptide bond decomposition that has been widely utilised. Hydrogels based on polypeptides can also undergo morphological adjustments in the form of sol-gel/gel-sol transitions or network shrinking. The materialisation of such is a direct result of changes in pH,[25] temperature,[26,27] chemical environment[28,29] or light.[30,31] Among synthetic polypeptides with stimuli triggered assemblies, there is a great deal of interest into responsiveness via redox mechanisms due to the nature of the cell. The tripeptide, glutathione (GSH), is the most abundant non-protein based thiol present in the intracellular environment. Its main role within the cell is to regulate the redox process through the generation of a highly reducing medium for biomolecules, preventing molecular oxidation.[32] Particularly interesting sites of action for GSH are residues consisting of disulphide linkages, which readily undergo cleavage in its presence.[33] This has generated much interest due to the straightforward nature of disulphide formation in thiol containing macromolecules.[34] Thus, many research groups have explored the use of these covalent bonds as active groups in their polymeric architecture for responsiveness.[35,36] A number of researchers have described the inclusion of oligo or poly-L-cysteine sequences in their synthetic polypeptides due to the spontaneous thiol-disulphide conversion.[37-39] The preparation of polypeptide based hydrogels have also been explored through the integration of disulphide forming residues.[40,41]

There are very few studies on the design and development of hydrogel systems based on star shaped polypeptides.[42,43] We have recently reported the design of a series of hydrogelating scaffolds from star block copolypeptides tethered to an 8-arm dendritic core.[44] The degree of polymerisation was identical for both the hydrophilic inner blocks (poly-L-lysine) and the hydrophobic outer blocks (poly-L-tyrosine, poly-L-phenylalanine, poly-L-valine). Contrasting chemical character of the side chain functionalities (phenol, phenyl, isopropyl) allowed for modulation of the rheological and gelation properties, which proved to be sensitive to the composition of the shell sequence. All hydrogels

exhibited shear thinning properties and could be injected with acceptable force with gelation concentrations ranging from 1.25 to 2.0 wt% and storage moduli from 180 to 2210 Pa. Superior mechanical properties are associated with hydrogels prepared from these star shaped architectures in comparison to linear polypeptides. Using the same principles, we have also used supramolecular star diblock copolypeptide hydrogels as bio-inspired inks in the development of constructs via 3D extrusion printing.[45] Based on short glutamic acid and valine chains tethered to a 32-arm dendrimer with a UV curable functionalities, the 3D hydrogel scaffolds produced could load molecular cargo, were hydrolytically degradable and showed non-cytotoxicity toward 3T3 fibroblasts. Moreover, both non-gelating and gelating stars display a more efficient loading capacity and improved delivery properties compared to conventional linear polypeptides.[46-48]

Inspired by previous reports on the influence of block sequence in linear block copolypeptides on their properties,[49,50] we present the synthesis of a series of star shaped diblock copolypeptide hydrogels possessing differing properties based on covalent interactions between disulphide bridges within the core and the shell of the star architecture. Changing sequence order from core disulphide to shell disulphide results in a transition from shear thickening to shear-thinning/self-recovering hydrogels. The materials were readily prepared via the sequential ring opening polymerisation (ROP) of N-carboxyanhydride (NCA) monomers benzyl-L-cysteine (BLC) and ε-carbobenzyloxy-L-lysine (ZLL) with two highly branched poly propylene imine (PPI) dendritic initiators. The characteristics, including the conformational and mechanical character, of each polypeptide hydrogel were studied. Results and evaluation of the secondary structure, rheological properties and reduction triggered drug release via dithiothreitol (DTT) are all outlined in order to demonstrate their suitability as biomedical hydrogels.

3.2 Experimental

3.2.1 Materials

All chemicals were obtained from Sigma-Aldrich unless otherwise stated. ε-Carbobenzyloxy-L-lysine and benzyl-L-cysteine were purchased from Novachem. Genration 4 (G4) and generation 5 (G5) poly-propylene imine (PPI) dendrimers were

obtained from SyMO-Chem BV. The NCAs of ε-carbobenzyloxy-L-lysine (ZLL) and benzyl-L-cysteine (BLC) were synthesised following literature procedures.[51]

3.2.2 Methods

^{1}H-NMR spectra were recorded on a Bruker Advance 400 (400 MHz) spectrometer at room temperature (21 °C) with trifluoroacetic acid-d (TFA-d) as a solvent. Attenuated total reflection (ATR) FTIR was recorded using a Thermo Scientific iS10 spectrometer in the region of 4000–400 cm^{-1}. A background measurement was initially performed before analysing the sample. Sixteen scans were completed using a resolution of 2 cm^{-1}. Circular dichroism spectra were acquired using a Jasco J-810 spectropolarimeter in the UV region (180 to 280 nm). The polypeptides were analysed at a concentration of 0.01 mg mL^{-1} (deionised water) in a quartz cell with a path length of 0.1 cm. Baseline correction was achieved by using deionised water as a reference before sample measurement. The scans were recorded at a speed of 20 nm min^{-1} with a data pitch of 0.1 nm. The sensitivity was set to 10 mdeg with a response time of 3 sec and a bandwidth of 1 nm. The mean residue ellipticity was calculated using the following equation:

$$[\Theta]_{MRW} \ / \ (10 \times l \times c) \qquad (1)$$

with experimentally determined (Θ) in mdeg, mean residue weight (MRW) in g mol^{-1}, path length (l) in cm and sample concentration (c) in mg mL^{-1}. The molecular weight and molecular weight distributions (dispersity, Đ = Mw/Mn) were determined by Size Exclusion Chromatography (SEC). Monodisperse polystyrene standards were used to generate a standard calibration curve. SEC measurements were carried out on a Waters 515 equipped with a Wyatt DAWN HELEOS-II (laser 658.0 nm) laser light scattering detector and a Wyatt Optilab rEX detector. The eluent was THF with a flow rate of 1 mL min^{-1}. The column temperature was set to 40 °C and the refractive index detector at 40 °C.

Imaging and Mechanical Analysis

Scanning Electron Microscopy (SEM) was carried out on a JEOL JSM 6490LV SEM with an excitation voltage of 15 kV. The sample was gelled at 3.0 wt% and then frozen in small spherical moulds prior to imaging. Rheological measurements were performed on an Anton Paar Physica MCR 301 digital rheometer. All experiments were conducted at room temperature (21 °C) using a conical plate consisting of a 50 mm diameter geometry and a 1° cone angle with a gap length of 0.097 mm. The use of a temperature-controlled hood was employed to prevent evaporation of water from the hydrogels. The weight swelling ratio (Q) of the hydrogel samples was determined using the following equation:

$$Q = (m_s - m_r)/m_r \quad (2)$$

Where m_r is the hydrogel mass in dry state and m_s is the hydrogel mass in the swollen state.

Drug Release

DOX.HCl was prepared as a 1 mg mL^{-1} solution in deionised water. The hydrogel/drug depot was prepared resuspending the lyophilised polypeptides using the DOX.HCl solution (1 mg mL^{-1}) at a polypeptide concentration of 3.0 wt%. The samples were stirred overnight and allowed to sit for two days before analysis. The drug loaded hydrogel samples were dialysed (12-14kDa MWCO) against 50 mL of PBS (pH 7.5, room temperature), with the addition of 10 mM DTT to the media for the reduction assay, to determine drug release over time. Aliquots of the dialysate were assayed for DOX.HCl content at specific time intervals using a UV/vis spectrometer at 490 nm. Quantification was determined using a calibration curve and samples were then returned to the media.

3.2.3 Synthesis of 64-arm oligo(L-cysteine)-b-poly(L-lysine)

The NCA of benzyl-L-cysteine (176.36 mg, 7.43×10^{-1} mmol) was dissolved in anhydrous $CHCl_3$ (6 mL) under a N_2 atmosphere. The flask was placed in a thermostatically controlled water bath containing 5M NaCl at 0°C. The 64-arm G5 PPI dendrimer (16.65 mg, 2.32×10^{-3} mmol) was solubilised in 4 mL of dry $CHCl_3$, and quickly added to the Schlenk flask. The flask was evacuated under vacuum to remove the CO_2 generated and

stirring was allowed for 20 hours at 0°C. FTIR was used to confirm total consumption of the BLC NCA monomer. The NCA of ε-carbobenzyloxy-L-lysine (1.82 g, 5.95 mmol) was dissolved in 15 mL anhydrous $CHCl_3$ and charged to the Schlenk flask. The solution was allowed to stir at 0°C until full conversion of the ZLL NCA monomer was confirmed by FTIR. The polymer was precipitated into excess diethyl ether and dried under vacuum in a desiccator to give the 64-PLC_5-b-PLL_{40} star polymer (yield 82 %). Subsequently, the dried polymer (1.1 g) was dissolved in 15 mL trifluoroacetic acid and allowed to stir until fully dissolved. Then, 6 mL of HBr (33 wt% in acetic acid) was added drop wise to the solution in a six-fold molar excess with respect to ε-carbobenzyloxy-L-lysine and benzyl-L-cysteine protecting groups and stirring continued for 16 hours. The polymer was precipitated twice into diethyl ether (40 mL) and centrifuged. The TFA/HBr/diethyl ether waste was decanted and the precipitate was washed once more with diethyl ether. The material was dried under vacuum and then subsequently dissolved in deionised water. Dialysis was performed against deionised water for 4 days using a 12-14 kDa MWCO membrane, with frequent water replacement. The polymer was then lyophilised (yield 60%). *The other diblock copolypeptides were prepared accordingly replacing the 64-arm G5 PPI dendrimer initiator with the 32-arm G4 PPI dendrimer while propargylamine was used for the linear copolymer. For the homopolypeptide ZLL NCA was used.

3.3 Results and Discussion

3.3.1 Preparation of disulphide star copolypeptides

The 32-arm star diblock copolypeptides with alternating sequences of oligo(benzyl-L-cysteine)-b-poly(Z-L-lysine) were synthesised via the ROP of corresponding NCA amino acid monomers using a G4 poly(propylene imine) (PPI) dendrimer initiator. Alternating between the amino acid monomer addition allowed for core tethered sequences using BLC NCA followed by peripheral polymerisation of ZLL NCA or vice versa, maintaining a ratio of 5 cysteine to 40 lysine per arm (Scheme 3.1). FTIR spectroscopy confirmed the consumption of the first NCA monomer, after which the second monomer was added.

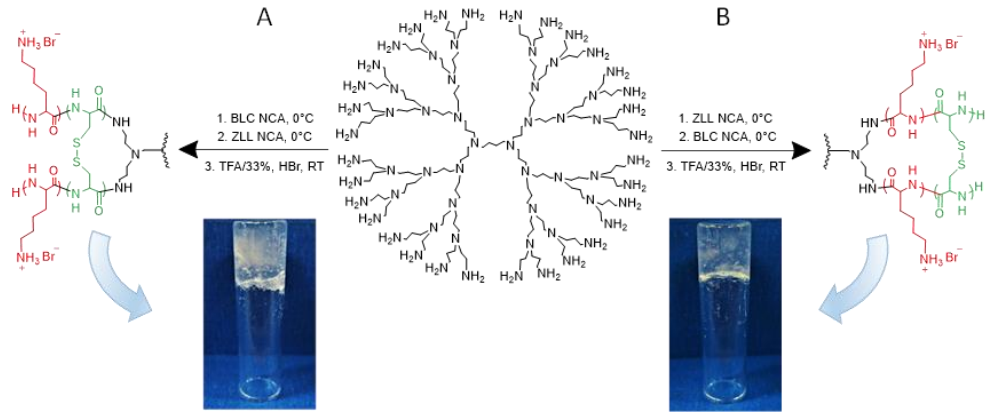

Scheme 3.1: A) Synthetic route for 32-OLC_5-b-PLL_{40} with an image of its subsequent aqueous gelation and B) Synthetic route of 32-PLL_{40}-b-OLC_5 with an image of its subsequent aqueous gelation. *two neighbouring arms denoted in each of the final chemical structures

Subsequent macroinitiation of the second monomer was achieved through the terminal amine in order to propagate the polypeptide shell sequence. ^{1}H-NMR was used to confirm the successful growth of the polypeptide chains from the terminal amine on the dendrimer and from the terminal amine first block (Figure 3.1).

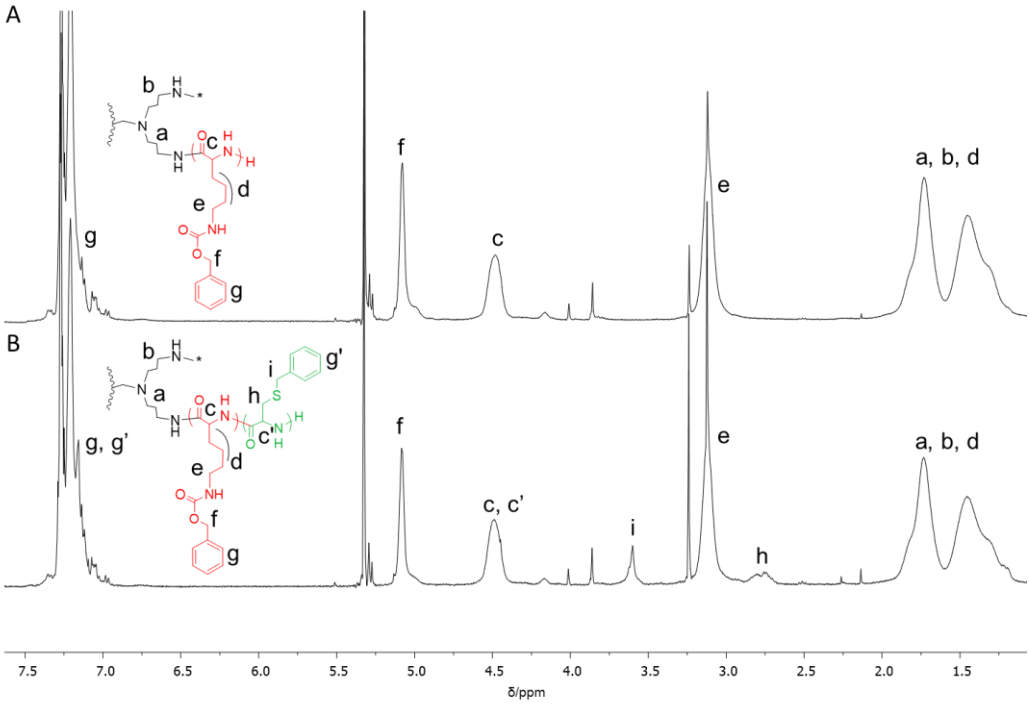

Figure 3.1: ^{1}H-NMR spectra of A) 32-$PZLL_{40}$ and B) 32-$PZLL_{40}$-b-$OBLC_5$.

An additional 64-arm star copolypeptide with an inner oligo(benzyl-L-cysteine) and shell poly(Z-L-lysine) sequence was synthesised in order to investigate the correlation between degree of branching and material properties. The architecture was composed of the same arm length but double the number of arms relative to each 32-arm dendritic initiator. The relative molecular weights were analysed via size exclusion chromatography (Figure 3.2, Table 3.1), showing a trace shift in agreement with target degree of polymerisation (DP).

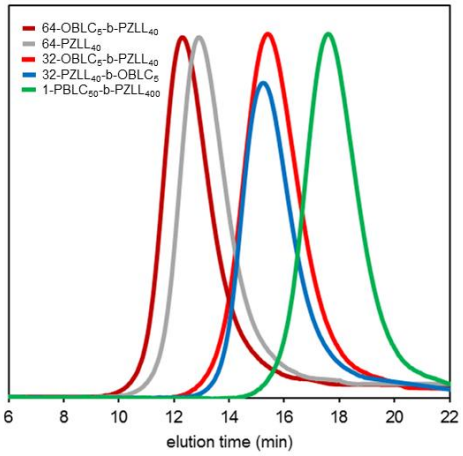

Figure 3.2: SEC traces of homopolypeptide and copolypeptides.

Table 3.1: Molecular weight and polydispersity of polypeptides.

polymer	M_n [a]	M_n [b]	$Đ$ [a]
32-PZLL$_{40}$-b-OBLC$_5$	321 kDa	366 kDa	1.17
32-OBLC$_5$-b-PZLL$_{40}$	346 kDa	366 kDa	1.11
64-OBLC$_5$-b-PZLL$_{40}$	714 kDa	733 kDa	1.13
64-PZLL$_{40}$	640 kDa	671 kDa	1.13
1-PBLC$_{50}$-b-PZLL$_{400}$	103 kDa	114 kDa	1.32

[a] As confirmed by SEC. [b] Theoretical full conversion.

In order to reveal the pendant functionalities of the polypeptides (amine and thiol), cleavage of the protecting groups was achieved with TFA and HBr (33 %) in acetic acid. The polymers are denoted as 32-OLC$_5$-b-PLL$_{40}$, and 32-PLL$_{40}$-b-OLC$_5$, respectively. After purification, each of the star diblock copolypeptides formed hydrogels at low material

concentration. No pretreatment was necessary as they spontaneously gelled in aqueous media. The critical gelation concentration (CGC) was determined using the inversion vial method (Table 3.2). It was considered a gel since no flow was evident within five minutes of inversion. Interestingly, the network of hydrogel samples formed at very low concentrations, in particular for the 32-arm shell crosslinked star copolypeptide, which remained a stable gel at 0.05 wt%. The CGC increased significantly to 0.5 wt% for the 32-arm core crosslinked hydrogel, with a slightly lower polymer concentration sufficient for gelation of its 64-arm analogue (0.3 wt%). Switching the peptide sequence pattern has a definitive effect on the gelation, with a magnitude of ten difference observed for alternative 32-arm hydrogels. A linear copolymer with a DP ten times that of the equivalent arms of the stars was synthesised (1-$PBLC_{50}$-b-$PZLL_{400}$) and did form a hydrogel but at notably higher concentrations than the stars.

Table 3.2: Properties of hydrogels at room temperature. CGC and G' are the critical gel concentration (determined using inversion method) and storage modulus in the linear visco-elastic region. Q is calculated using equation 2.

polymer	CGC (wt%)	G' (Pa)	Q
32-PLL_{40}-b-OLC_5	0.05	4530 [a]	87.4 [a]
32-OLC_5-b-PLL_{40}	0.5	820 [a]	63.1 [a]
64-OLC_5-b-PLL_{40}	0.3	1230 [a]	67.4 [a]
1-$PBLC_{50}$-b- $PZLL_{400}$	4.5	430 [b]	45.6 [b]

[a] Analysed at 3.0 wt%. [b] Analysed at 6.5 wt%.

Visual inspection of core and shell disulphide hydrogel networks under SEM, which were obtained from a hydrated gel sample that was frozen prior to imaging, show porous interconnected networks (Fig. A5). Irregular assemblies can be observed denoting parallel structures with many interwoven fibres observed. The alignment of such fibres depicts accumulation of aggregates possibly representing micellar assemblies.[52,53] It is anticipated that the core crosslinked hydrogel network is governed by the conformation stemming from disulphide linkages primarily formed through intramolecular crosslinking junctions with thiol residues on the same star or intramolecular folding on the same arm.

Intermolecular crosslinking of adjacent thiol in the core stars would be difficult considering their location within the star structure, although this would be more viable for the shell crosslinked hydrogel network with pendant thiols on the periphery of the architecture. In order to investigate the orientation of disulphide from the short chain oligo(L-cysteine) sequences close to the core and on the periphery, FTIR and CD spectroscopy was used.

3.3.2 Conformational analysis

FTIR analysis of the polypeptides in the solid and gelled state uncovered the conformational changes resulting from the polypeptide chain folding in the amide I and II regions from 1500-1700 cm^{-1} (Figure 3.3). Of the star polypeptides made with core and shell disulfide linkages, there are significant deviations in the FTIR pattern when compared to the star homopolypeptide 64-PLL_{40} (Figure A6). For each of the shell and core disulfide crosslinked polypeptide materials, there is a nominal shift in the bands from alternative conformations arising from both gelled and solid states. For lyophilised 32-OLC_5-b-PLL_{40}, the bands at 1670 and 1629 cm^{-1} become significantly more pronounced after gelling in D_2O (Figure 3.3A), with each of the bands representing characteristic β-turn and β-sheet conformations respectively.[54]

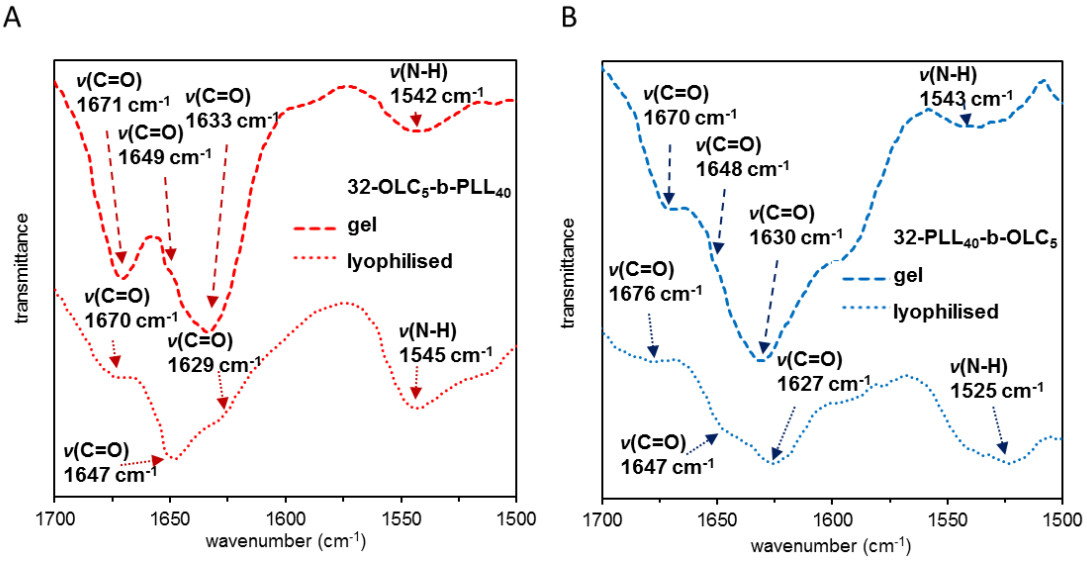

Figure 3.3: FTIR spectra of solid (dotted lines) and gelled (dashed lines) state core A) and shell B) disulphide crosslinked copolypeptides.

The characteristic β-sheet band at 1633 cm^{-1} becomes apparent after swelling overlapping the random coil band at 1649 cm^{-1}. The increase of the β-turn band 1671 cm^{-1} could possibly signify the presence of multiple intramolecular disulphides arising from linkages of neighbouring cysteine residues from the core oligo-L-cysteine sequences.[55] The intramolecular crosslinking of cysteines on the same polypeptide arm sequence and on neighbouring arm sequences could influence the presence of β-motifs, which are well established in short hydrophobic peptide sequences.[56,57] Comparatively for the gelled 32-PLL_{40}-b-OLC_5 material (Figure 3.3B), the intensity of the characteristic β-turn band at 1670 cm^{-1} is modest considering the intensity of the β-sheet band at 1630 cm^{-1}, which could imply the presence of intermolecular disulphide formation between adjacent star copolypeptides with shell oligo-L-cysteine.[58,59] In addition to FTIR, CD spectroscopy provides further insight into the conformation associated with polypeptide macromolecular architecture in solution.

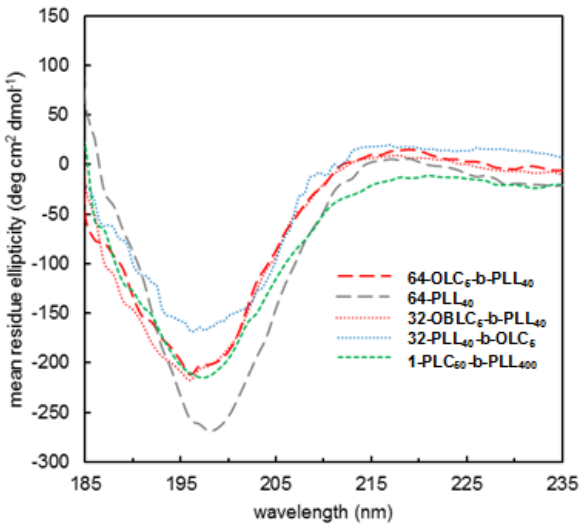

Figure 3.4: CD (circular dichroism) spectra of copolypeptide samples in aqueous solution.

CD analysis was used in conjunction with FTIR in order to correlate the spectroscopic results. In the spectral traces depicted, all polypeptides display a broad centred minimum at 197 nm, which is characteristic of predominate random coil conformation (Figure 3.4). A star homopolypeptide in the form of 64-PLL_{40} was analysed as a reference in order to compare the influence of the oligo(L-cysteine) block on the secondary structure. A large minimum (random coil) was observed for star PLL, indicative of the conformation noted

due to interchain repulsion of cationic chains.[60] For the 32-arm core and shell copolypeptides, there is a moderate wavelength shift in the random coil minima, suggesting disparate disulphide crosslinking of the architectures via alternative β motifs. Although the slight increase from the disulphide β conformers is apparent, the individual characterisation of β turns and sheets are known to be difficult to determine from CD alone.[61] The position of the spontaneously formed cystine crosslinks on the periphery would contribute to a highly dense concentration of disulphides on the exterior of the hydrophilic poly-L-lysine segments, restricting the mobility of these inherently random coiling chains (Figure 3.5).

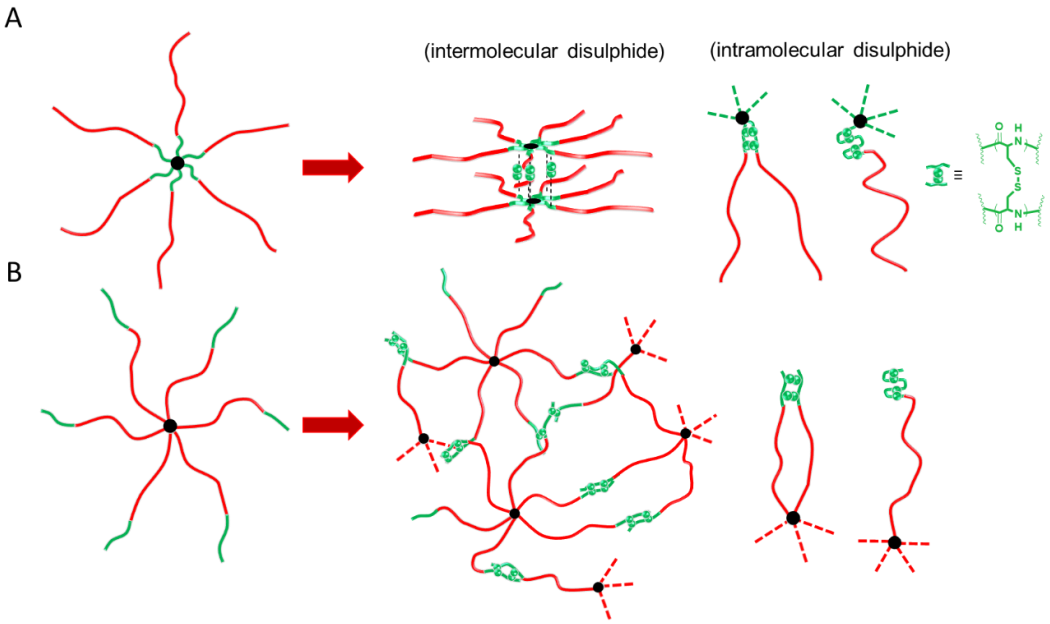

Figure 3.5: Schematic representation of possible arrangements of core and shell disulphide crosslinked star copolypeptide hydrogels. A) Star copolypeptide with OLC in the core and B) star copolypeptide with OLC on the shell.

While the core disulphide crosslinking would contribute to an inferior restriction of the shell PLL domains, allowing for an apparent increase in random coiling. Similarly, the CD spectral trace of 64-OLC_5-b-PLL_{40} did not deviate much from its 32-arm analogue, showing an almost identical intensity at the 197 nm minima. The inclusion of these alternate OLC blocks appears to reduce the degree of random coiling of PLL, which is known to undergo conformational shift in the presence of integrated assemblies.[62] The

CD spectra of the linear block copolymer 1-PLC_{50}-b-PLL_{400}, with analogous composition, is in agreement with the prevailing disordered content. Although since the linear copolypeptide permits a mix of parallel and antiparallel assemblies, this could contribute to the evident broadening in the spectral region from 197-216 nm. Another interesting characteristic of the spectra, in addition to the minima mentioned, is the wide centered maxima at ~216 nm. Reports suggest such moderately intense maxima are indicative of the influence of β-motifs in a peptide-based architecture, signifying the impact of disulphide residues. These data suggest that indeed the majority of disulphide linkages occur through intermolecular interactions with the shell crosslinked hydrogel since the adjacent cysteine residues on the star architecture are ideally orientated for this. While the core oligo-L-cysteine containing hydrogel system appears to be mediated through primarily intramolecular interactions due to length and orientation of those sequences in the core. The highly ordered arrangement of β-turns or sheets from the alternative cysteine mediated assemblies provides core and shell diblock copolypeptide materials with different architecture and thus different spectral conformations.

3.3.3 Mechanical properties

The core and shell crosslinked star copolypeptides (32-OLC_5-b-PLL_{40} and 32-PLL_{40}-b-OLC_5) exhibited a distinctive linear visco-elastic (LVE) region in which storage modulus (G') exceeds the loss modulus (G''), (Figure 3.6A and B). This is characteristic of materials that exhibit 'true gel' behaviour. The position of the oligo(L-cysteine) sequence appears to afford different hydrogel mechanical properties as the recorded G' (in the LVE region) of the shell disulphide hydrogel was 4530 ± 8 Pa, which is far superior in strength to the core disulphide hydrogel, which has a G' of 820 ± 10 Pa. The length of the LVE region was different for the core and crosslinked copolypeptides hydrogels. For example, the *G'* value of 32-PLL_{40}-b-OLC_5 decreased upon reaching 2% (indicating the end of the LVE region) and had a crossover point with *G''* at 48%. This is representative of a gel-sol transition related flow behaviour. In comparison, the crossover point was at 5% strain for the shell crosslinked 32-OLC_5-b-PLL_{40} hydrogel.

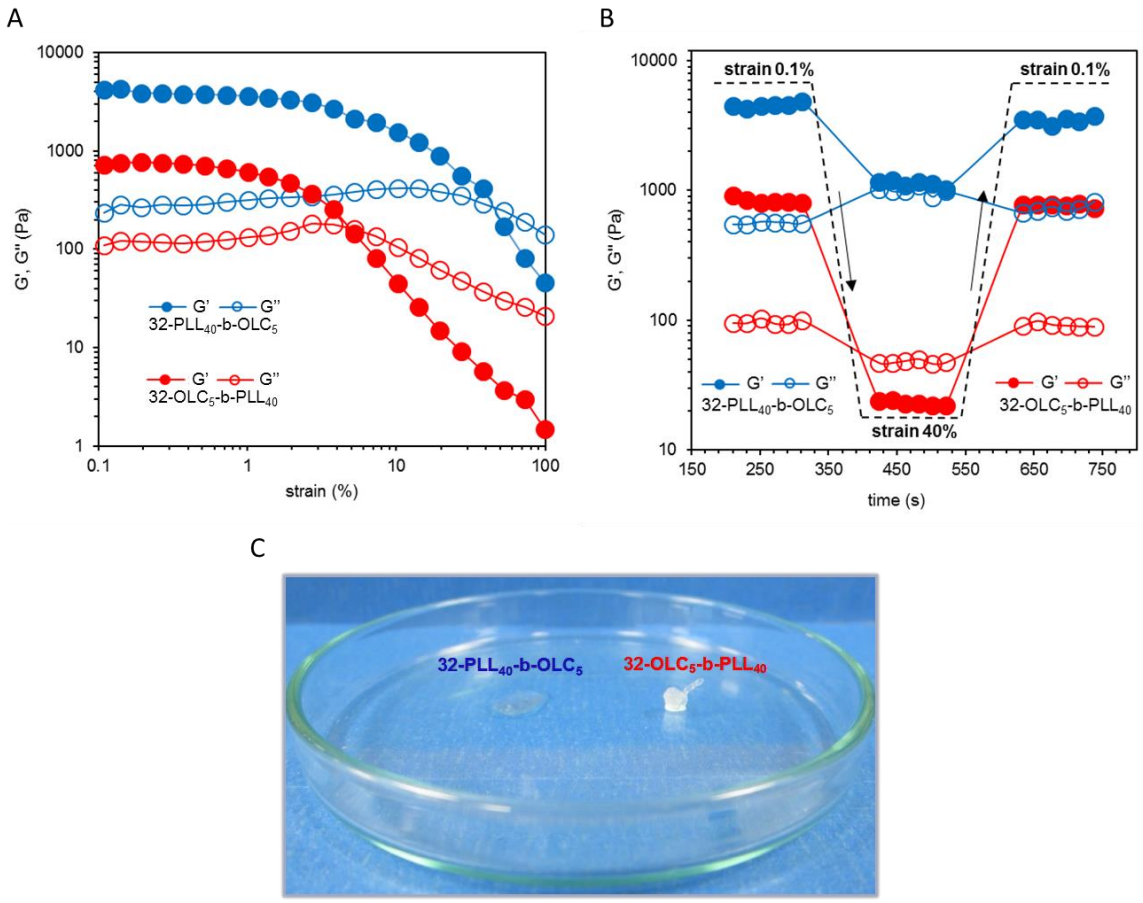

Figure 3.6: Rheological A) amplitude sweep of core and shell star copolypeptide hydrogels with storage and loss modulus as a function of increasing strain and constant frequency (sheared at γ = 0.1–100, ω = 1 rad s^{-1}). Rheological B) short stepping strain sweep of core and shell disulphide crosslinked star copolypeptides (at constant frequency ω = 1 rad s^{-1}). C) Image of both hydrogels after shearing through 21G gauge needle.

The hydrogels' self-recovery behaviour was investigated through a short step strain sweep experiment (Figure 3.6B). The use of 40% strain was insufficient to induce a gel-sol transition of 32-PLL_{40}-b-OLC_5 as G'' did not exceed G'. Although, the large amplitude strain did have an effect on the self-recovery behaviour of the hydrogel network. The initial G' of 32-OLC_5-b-PLL_{40} was 811 ± 15 Pa, which reverted to 782 ± 12 Pa after the strain cycling, corresponding to full self-recovery (within error margins). In contrast, the hydrogel formed for 32-PLL_{40}-b-OLC_5 exhibited a self-recovery of about 75%, i.e. initial G' value of 4521 ± 9 Pa, which recovered to 3515 ± 11 Pa after returning to original strain. The results demonstrate that the position of the disulphide crosslinks within these star

copolypeptide hydrogels can impart two distinctively different mechanical behaviours otherwise unattainable in linear polypeptide analogues.

The practical aspect of this was demonstrated by assessing the ability to inject these hydrogels through a standard 21G syringe needle (Figure 3.6C). The core crosslinked hydrogel underwent shear deformation reforming almost instantaneously after passing through the needle while the shell crosslinked hydrogel expelled water when subject to the same shear (video, ESI), further substantiating the rheological analysis. For the 32-arm and 64-arm core crosslinked hydrogels, there is a direct correlation between relative strength of the gel and increasing degree of branching (G' values of 820 ± 10 Pa and 1230 ± 13 Pa, respectively).

In comparison to its 32-arm counterpart, the 64-arm hydrogel sample showed network breakdown (end of LVE region) at >5% strain (Figure 3.7A) while both hydrogels were insensitive to frequency fluctuation (Figure 3.7B). A step strain sweep experiment (Figure 3.7C) demonstrated the self-recovery behaviour of the core crosslinked hydrogels. Above the significant amplitude oscillatory strain (40%), expected deformation was evident as G' sharply reduced. Reverting back to 0.1% strain which was within the viscoelastic threshold allowed for recovery of G' to its original value. Even after stepping the strain to a higher amplitude (60%), the G' of both star copolypeptides promptly returned to their original state upon a return to 0.1% strain (indicating self-recovery behaviour).

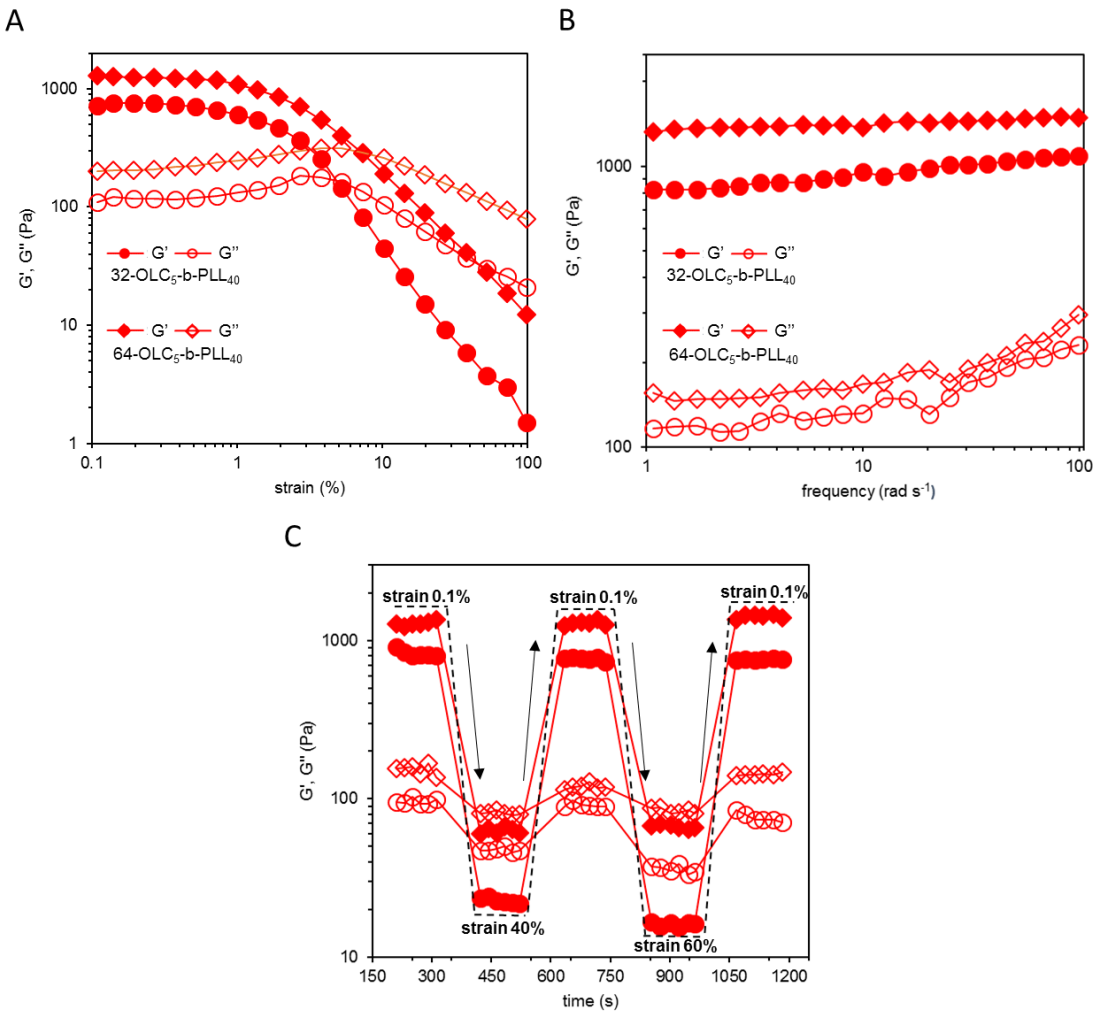

Figure 3.7: Rheological properties of 64 and 32 arm core crosslinked copolypeptides hydrogels. Amplitude sweep (A) of core disulphide crosslinked star copolypeptides hydrogels with storage and loss modulus as a function of increasing strain and constant frequency (sheared at ɣ = 0.1–100, ω = 1 rad s^{-1}). Frequency sweep (B) of core disulphide crosslinked star copolypeptides hydrogels with storage and loss modulus as a function of increasing angular frequency and constant strain (sheared at ɣ = 0.1, ω = 1–100 rad s^{-1}). Stepping strain sweep (C) of core disulphide crosslinked star copolypeptides (at constant frequency ω = 1 rad s^{-1}).

3.3.4 Drug release

Since the core crosslinked hydrogels exhibit favourable rheological behaviour in terms of shear-thinning, they were further examined for their drug release properties (Figure 3.8), based on their potential as injectable or 3D printable matrices for therapeutic delivery. DOX.HCl was loaded into each of the star block copolypeptide hydrogels (32- and 64-arm) by vigorously mixing the lyophilised samples with the DOC.HCl solution (1 mg mL^{-1}) at room temperature at a polypeptide concentration of 3.0 wt%.

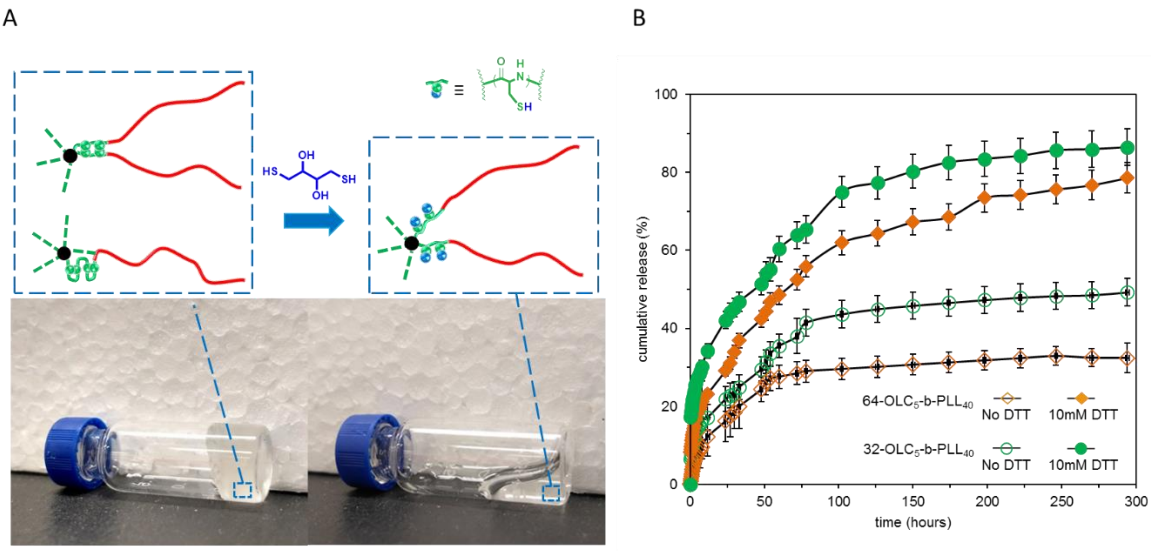

Figure 3.8: A) 64-OLC_5-b-PLL_{40} hydrogel and reduction of 64-OLC_5-b-PLL_{40} hydrogel using 10mM DTT and B) drug release profiles of DOX-loaded star copolypeptide hydrogels over 12-day period.

In order to illustrate the redox response of the disulphide linkages, two different concentrations of DTT were added to the hydrogels (5 mM and 10 mM). Almost instantly, the homogeneity of the hydrogels became unstable resulting in material flow (Figure 3.8A). The release profile of DOX from the star shaped hydrogels was examined in the absence and presence of DTT, in order to simulate both a redox free and redox environment (Figure 3.8B). The release of DOX for all samples eventually plateaued after the 300 hours (~12 day) of the study. Cumulative release of DOX reached 32% and 49% for the 64-arm and 32-arm block copolypeptide hydrogels respectively over 12 days. Interesting to note is the correlation between the release profile and the degree of

branching. The 64-arm hydrogel depot had a more delayed release of DOX which is most likely due to the increasing degree of branching of the star architecture in addition to the attached polypeptide arms, meaning simultaneous degradation and diffusion would be slower. Therefore, the closely aligned core would more readily envelop the loaded drug thus prolonging the release. DTT accelerated the release of DOX from both platforms via cleavage of the core disulphide bonds prompting destruction of the hydrogel network and thus diffusion through the corona of the star polypeptide.

After a period of 100 hours (~4 days), and in the absence of DTT, the sample 64-OLC_5-b-PLL_{40} released 29% of its cargo while in comparison 61% of DOX was released when the hydrogels were exposed to DTT. The hydrogels incubated with PBS without DTT present still triggered release without any prior stimulation from a reductant, implying that the dendrimer core of the molecule did not encapsulate a significant amount of the payload. This could be a result of the covalent crosslinks within the star copolypeptide. The density of disulphide residues on the edge in the inner core would promote slow diffusion of DOX into the PPI dendritic core, meaning the drug payload would localise at the periphery of the core.

3.4 Conclusions

A series of star shaped diblock copolypeptides containing core and shell disulphide crosslinks were synthesised by alternating oligo-L-cysteine and poly-L-lysine sequences. In aqueous solution, the star copolypeptides swelled and formed stable hydrogels with material content as low as polymer 0.05 wt%. The hydrogel behavior was monitored by switching the sequence composition and by increasing the degree of branching of the star copolypeptides. Changing the sequence on the 32-arm PPI dendrimer from core crosslinking to shell crosslinking had a significant effect on hydrogel storage modulus as it changed from 820 Pa to 4530 Pa. Moreover, the core crosslinked hydrogel underwent self-recovery almost instantaneously after passing through a standard syringe needle while the shell crosslinked hydrogel expelled water when subject to the same shear. Hydrogels readily underwent network disruption after the addition of the molecular reductant DTT, cleaving disulphide bonds resulting in a gel-sol transition, which was

utilised to accelerate the release of the model drug doxorubicin from the hydrogel depots. The diverse material properties associated with the star copolypeptide system employed here allows for fabrication of stable hydrogels bearing high mechanical strength or shear thinning properties by simply adjusting the sequence order, while simultaneously possessing redox responsiveness. The rheological behaviour of these core crosslinked copolypeptides coupled with their innate redox responsiveness makes them ideal for applications that require shear-thinning redox sensitive materials such as cardiac tissue engineering.

3.5 References

1 D. Seliktar, *Science,* 2012, 336, 1124.

2 O. Jeon, K. H. Bouhadir, J. M. Mansour, E. Alsberg, *Biomaterials*, 2009, 30, 2724.

3 J. T. Zhang, R. Bhat, K. D. Jandt, *Acta Biomaterialia*, 2009, 5, 488.

4 M. Nakahata, Y. Takashima, H. Yamaguchi, A. Harada, *Nat. Commun*., 2011, 2, 511.

5 A. B. South, L. A. Lyon, *Angew. Chem*., 2010, 122, 779.

6 M. Guvendiren, H. D. Lu, J. A. Burdick, *Soft Matter*, 2012, 8, 260.

7 S. Zhang, M. Altman, *React. Funct. Polym*., 1999, 41, 91.

8 B. S. Berlett, E. R. Stadtman, *J. Biol. Chem*., 1997, 272, 20313.

9 L. E. R. O'Leary, J. A. Fallas, E. L. Bakota, M. K. Kang, J. D. Hartgerink, *Nat. Chem*., 2011, 3, 821.

10 L. D. D'Andrea, L. Regan, *Trends Biochem. Sci*., 2003, 28, 655.

11 P. T. Lansbury Jr, P. R. Costa, J. M. Griffiths, E. J. Simon, M. Auger, K. J. Halverson, D. A. Kocisk, Z. S. Hendsch, T. T. Ashburn, R. G. S. Spencer, B. Tidor, R. G. Griffin, *Nature Struct. Biol*., 1995, 2, 990.

12 R. Fairman, K. S. Akerfeldt, *Curr. Opin. Struct. Biol*., 2005, 15, 453.

13 S. J. Shirbin, F. Karimi, N. J. A. Chan, D. E. Heath, Qiao, G. G. *Biomacromolecules*, 2016, 17, 2981.

14 C. C. Ahrens, M. E. Welch, L. G. Griffith, P. T. Hammond, *Biomacromolecules*, 2015, 16, 3774.

15 H. Cui, X. Zhuang, C. He, Y. Wei, X. Chen, *Acta Biomater*., 2015, 11, 183.

16 T. Stukenkemper, J. F. G. A. Jansen, C. Lavilla, A. A. Dias, D. F. Brougham, A. Heise, *Polym. Chem*., 2017, 8, 828.

17 T. Borase, A. Heise, *Adv. Mater*., 2016, 28, 5725.

18 J. Yuan, Y. Sun, J. Wang, H. Lu, *Biomacromolecules,* 2016, 17, 891.

19 T. J. Deming, *Chem. Rev*., 2015, 116, 786.

20 K. Ren, C. He, C. Xiao, G. Li, X. Chen, *Biomaterials*, 2015, 51, 238.

21 L. Yin, Z. Song, K. H. Kim, N. Zheng, H. Tang, H. Lu, N. Gabrielson, J. Cheng, *Biomaterials*, 2013, 34, 2340.

22 A. P. Nowak, V. Breedveld, L. Pakstls, B. Ozbas, D. J. Pine, D. Pochan, T. J. Deming, Nature, 2002, 417, 424.

23 E. F. Banwell, E. S. Abelardo, D. J. Adams, M. A. Birchall, A. Corrigan, A. M. Donald, M. Kirkland, L. C. Serpell, M. F. Butler, D. N. Woolfson, *Nat. Mater.*, 2009, 8, 596.

24 M. C. Giano, D. J. Pochan, J. P. Schneider, *Biomaterials,* 2011, 32, 6471.

25 C. Zhao, X. Zhuang, P. He, C. Xiao, C. He, J. Sun, X. Chen, X. Jing, *Polymer*, 2009, 50, 4308.

26 S. Zhang, D. J. Alvarez, M. V. Sofroniew, T. J. Deming, *Biomacromolecules*, 2015, 16, 1331.

27 J. Huang, C. L. Hastings, G. P. Duffy, H. M. Kelly, J. Raeburn, D. J. Adams, A. Heise, *Biomacromolecules*, 2013, 14, 200.

28 M. Zhu, Y. Wu, C. Ge, Y. Ling, H. Tang, *Macromolecules*, 2016, 49, 3542.

29 J. R. Kramer, T. J. Deming, *J. Am. Chem. Soc.*, 2012, 134, 4112.

30 G. E. Negri, T. J. Deming, *ACS Macro Letters,* 2016, 5, 1253.

31 G. Liu, C. M. Dong, *Biomacromolecules*, 2012, 13, 1573.

32 M. L. Circu, T. Y. Aw, *Free Radic. Res.*, 2008, 42, 689.

33 E.P. Feener, W.C. Shen, H. J. P. Ryser, *J. Biol. Chem.*, 1990, 265, 18780.

34 H. F. Gilbert, *Methods Enzymol.*, 1995, 251, 8.

35 D. Wu, X. J. Loh, Y. L. Wu, C. L. Lay, Y. Liu, *J. Am. Chem. Soc.*, 2010, 132, 15140.

36 X. Wang, D. Li, F. Yang, H. Shen, Z. Li, D. Wu, *Polym. Chem.*, 2013, 4, 4596.

37 B. S. McAvan, M. Khuphe, P. D. Thornton, *Eur. Polym. J.*, 2017, 87, 468.

38 Y. X. Zhang, Y. F. Chen, X. Y. Shen, J. J. Hu, J. S. Jan, *Polymer,* 2016*,* 86*,* 32.

39 J. Zhou, P. Chen, C. Deng, F. Meng, R. Cheng, Z. Zhong, *Macromolecules*, 2013, 46, 6723.

40 T. Xing, C. Mao, B. Lai, L. Yan, *ACS Appl. Mater. Interfaces*, 2012, 4, 5662.

41 Y. Ma, X. Fu, Y. Shen, W. Fu, Z. Li, *Macromolecules*, 2014, 47, 4684.

42 S. Zhang, Y. Wan, W. Fu, Z. Li, *Soft Matter*, 2015, 15, 2945.

43 P. D. Thornton, S. M. R. Billah, N. R. Cameron, *Macromol. Rapid Commun.*, 2013*,* 34*,* 257.

44 R. Murphy, T. Borase, C. Payne, J. O'Dwyer, S. A. Cryan, A. Heise, *RSC Adv.*, 2016*,* 6, 23370.

45 R. Murphy, D. P. Walsh C. A. Hamilton, S. A. Cryan, M. in het Panhuis, A. Heise, *Biomacromolecules*, 2018, 19, 2691.

46 D. L. Liu, X. Chang, C. M. Dong, *Chem. Commun*., 2013, 49, 1229.

47 M. Byrne, D. Victory, A. Hibbitts, M. Lanigan, A. Heise, S. A. Cryan, *Biomater. Sci.*, 2013, 1, 1223.

48 M. Byrne, P. D. Thornton, S. A. Cryan, A. Heise, *Polym. Chem*., 2012, 3, 2825.

49 C. Lavilla, M. Byrne, A. Heise, *Macromolecules,* 2016, 49, 2942−2947.

50 C. Lavilla, G. Yilmaz, V. Uzunova, R. Napier, C. R. Becer, A. Heise, *Biomacromolecules,* 2017, 18, 1928.

51 G. J. Habraken, M. Peeters, C. H. Dietz, C. E. Koning, A. Heise, *Polym. Chem*., 2010, 1, 514.

52 A. Sulistio, A. Widjaya, A. Blencowe, X. Zhang, G. G. Qiao, *Chem. Commun.*, 2011, 47, 1151.

53 Q. Chen, F. Han, C. Lin, X. Wen, P. Zhao, *Polymer*, 2018, 146, 378.

54 S. S. Cheng, K. K. Chittur, C. N. Sukenik, L. A. Culp, K. J. Lewandowska, *J. Colloid Interface Sci.*, 1994, 162, 135.

55 A. Ravi, P. Balaram, *Tetrahedron*, 1984, 40, 2577.

56 V. Moretto, M. Crisma, G. M. Bonora, C.Toniolo, *Macromolecules*, 1989, 22, 2939.

57 M. Hollosi, Z. Majer, A. Z. Ronai, A. Magyar, K. Medzihradszky, S. Holly, A. Perczel, G. D. Fasman, Biopolymers, 1994, 34, 177.

58 T. J. Cashman, B. R. Linton, *Org. Lett.*, 2007, 9, 5457.

59 R. Kishore, S. Raghothama, P. Balaram, 1987, *Biopolymers*, 26, 873.

60 J. S. Chiou, T. Tatara, S. Sawamura, Y. Kaminoh, H. Kamaya, A. Shibata, I. Ueda, *Biochim. Biophys. Acta.*, 1992, 1119*,* 211.

61 A. Glattli, X. Daura, D. Seebach, W. F. van Gunsteren, *J. Am. Chem. Soc.*, 2002, 124*,* 12972.

62 A. Harada, S. Cammas, K. Kataoka, *Macromolecules*, 1996, 29*,* 6183.

CHAPTER 4

3D PRINTABLE STAR COPOLYPEPTIDE HYDROGELS

This chapter was published in; *Biomacromolecules*, **2018**, 19, 2691.

Abstract

We present a star copolypeptide based hydrogel ink capable of structural microfabrication using 3D extrusion printing. The material comprises an amphiphilic block copolymer structure of poly(benzyl-L-glutamate)-*b*-oligo(L-valine), which spontaneously form hydrogels through conformationally induced hydrophobic interactions. The chemical design allows the bulk phase of the hydrogel to remain intact after application of shear due to its self-recovery behavior. It is demonstrated that the composition of the materials is ideally suited for 3D printing; with scaffolds capable of maintaining structural cohesion after extrusion. Post extrusion UV-triggered fixation of the printed structures is carried out resulting in stable hydrogel constructs. The constructs were found to be degradable, exhibited favorable release of encapsulated molecular cargo and did not affect the metabolic health of the commonly used fibroblastic cell line, Balb/3T3 cells in the absence of the reactive diluent N,N'-methylenebisacrylamide. The star copolypeptide inks allow for rapid prototyping enabling the fabrication of defined intricate microstructures, providing a platform for complex scaffold development that would be otherwise unattainable with other processing techniques such as molding or casting.

David P. Walsh conducted the cell viability assays at RCSI.

Charles A. Hamilton designed the Gcode files and assisted with 3D printing and rheology at UOW.

Sepehr Talebian assisted with the SEM imaging at UOW.

4.1 Introduction

The field of tissue engineering and regenerative medicine aims to regenerate damaged tissues rather than their replacement via the creation of well defined, surgically implantable biomaterial constructs.[1,2] The development of defined three-dimensional (3D) architecture fabrication for tissue engineering has been a recent emergence within the field.[3] In particular, 3D printing represents a promising rapid prototyping technology for the production of intricate bio-inspired scaffolds/constructs.[4] Highly defined complex structures can be readily developed with computer-aided design (CAD) and deposited with stereolithography,[5,6] extrusion[7,8] or ink-jet[9] based printing. For the development of tissue engineering scaffolds, extrusion or ink-jet based approaches are mainly employed. The primary feedstock materials used are polymeric hydrogels, which possess ideal physicochemical properties for these rapid 3D patterning techniques. Hydrogels encompass the capability to augment native tissue due to their comparative 3D nano-architecture while holding the potential to act as a mimetic of the extracellular environment.[10-12] Recent work on 3D rapid prototyping with hydrogels has mainly focused on the use of natural polymers. Polysaccharides such as chitosan[13] and alginate[14] have been chemically functionalised and used as carriers within hydrogel inks. Recent reports also detail the fabrication of modified bio-native gelatin[15] and hyaluronic acid[16] hydrogels which were 3D printed into cell laden constructs and self-healing structures respectively. More synthetic approaches have utilised poly(ethylene glycol)[17] or acrylic monomer loaded inks.[18] Despite these efforts, the limited number of suitable bio-inks has been identified as the major barrier to progress and the development of new advanced hydrogel applications.[3] It is envisaged that a possible solution lies in the synthesis of hydrogel polymers but application demands are high. For example, control over the mechanical properties for the 'printability' is a vitally important factor for the choice of new bioinks in the fabrication of constructs with desired spatial resolution. In some cases, defined layer-by-layer production requires the use of a high polymer fraction in hydrogel inks (>10 wt%) in order to obtain desired rheological behavior for printing.[19] Other processing involved in the fabrication of self-supporting structures is stimuli triggered gelation

generally using post-printing crosslinking methodologies such as UV curing.[20,21] The process is rather straightforward, whereby a highly viscous hydrogel ink is extruded and simultaneously cured into the desired shape with the assistance of UV irradiation. However, this method requires rapid gelation upon extrusion onto the substrate in order to maintain the predetermined print resolution. Thus, the essential prerequisites for advancing the process would be to develop polymeric hydrogels that can encapsulate high fractions of water (>97%), display shear thinning behavior and instantaneously reassemble upon extrusion, yielding a stabilised construct.

Of those existing materials available, hydrogels based on synthetic polypeptides derived from the polymerisation of amino acid *N*-carboxyanhydride (NCA) would possess ideal properties when considering these criteria.[22,23] Their secondary structure arrangements play a vital role in the self-assembly of the adjacent peptide domains into hydrogelating matrices.[24-27] Additionally, the amino acid building blocks contain side groups with tunable functional groups, holding potential for customizing the physicochemical, mechanical and biological features of hydrogels.[28-30] Although relatively unexplored, these materials could pave the way for the development of tailor made cell-compatible hydrogel inks which can create bio-functional structures. The versatility of the polypeptide system allows for seamless modulation of mechanical properties, thus expanding the range of materials and facilitating the use of more advanced hydrogel inks in the field of 3D printing. A recent example used dual extrusion of a polypeptide-DNA conjugate and a DNA linker to create a bio-ink capable of yielding uniform structures based on DNA hybridisation crosslinking.[31] Here, we report for the first time the rational design of star shaped block copolypeptides suitable as 3D printing inks. The materials combine appropriate shear-thinning behavior with fast recovery to form stable, degradable, hydrogel constructs which are non-toxic towards commonly used Balb/3T3 cells. The exceptional 3D printing processability was demonstrated in the fabrication of various complex self-supporting hydrogel constructs. The polypeptide inks disclosed here overcome limitations usually encountered with 3D printing inks and could open new avenues for rapid prototyping in areas such as tissue engineering scaffolds not achievable otherwise.

4.2 Experimental

4.2.1 Materials

All chemicals were obtained from Sigma-Aldrich unless otherwise stated. Benzyl-L-glutamate, L-valine, N',N'-dicyclohexylcarbodiimide (DCC) and 4-dimethylaminopyridine (DMAP) were purchased from Novachem (Australia). The generation 4 (G4) 32-arm polypropylene imine (PPI) dendrimer (DAB-Am-32) was obtained from SyMO-Chem BV (Netherlands). The NCAs of benzyl-L-glutamate and L-valine were synthesised following literature procedures.[32]

4.2.2 Methods

Nuclear Magnetic Resonance (^{1}H NMR) analysis was completed using a Bruker Avance 400 (400 MHz) spectrometer at room temperature with $CDCl_3$ and trifluoroacetic acid-d (TFA-d). Attenuated total reflection (ATR) FTIR was recorded using a spectrometer (IR Prestige-21 Shimadzu, Japan) in the region of 4000–700cm^{-1}. A background measurement was initially performed before analysing the sample. Thirty scans were completed using a resolution of 2 cm^{-1}. The molecular weight and molecular weight distributions (dispersity, $Đ = M_w/M_n$) were determined by size exclusion chromatography (SEC). Measurements were carried out on a Waters 515 equipped with a Wyatt DAWN HELEOS-II (laser 658.0 nm) laser light scattering detector and a Wyatt Optilab rEX detector. The eluent was THF with a flow rate of 1 mL min^{-1}. The column temperature was set to 40 °C and the refractive index detector at 40 °C. Rheological measurements were conducted on a MCR 301 digital rheometer (Anton Paar, Physica, Australia). Frequency sweeps (ω = 1-100 rad s^{-1} and γ = 0.1%), strain sweeps (γ = 0.1%-100% and ω = 1 rad s^{-1}) and time sweeps with oscillation in strain (stepping between γ = 0.1% and 40%, then 0.1% and 100%, and returning to γ = 0.1%, constantly at ω = 1 rad s^{-1}) were conducted at room temperature (21 °C) using a conical plate (CP50-1, Anton Paar, Australia) consisting of a 50 mm diameter geometry and a 1° cone angle with a gap length of 0.097 mm. The use of a protective hood was employed to prevent evaporation. UV stimulated measurements (γ = 0.1%, ω = 1 rad s^{-1}) were conducted using a pyrex base rheometer attachment and a Dymax BlueWave 75 Rev 2.0 UV system with a 19+ W cm^{-2} light source. Printed hydrogel

constructs were video recorded and photographed with a 16MP Nikon camera and a 16MP smart phone camera (Motorola Moto G4 Plus). Morphological imaging of the constructs was performed with a JEOL JSM-6460A scanning electron microscope (SEM). The samples were 3D printed, UV cured and then a cross-section of the construct was imaged.

Ink preparation

Three hydrogel-forming inks were prepared to find the optimum formulation for yielding well resolved stabilised constructs after 3D extrusion printing. Inks consisted of a constant concentration of polymer (2.0 wt%), with a small variation in photo initiator concentration and in one ink, the difunctional monomer N,N'-methylenebisacrylamide.

3D printing

3D printing was done on a custom built extrusion printer, i.e. a computerised numerical control (CNC) milling machine (Sherline Products, 5400) was used as a positioning stage, upon which independent linear actuators (Zaber Technologies, T-LA60A) were mounted onto the z-axis of the stage as syringe pumps. The hydrogel ink was prepared and then loaded into a 5mL syringe barrel and centrifuged to remove air bubbles. The material was then extruded by the linear actuators moving at 25 data points/s (where each data point represents 0.047625 μm). The Gcode to dictate the movement of the printhead (at 300 mm/min) was written in the Linux Gedit program. All prints were done using 32 or 25 gauge extrusion tips purchased from Nordson EFD unless otherwise stated. Completed prints were subject to UV curing (Dymax BlueWave 75 Rev 2.0 UV system/19+ W cm^{-2} light source) as a post-processing method to produce stabilised constructs.

Drug Loading

Doxorubicin.HCl (DOX) was used as the drug to be loaded into the hydrogel ink. DOX was prepared as a 1 mg mL^{-1} solution in deionised water. The hydrogel/drug depot was then formed using the lyophilised polypeptides at a concentration of 2.0 wt%. 3D

extrusion printing was carried out as described above with a longer UV exposure time. The constructs were then incubated in PBS (pH 7.5) and aliquots were examined at specific time intervals. The samples were analysed using a UV/vis spectrometer at a wavelength of 490nm and quantification was completed using a calibration curve, samples were then returned to the media. Experiments were carried out in triplicate.

Degradation Studies

UV crosslinked constructs were subject to immersion in acidic (pH 2.0), neutral (pH 7.4) and basic (pH 12.0) commercial PBS media. Samples were then incubated in a cell culture incubator at 37 °C for a period of 4 weeks, with regular sampling intervals. Degradation was determined by loss of hydrogel mass over time and was indicated by dissolution of printed structures. Experiments were carried out in triplicate.

Balb/3T3 Cell Culture

Balb/3T3 clone A31 mouse fibroblasts were cultured in T175 adherent cell flasks (Sarstedt, Germany) at a seeding density of $1x10^6$ cells per flask. Complete culture media consisted of Dulbecco's Modified Eagles Medium (DMEM) – high glucose which was supplemented with 10% v/v Foetal Bovine Serum, 2% v/v Glutamine and 1% v/v Penicillin/Streptomycin. Flasks were maintained in an incubator at 37 °C with 5% CO_2 and 90% humidity. Cells were passaged with 0.25% v/v trypsin/EDTA every 3-4 days once 70-80% confluency had been reached. All experiments were carried out using passage 6-8 cells.

In vitro biocompatibility of star shaped diblock copolypeptides

The metabolic activity of Balb/3T3 fibroblasts in the presence of extracted leachates from sliced segments of P1, P2 & P3 copolymers was assessed using a protocol described by Kiser et al. Briefly, 100mg segments of ring from P1, P2 or P3 were cut under sterile conditions and incubated in 10mls of Phosphate Buffered Saline (PBS) in a shaking water bath at 37 °C for 7 days. The supernatant was filtered through a sterile 0.2µm filter (Merck Millipore, Ireland) before being diluted 1:4 with complete culture media to form the respective treatment solution. Cytotoxicity assessment was

performed using a colorimetric MTT Cell Growth Assay (Merck Millipore, Ireland) and Live/Dead staining (Molecular Probes, Invitrogen, Ireland). With regard to the MTT assay, cells were cultured as previously described and seeded at a density of $1.5x10^4$ cells per well of a 96 well plate. Following 24 hours' incubation the cells were washed and incubated in 100µl of extracted leachates from P1, P2 or P3 prepared as previously described. At each timepoint of 24 hours, 72 hours or 168 hours approximately 10ul of MTT substrate was added to each well. Viable cells cleave yellow MTT substrate to form formazan crystals in a process which requires activate mitochondria. Cells were incubated in the presence of MTT substrate for four hours at 37 °C. The supernatant was then removed and 100ul of DMSO added to each well to dissolve the formazan crystal protocol. Absorbance was determined at 570nm with a reference wavelength of 630nm. A 1:4 mixture of PBS: Complete Culture Media served as a 100% viable control. Images were obtained using a Leica DMIL microscope (Leica Microsystems, Switzerland). For Live/Dead imaging cells were seeded into 12 well plates at a density of $2x10^4$ cells per well. Following 24 hours incubation at 37 °C, cells were washed and media replaced with 1ml of extracted leachates from each of P1, P2 or P3. A 1:4 mixture of PBS: Complete Culture Media served as a 100% untreated control. At each time point of 24 hours, 72 hours or 168 hours each well was washed with 1ml PBS and approximately 300µl LIVE/DEAD stain added. Following a 15 minute incubation cells were imaged by fluorescence microscopy using a Leica DMIL microscope (Leica Microsystems, Switzerland). Live cells will fluoresce green due to the accumulation of calcein-AM while dead cells will fluoresce red due to the accumulation of ethidium homodimer-1.

4.2.3 Synthesis of 32-arm star shaped poly(L-glutamate)-*b*-oligo(L-valine)

Benzyl-L-glutamate NCA (2.10 g, 7.98 mmol) was dissolved in a 5:1 mixture of dry $CHCl_3$/DMF (25 mL) under a N_2 atmosphere in a schlenk flask at 0°C. G4 32-arm PPI dendrimer (25.02 mg, 7.12×10^{-6} mmol) in 5 mL of dry $CHCl_3$ was quickly charged to the Schlenk flask. The flask was evacuated under vacuum to remove CO_2 and was allowed to stir for 16 hours at 0°C. FTIR was used to confirm total monomer consumption. An aliquot was taken directly via syringe to monitor the molecular mass

using SEC. L-valine NCA (203.92 mg, 1.42 mmol) was dissolved in a 7 mL mixture of anhydrous $CHCl_3$/DMF (5:1) and charged to the flask. The solution was allowed to stir at 0°C until full conversion was confirmed by FTIR. The polymer was precipitated into excess diethyl ether and dried under vacuum in a dessicator to give the 32-$PBLG_{35}$-b-OLV_5 star polymer (yield 76%). The diblock copolymer (1.6 g) was dissolved in 20 mL trifluroacetic acid and allowed to solubilise. Then, 6 mL of HBr (33 wt% in acetic acid) was added drop wise to the solution in a six-fold excess with respect to benzyl-L-glutamate repeat units and stirred for 16 hours. The polymer was precipitated thrice into diethyl ether (50 mL) and centrifuged at 6000 rpm. The supernatant was decanted and the precipitate was washed once more with diethyl ether (40 mL). It was then dried under vacuum and then subsequently dissolved in deionised water with NaOH. Dialysis was performed against deionised water for 5 days using a 12 kDa MWCO membrane, with frequent water replacement. The polymer was then lyophilised (yield 80%).

4.2.4 Preparation of allyl functionalised copolypeptide

The star copolypeptide (1.8 g, 0.02 mmol), DCC (1.04 g, 5.00 mmol) and DMAP (0.25 g, 2.07 mmol) were dissolved in 130 mL anhydrous DMSO and stirred for 30 mins. Allyl alcohol (0.12 g, 2.07 mmol) was dissolved in 1 mL anhydrous DMSO and then charged to the flask, and the solution was stirred for 3 days. The dicyclohexylurea (DCU) precipitate was filtered off and the reaction solution was diluted in water, which was then dialysed against deionised water for 4 days using a 12 kDa MWCO membrane, with frequent water replacement. The polymer was then lyophilised (yield 91%).

4.3 Results and Discussion

4.3.1 Preparation of star copolypeptide

Star (block) copolypeptides can be readily obtained by NCA polymerisation from multi-amine initiators.[33-37] In this work, the physically crosslinked hydrogels are composed of a 35mer of glutamic acid, chain extended with a 5mer of valine, which are tethered from the terminal amine ends of a 32-arm polypropylene imine (PPI) dendrimer core (Scheme 4.1).

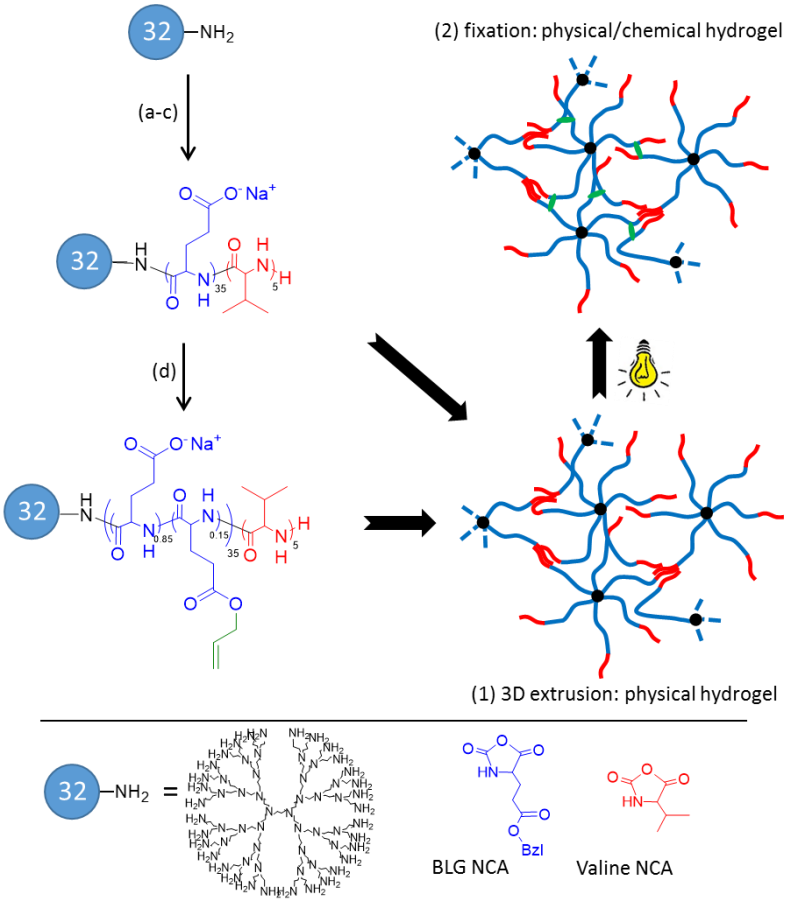

Scheme 4.1: Structure of star shaped diblock copolypeptides and hydrogel formation through valine block self-assembly during extrusion (1) and post-extrusion UV crosslinking of star copolypeptide hydrogels (2). (a) Benzyl-L-glutamate (BLG) NCA, DMF/$CHCl_3$, 0°C; (b) Valine NCA, DMF/$CHCl_3$, 0°C. (c) Trifluoroacetic acid/33% HBr in acetic acid, rt. (d) Allyl alcohol, DCC/DMAP, DMSO, rt. Note: Star block copolypeptides comprise 32-arms; for simplicity only 6-arm star block copolypeptides are depicted.

SEC traces and ^{1}H-NMR spectra confirmed the successful development of the diblock copolypeptide architecture (Figure 4.1, 4.2). After deprotection, these amphiphilic star block copolypeptides spontaneously form hydrogels, presumably through hydrophobic interactions stemming from the self-assembly of the valine domains, which are known to cluster in beta motif arrangements.[38] The importance of the star shaped structure and sequence length is underpinned by the fact that the linear equivalents of the block copolypeptide does not form hydrogels. It would appear that the covalent point-like junctions of the star polypeptide core crucially contribute to the stable network formation. It was envisaged that the inclusion of physical

crosslinking domains in the form of valine isopropyl groups would facilitate the self-recovery and dissipation of shear stress when subject to needle-based extrusion. The reversibility of the bonding arises from the mobility of these noncovalent moieties which allow the initial mechanical properties of the hydrogel to remain uncompromised after shear processing.[39]

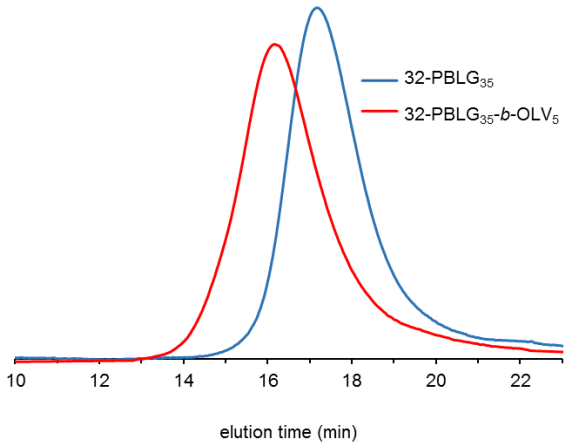

Figure 4.1: SEC trace showing peptide chain extension; 32-PBLG$_{35}$ (M_w 203,000, *Đ 1.14*) and 32-PBLG$_{35}$-*b*-OLV$_5$ (M_w 211,000, *Đ 1.22*).

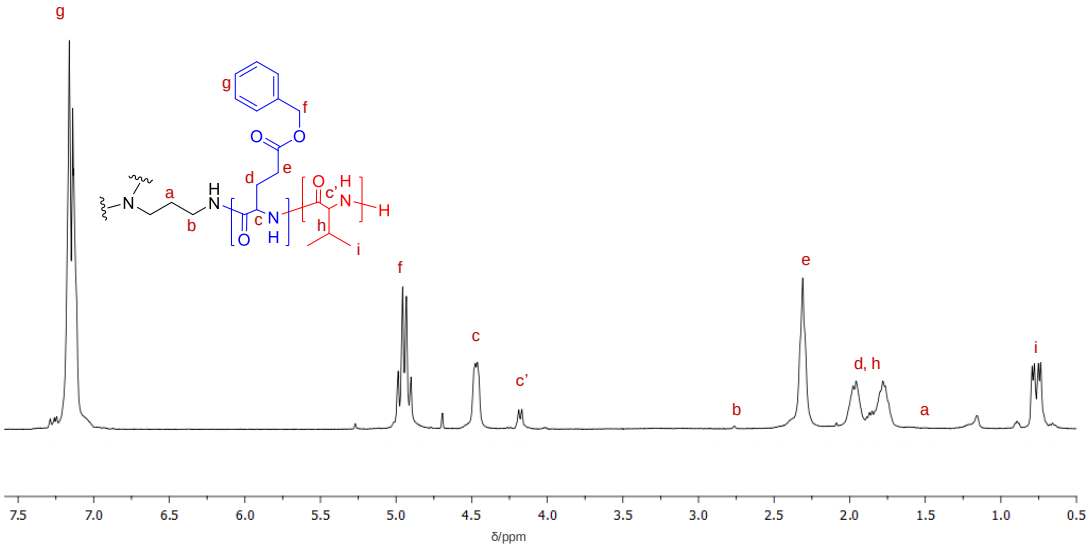

Figure 4.2: ^{1}H-NMR spectra of star shaped poly(benzyl-L-glutamate)-*b*-oligo(L-valine) in $CDCl_3$ (15% TFA-d).

As a robust construct was sought, a secondary crosslinking mechanism was included for mechanical stabilisation.[40] Prompting this, the copolypeptide was designed to include photo-crosslinkable allyl groups (Scheme 4.1). Post and pre-polymerisation modifications were carried out to identify the most suitable copolymer arrangement for UV crosslinking. Initially triblock star copolypeptides were prepared with set block sequence ratios in which an allyl-glutamate 5mer central block was incorporated (Scheme 4.2). However, this arrangement proved unsuitable for 3D printing purposes as after photo-crosslinking, shrinkage of the constructs was evident, structural resolution was lost and the materials became brittle.

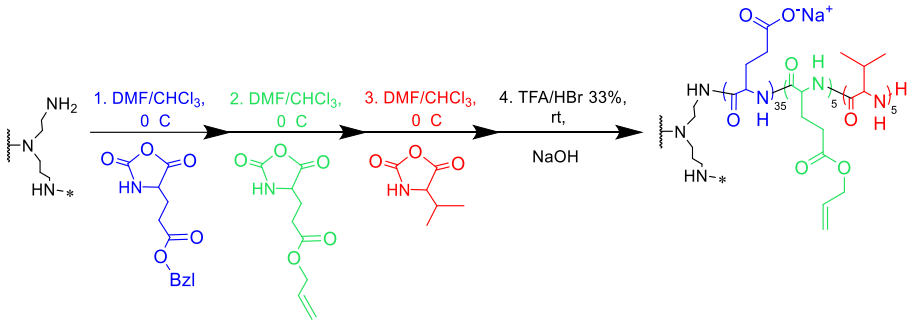

Scheme 4.2: Synthesis of star triblock copolypeptide denoting one single arm of the 32-arm PPI dendrimer.

As an alternative strategy, the diblock star copolypeptide was used with a post polymerisation esterification protocol. The poly(L-glutamic acid) (PGA) carboxyl groups were randomly condensed with allyl alcohol using DCC/DMAP to generate the crosslinkable allyl moieties with a targeted degree of substitution (~15% of PGA repeat units). Quantification of the allyl functionalities could not be determined due to the materials' high tendency to gel. The ratio of signal to noise in the ^{1}H-NMR spectra was almost identical due to the material swelling so representative allyl ester peaks were not observable but an ester band shift was noted in the FTIR spectra of the native and functionalised polymers (Figure A7).

4.3.2 Hydrogel properties

The hydrogel ink was trialed using handheld syringe-needle extrusion of structures with undefined patterns. These structures were found to maintain their shape and

conformity post UV curing so were deemed suitable for 3D printing. The hydrogel inks, were formulated as described in Table 4.1. The star polypeptide concentration in all aqueous formulations was 2.0 wt%. All formulations further contained photo initiator IRGACURE 2959 at different concentrations and, in the case of P3, N,N'-methylenebisacrylamide as a hydrophilic monomeric acrylate. The latter was envisaged to act as a reactive diluent to facilitate the crosslinking process.

Table 4.1: Summary of composition and water uptake ratios of the printable ink formulations developed from star copolypeptide hydrogels (PI: IRGACURE 2959; S1: star copolypeptide hydrogel; NMBAA: N, N'-methylenebisacrylamide).

Entry	Ink composition (per 1 mL ink)	Water uptake ratio[(a)] (hydrogel ink)	Water uptake ratio[(b)] (printed, UV crosslinked)
P1	20 mg S1, 1 mg PI	64.1 ± 1.5	11.2 ± 0.3
P2	20 mg S1, 5 mg PI	75.4 ± 1.7	12.4 ± 0.4
P3	20 mg S1, 5 mg PI, 8 mg NMBAA	74.3 ± 1.5	15.7 ± 0.2

(a) The water uptake ratio was determined from the equation $(W_S - W_D) / W_D$, where W_D is the mass of the polymer and starting materials in dry state and W_S is the hydrogel mass in the swollen state. (b) For the UV crosslinked construct, the water uptake ratio was determined from the same equation $(W_S - W_D) / W_D$, where W_D is the mass of the dried UV crosslinked construct and W_S is the mass of the construct in the swollen state.

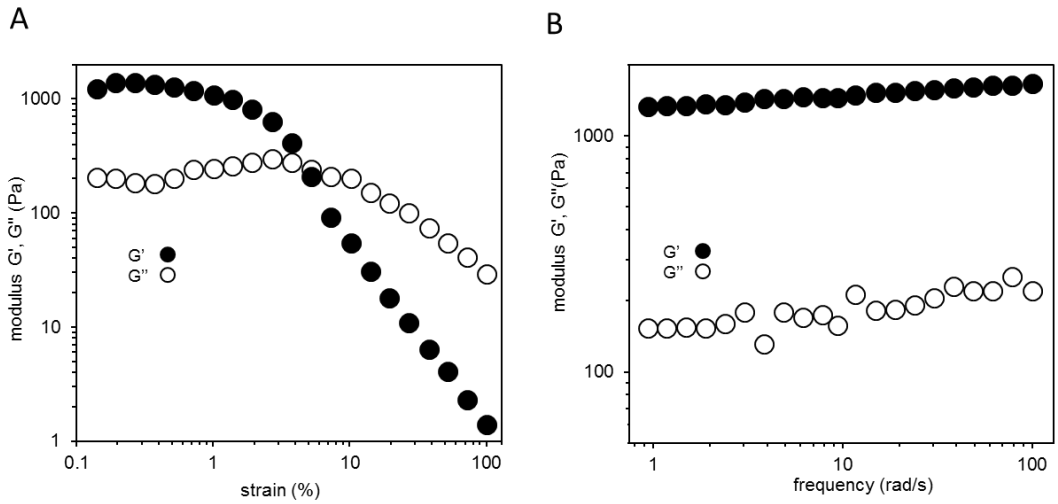

Figure 4.3: Rheological A) amplitude sweep (γ = 1-100%, ω = 1 rad s^{-1}) and B) frequency sweep (γ = 0.1%, ω = 1-100 rad s^{-1}) of the P1 hydrogel at 1.0 wt%. Closed and open spheres indicate storage (G') and loss (G") modulus values respectively.

To elucidate the ink formulations' suitability for 3D extrusion printing, the rheological properties of P1, P2 and P3 were evaluated. An amplitude sweep was carried out to identify the viscoelastic linear region of the star copolypetide hydrogel and determine its yield stress point (Figure 4.3A). The hydrogel maintained its rheological behavior until 4% strain was reached, the point in time when gel network collapse was observed. The hydrogel also exhibited oscillatory stability when subject to analysis over a wide range of frequencies (Figure 4.3B).

In order to mechanically simulate the shear induced self-recovery after the extrusion process, the dynamic modulus of the star copolypeptide inks were measured through a time sweep with steps in strain (Figure 4.4A). Alternating the strain from low to high had no significant impact on the storage modulus and loss modulus. The initial storage modulus value of 1513 ± 5 Pa (at 0.1% strain) recovered almost instantaneously to 1495 ± 6 Pa after stepping in strain (between 0.1% and 40%). Similarly, after subjecting the hydrogel to steps in strain (between 0.1% and 100%), the modulus recovered rapidly to 1522 ± 10 Pa. Once strain is reduced, rapid self-recovery of the hydrogel network occurs (30 seconds) as the bulk flow of the material is unhindered by the strain process. A UV mediated time sweep (Figure 4.4B) conveys enhanced

modulation of storage modulus values confirming the expected formation of covalent crosslinks. Once the hydrogel ink was UV irradiated, the allyl-glutamate residues polymerise with neighboring moieties forming a secondary hydrophobic chain within the hydrogel, resulting in the formation of a stronger gel network and thus an increase in storage modulus.

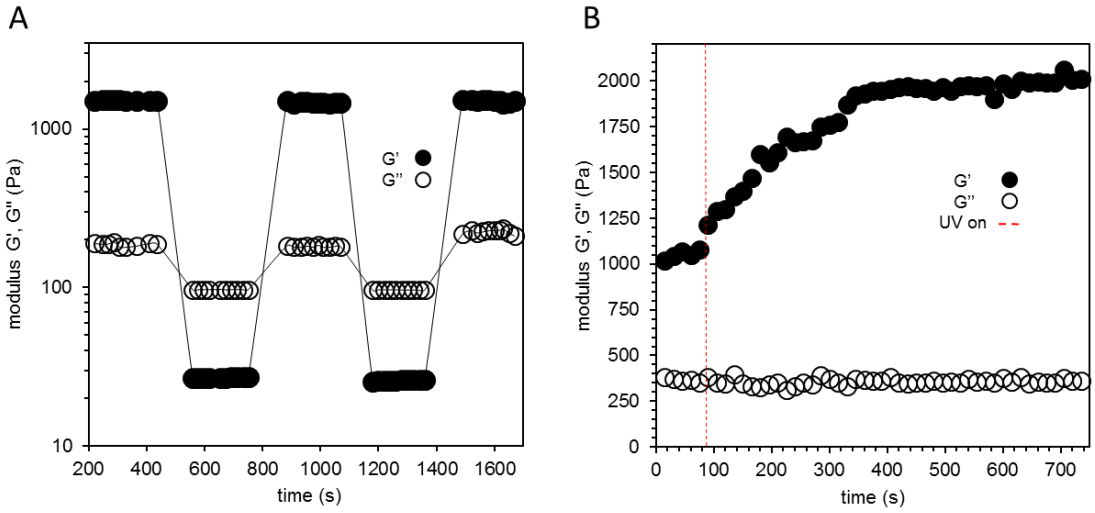

Figure 4.4: A) Rheological stepping strain based time sweep of hydrogel at 1.0 wt% (γ = 0.1% for 240 s, then γ = 40% for 240 s, then γ = 0.1% for 240 s, then γ = 100% for 240 s, then γ = 0.1% for 240 s; ω = 1 rad s^{-1}). B) UV mediated time sweep of the P1 hydrogel at 1.0 wt% (γ = 0.1%; ω = 1 rad s^{-1}).

4.3.3 3D extrusion of hydrogels

3D printing of hydrogels was carried out using a 3D printer comprised of a precision positioning system and an ink extrusion system. The hydrogel ink was loaded into a 5 mL syringe and centrifuged to remove any air bubbles present. The material was then extruded using 32 or 25-gauge extrusion tips at a constant speed and a programmed printhead movement (300 mm/min) onto a planar platform yielding well resolved constructs. As predicted by rheological analysis, all tested star block copolypeptide hydrogel formulations could form self-supporting micron sized structures at heights of up to 12 layers before UV curing (Figure 4.5A), demonstrating their remarkable mechanical robustness.

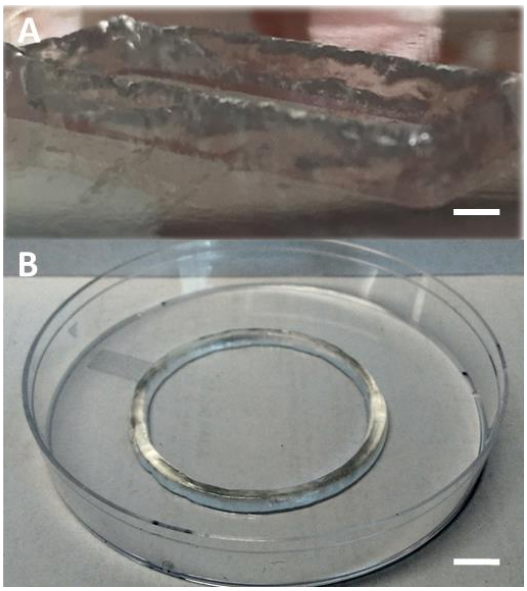

Figure 4.5: A) Image of 12 layered construct after 3D extrusion but before UV curing. B) Image of ring construct after 3D extrusion and UV curing. Scale bar = 10 mm.

Furthermore, intricate printing patterns were easily attained with resulting structures devoid of any shear related flow behavior. The constructs were then immobilised through UV initiation of surface allyl-glutamate residues with the radical species of IRGACURE 2959, yielding stabilised hydrogel prints. Both arbitrary grid and ring-shaped structures (Figure 4.5B, 4.6A, 4.6B) were 3D patterned with the printed track resolution ranging from the mm to μm scale as a result of alternating the extrusion parameters. Markedly improved deposition and structural definition was observed after switching the nozzle size (32 to 25 gauge) and changing the extrusion deposition speed (30 mm/s to 25 mm/s). The resulting structures maintained micrometer spacing between adjacent tracks even after UV curing. A cross section of the printed ring was analysed using a scanning electron microscope revealing a micro-porous network of intertwined fibers. The position of elongated fibers in the core with more densely packed antiparallel/parallel fibers present near the edges suggest bulk chemical crosslinking towards the surface of the construct (Figure 4.6D).

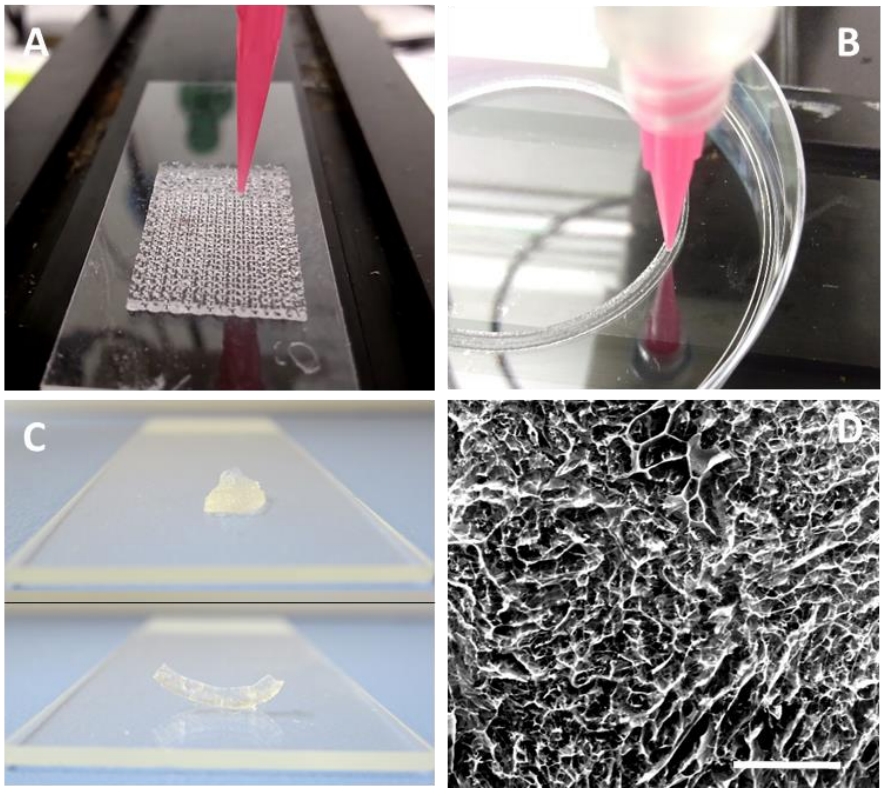

Figure 4.6: A) Image of hydrogel grid structure during 3D extrusion printing and before UV crosslinking at a polymer fraction of 2.0 wt%. B) Image of hydrogel ring structure (8 cm diameter) during 3D extrusion and before UV crosslinking at a polymer fraction of 2.0 wt%. C) Hydrogel ink before (top) and after (bottom) 3D fabrication and UV curing. D) Scanning electron microscopy image of cross section of hydrogel construct after UV curing. Scale bar = 100µm.

4.3.4 Degradation, drug release and cell studies

Without any intermediate work up, a portion of the printed structures were then subject to pH responsive degradation, highlighting a desirable feature of the star block copolypeptide material. No initial swelling was observed in the degradation analysis which could be a result of a maximum capacity of water already in the constructs. The expulsion of water during crosslinking in addition to the evaporation effects of the heat generated from UV irradiation would cause the structures to become less hydrated. This is demonstrated in the reduced water uptake of constructs after UV crosslinking (Table 4.1). In terms of bulk mass loss, the profile of P1 was quicker than that of the P2 construct when subject to incubation in neutral isotonic media over a 30-day period (Figure 4.7A). Moreover, the decomposition of P3 was found to be even

more prolonged in comparison to P1 and P2 as deduced from the linear curve fit. This could be due to the higher degree of crosslinking caused by the presence of the reactive diluent in addition to the inferior degradation profile of poly(acrylamide)s in comparison to poly(allylester)s.

A stark profile change was observed in both basic and acidic pH, which accelerate peptide degradation through hydrolysis (Figure 4.7B, 4.7C). After a 21-day period at neutral pH, 55 ± 3 % of scaffold P1 remained compared to 36 ± 2 % when subject to incubation at pH 2.0. Hydrolytic cleavage of the ester bonds and the peptide backbone would result in deconstruction of chemical and physical crosslinks and subsequent chain scission.[41] Significant disassembly of the hydrogel construct started to become evident after 22 days when small portions became deconstructed from the bulk structure, suggesting unravelling of the secondary structure and the supramolecular crosslinks within the network in each pH medium. We can deduce that the hydrogel constructs possess labile bonding for degradation in a variety of pH environments and thus potentially in biological-fluids, meaning the polymer fraction can diminish and ultimately degrade fully in a biological environment.

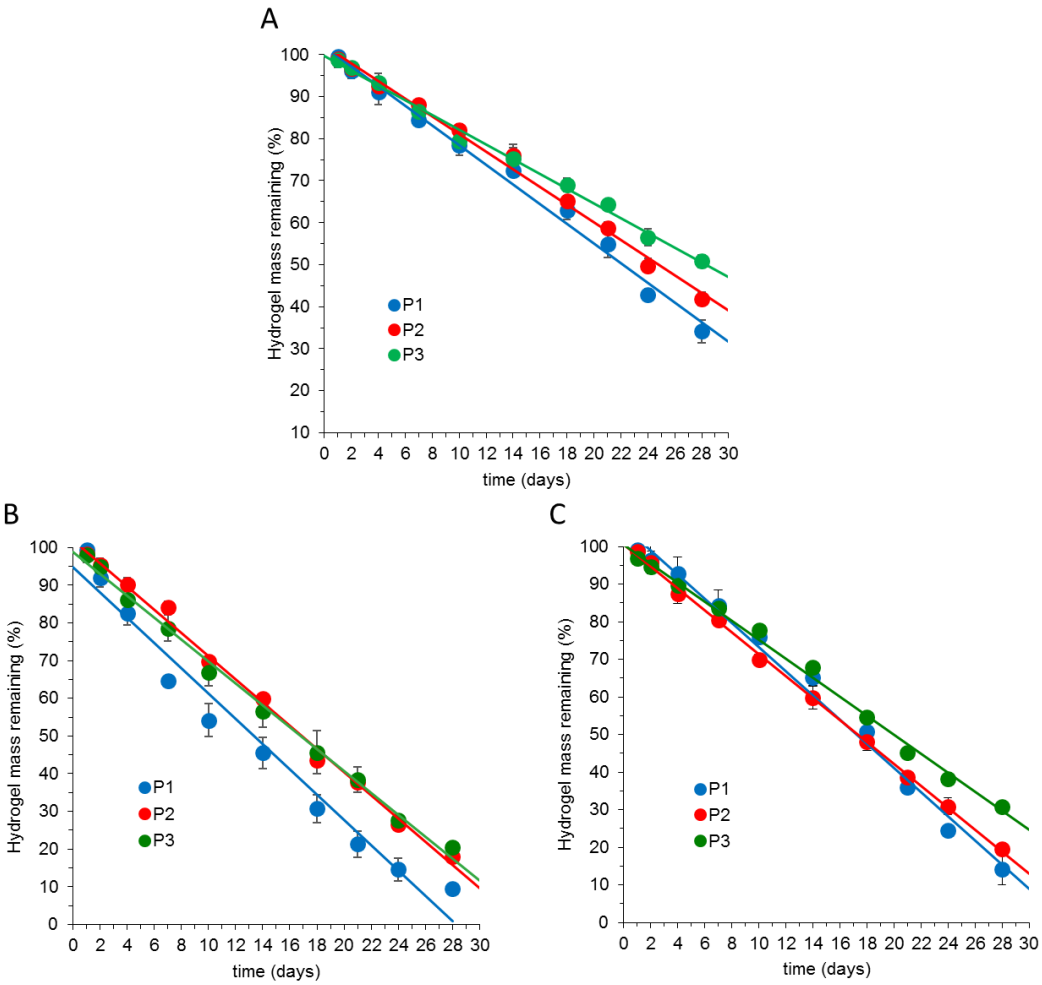

Figure 4.7: Hydrolytic degradation of small portions (150 – 200 mg) of UV-cured P1, P2 and P3 ring constructs in A) neutral PBS buffer media, B) basic PBS buffer media and C) acidic PBS buffer media (Straight lines denote linear fit).

The degradation profile coupled with the presence of both hydrophobic physical and chemical domains, indicated the capability to encapsulate and release molecular cargo. Initially, the hydrogel inks were loaded with the small molecule drug doxorubicin hydrochloride (DOX.HCl). 3D extrusion was carried out in a similar manner as described albeit with the addition of 2% DOX.HCl (w/w). Ring shaped structures were readily attained although a longer exposure to UV was necessary in order to form a mechanically supported drug loaded gel construct, which is potentially due to inferior penetration of UV light through the slightly red colored hydrogel construct and thus slower activation of the photo initiator. All hydrogel constructs were subject to release at neutral pH and the released drug was quantified

by UV spectroscopy (Figure 4.8A). DOX.HCl loaded P1 exhibited an initial burst release (28 ± 3 %) within the first 50 hours followed by a steady release of another 10 % up to 350 hours. In comparison, a less pronounced burst release was observed for P2 resulting in lower release after 50 hours (13 ± 2 %), potentially due to the higher degree of inter network crosslinking in the P2 structure. This is presumably due to the use of 5-fold excess of photo initiator in P2 which would contribute to a higher concentration of radicals upon UV stimulation resulting in higher density of radically mediated crosslinks.[19] A lower burst release was also observed for P3, possibly for the same reason of higher crosslink density. Following the initial burst release all samples display a continuous steady drug release, which correlates with the material degradation and simultaneous diffusion. The P1 loaded construct was also subject to acid stimulated release as a comparison (Figure 4.8B). After 168 hours (7 days) in neutral media 33% ± 2 % was released at neutral pH while 45 ± 4 % was released in the acidic media. This could be prompted by the deionisation of sodium glutamate residues to the corresponding free acid resulting in condensation of the hydrogel construct triggering an increased amount of DOX.HCl to be released.

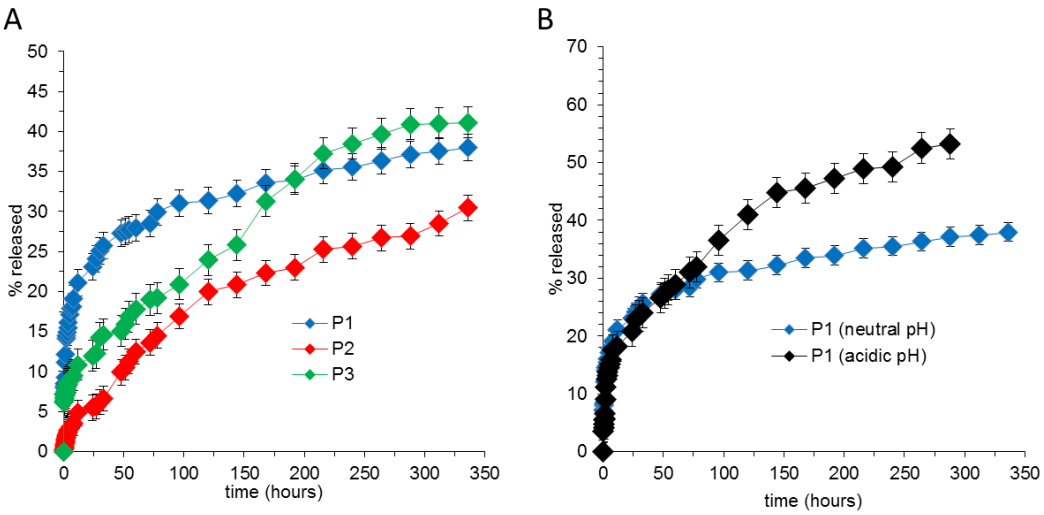

Figure 4.8: A) DOX.HCl release of P1-P3 in neutral PBS buffer media. B) DOX.HCl release of P1 in neutral and acidic pH.

The cytotoxicity of polymer constructs was investigated by incubating Balb/3T3 cells in the presence of 1 ml of extracted leachates from each of P1, P2 and P3. Balb/3T3

cells are an adherent, fibroblastic cell line which are a commonly utilised cell type within the literature for assessing the potential *in vitro* cytotoxicity of novel polymeric materials.[42]

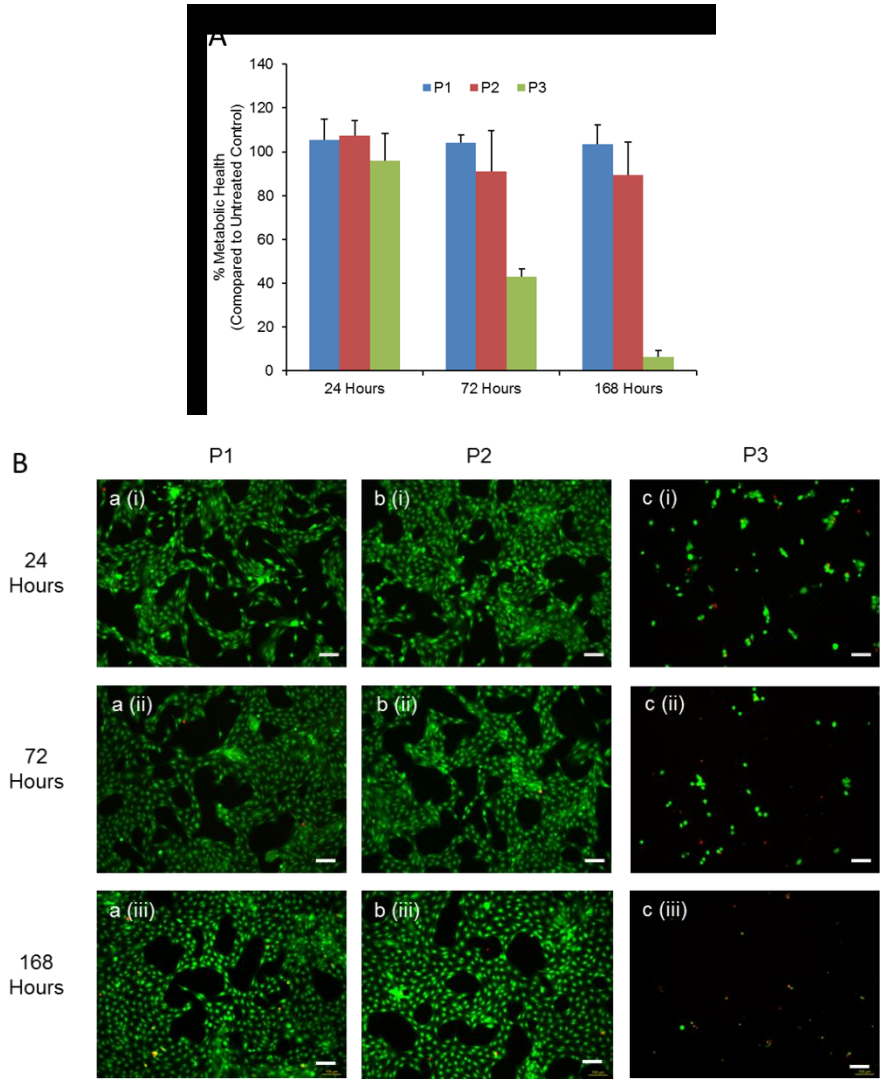

Figure 4.9: A) Effect of extracted ring construct leachates on Balb/3T3 metabolic health. Balb/3T3 cells were incubated in the presence of 1 ml of extracted leachates from each of P1, P2 and P3. A significant reduction in the metabolic health of Balb/3T3 cells was evident following incubation with extracted leachates from P3. B) Live/Dead fluorescence microscopy images of Balb/3T3 Cells Following Incubation with extracted leachate. Balb/3T3 cells which been incubated in the presence of extracted leachates from each of P1 (a), P2 (b) and P3 (c) at 24 hours (i), 72 hours (ii) and 168 hours (iii). Viable cells will fluoresce green while dead cells fluoresce red. Scale bar = 100µm.

It was found that the cells do not suffer from a reduced metabolic state due to being exposed to the extracted leachates from P1 and P2 for up to 7 days (Figure 4.9). This implies that these two polymers are not leaching out any materials/by-products which could result in either acute or delayed toxicity effects on these cells. Indeed, cells treated with P1 extracted leachates have a metabolic health of 105.5 ± 9.3% at 24 hours which is maintained at 103.5 ± 8.9 % by 168 hours. Similarly, P2 has an initial metabolic health of 107.5 ± 6.7 % at 24 hours which falls to 90 ± 14 % by 168 hours. In contrast, P3 resulted in a significant reduction in cell metabolic health over the time course of the study. Initial, acute toxicity of exposure to extracted leachates from P3 was not evident as observed by an initial metabolic activity of 95.9 ± 12% at 24 hours. However, delayed toxicity of exposure to these leachates is clearly present as evident by a reduction in the metabolic health to 6.2 ± 3% by 168 hours. In corroboration of these results, Live/Dead imaging demonstrated a healthy monolayer of live (green) cells for both P1 and P2 leachate treated Balb/3T3 cells (Figure 4.9). In this instance, the cell density appeared to increase over time, indicating a proliferating monolayer, a result also observable using phase contrast imaging (Figure A8). In contrast, cells treated with P3 leachates displayed a decrease in cell density over time, with both reduced live (green) and dead (red) cells suggesting the leachates were causing cells to detach from the adherent plastic. These findings are hypothesised to be due to the delayed intracellular processing of excess unreacted N,N'-methylenebisacrylamide monomer present in P3. Overall, the extracted leachates from P1 and P2 do not appear to be toxic to the commonly used Balb/3T3 fibroblast cell line similar to that of the untreated control (Figure A9) while those extracted from P3 are associated with a delayed toxicity effect.

4.4 Conclusions

Novel hydrogels based on amphiphilic star block copolypeptide capable of structural microfabrication using 3D extrusion printing were developed. It was demonstrated that the composition of the materials is ideally suited for 3D printing; with scaffolds capable of maintaining structural cohesion after extrusion. In particular, extrusion

printing allows for rapid prototyping enabling the fabrication of defined intricate microstructures, providing a platform for complex scaffold development that would be otherwise unattainable with other processing techniques such as molding or casting. Alternatively, multiscale structures could also be readily attained through varying the printing parameters. The constructs were found to be degradable, exhibited favorable release of encapsulated molecular cargo and did not affect the metabolic health of the commonly used fibroblastic cell line, Balb/3T3 cells. The versatility of the material can allow for modulation of hydrogel ink properties, thus providing a plethora of possibilities for optimised tissue construction using 3D printing.

4.5 References

1 M. E. Furth, A. Atala, M. E. Van Dyke, *Biomaterials,* 2007, 28, 5068.

2 F. J. O'Brien, *Mater. Today,* 2011, 14, 88.

3 R. R. Jose, M. J. Rodriguez, T. A. Dixon, F. Omenetto, D. L. Kaplan, *ACS Biomater. Sci. Eng.,* 2016, 2, 1662.

4 J. Li, M. Chen, X. Fan, H. Zhou, *J. Transl. Med.*, 2016, 14, 271.

5 Y. Shanjani, C. C. Pan, L. Elomaa, Y. A. Yang, *Biofabrication,* 2015, 7, 045008.

6 Z. Wang, R. Abdulla, B. Parker, R. A. Samanipour, *Biofabrication,* 2015, 7, 045009.

7 L. Ouyang, C. B. Highley, W. Sun, J. A. Burdick, *Adv. Mater.*, 2017, 29, 1604983.

8 S. E. Bakarich, M. in het Panhuis, S. Beirne, G. G. Wallace, G. M. Spinks, *J. Mater. Chem. B*, 2013, 1, 4939.

9 T. Xu, W. Zhao, J. M. Zhu, M. Z. Albanna, J. J. Yoo, A. Atala, *Biomaterials* 2013, 34, 130.

10 B. V. Slaughter, S. S. Khurshid, O. Z. Fisher, A. Khademhosseini, N. A. Peppas, *Adv. Mater.,* 2009, 21, 3307.

11 M. W. Tibbitt, K. S. Anseth, *Biotechnol. Bioeng.,* 2009, 103, 655.

12 S. Van Vlierberghe, P. Dubruel, E. Schacht, *Biomacromolecules*, 2011 12, 1387.

13 W. L. Ng, W. Y. Yeong, M. W. Naing, *Int. J. Bioprinting,* 2016*,* 2, 53.

14 J. Jia, D. J. Richards, S. Pollard, Y. Tan, J. Rodriguez, R. P. Visconti, T. C. Trusk, M. J. Yost, H. Yao, R. R. Markwald, Y. Mei, *Acta Biomater*., 2014*,* 10, 4323.

15 C. Colosi, S. R. Shin, V. Manoharan, S. Massa, M. Costantini, A. Barbetta, M. R. Dokmeci, M. Dentini, A. Khademhosseini, *Adv. Mater.*, 2016, 28, 677.

16 C. B. Highley, C. B. Rodell, J. A. Burdick, Direct *Adv. Mater.*, 2015, 27, 5075.

17 A. L. Rutz, K. E. Hyland, A. E. Jakus, W. R. Burghardt, R. N. Shah, *Adv. Mater.,* 2015, 27, 1607.

18 S. E. Bakarich, R. Gorkin, M. in het Panhuis, G. M. Spinks, *Macromol. Rapid Commun.*, 2015, 36, 1211.

19 R. Gaetani, P. A. Doevendans, C. H. G. Metz, J. Alblas, E. Messina, A. Giacomello, J. P. G. Sluijter, *Biomaterials,* 2012, 33, 1782.

20 K. S. Lim, B. S. Schon, N. V. Mekhileri, G. C. Brown, C. M. Chia, S. Prabakar, G. J. Hooper, T. B. Woodfield, *ACS Biomater. Sci. Eng.,* 2016, 10, 1752.

21 L. Shi, H. Carstensen, K. Hölzl, M. Lunzer, H. Li, J. Hilborn, A. Ovsianikov, D. A. Ossipov, *Chem. Mater.,* 2017, 29, 5816.

22 N. Hadjichristidis, H. Iatrou, M. Pitsikalis G. Sakellariou, *Chem. Rev.,* 2009, 109, 5528.

23 C. M. González-Henríquez, M. A. Sarabia-Vallejos, J. Rodríguez-Hernández, *Polymers,* 2017, 9, 551.

24 A. P. Nowak, V. Breedveld, L. Pakstls, B. Ozbas, D. J. Pine, D. Pochan, T. J. Deming, *Nature*, 2002, 417, 424.

25 J. Huang, C. L. Hastings, G. P. Duffy, H. M. Kelly, J. Raeburn, D. J. Adams, A. Heise, *Biomacromolecules,* 2013, 14, 200.

26 C. Bonduelle, *Polym. Chem.,* 2018, 9, 1517.

27 Y. Chen, X. H. Pang, C.M. Dong, *Adv. Funct. Mater.,* 2010, 20, 579.

28 T. J. Deming, *Chem. Rev*., 2016, 116, 786.

29 S. B. Hanay, B. Ritzen, D. Brougham, A. A. Dias, A. Heise, *Macromol. Biosci.,* 2017, 17, 1700016.

30 S. B. Hanay, D. F. Brougham, A. A. Dias, A. Heise, *Polym. Chem.,* 2017, 8, 6594.

31 C. Li, A. Faulkner-Jones, A. R. Dun, J. Jin, P. Chen, Y. Xing, Z. Yang, Z. Li, W. Shu, D. Liu, R. R. Duncan, *Angew. Chem. Int. Ed.,* 2015, 54, 3957.

32 G. J. Habraken, M. Peeters, C. H. Dietz, C. E. Koning, A. Heise, *Polym. Chem.*, 2010, 1, 514.

33 M. Byrne, R. Murphy, A. Kapetanakis, J. Ramsey, S. A. Cryan, A. Heise, *Macromol. Rapid Commun.,* 2015, 36, 1862.

34 N. Higashi, T. Koga, N. Niwa, M. Niwa, *Chem. Commun*., 2000, 0, 361.

35 S. J. Lam, N. M. O'Brien-Simpson, N. Pantarat, A. Sulistio, E. H. H. Wong, Y. Chen, J. C. Lenzo, J. A. Holden, A. Blencowe, E. C. Reynolds, G. G. Qiao, *Nat. Microbiol.*, 2016, 1, 16162.

36 M. Byrne, P. D. Thornton, S. A. Cryan, A. Heise, *Polym. Chem.*, 2012, 3, 2825.

37 R. Murphy, T. Borase, C. Payne, J. O'Dwyer, S. A. Cryan, A. Heise, *RSC Adv.*, 2016, 6, 23370.

38 V. Munoz, P. A. Thompson, J. Hofrichter, W. A. Eaton, *Nature,* 1997, 390, 196.

39 M. Guvendiren, H. D. Lu, J. A. Burdick, *Soft Matter,* 2012, 8, 260.

40 W. Schuurman, P. A. Levett, M. W. Pot, P. R. van Weeren, W. J. A. Dhert, D. W. Hutmacher, F. P. W. Melchels, T. J. Klein, J. Malda, *Macromol. Biosci.,* 2013, 13, 551.

41 T. Akagi, M. Higashi, T. Kaneko, T. Kida, M. Akashi, *Biomacromolecules*, 2006, 7, 297.

42 A. A. Ignatius, L. E. Claes, *Biomaterials*, 1996, 17, 831.

CHAPTER 5

POLYPEPTIDE ORGANO/HYDROGELS FROM DIFUNCTIONAL NCA

Abstract

The design of both solvent and water gelators from the same structural scaffold is challenging, so a chemical transformation is usually necessary in order to realise both material properties. In this work we report the synthesis of a new difunctional N-carboxyanhydride (NCA) monomer, namely diaminopimelic acid (DAPA), and its use in the one-pot preparation of an organogelating copolypeptide. The organogel is formed *in situ* through ring opening polymerisation (ROP) of DAPA NCA with helical poly(-carbobenzyloxy-L-lysine) (PZLL) sequences in a mixture of DMF/chloroform. After removing the solvent, the copolypeptide was tested for its uptake of a range of different organic solvents. Interestingly, after removal of the carbobenzyloxy (cbz or Z) protecting groups, the network remained intact in exceedingly high aqueous concentrations (99.5%). FTIR was used to characterise the secondary structure, revealing the crosslinking arrangements that contributed to gelation with the mechanical properties of the gel analysed via rheological assays.

5.1 Introduction

Gelators are an important class of three-dimensional networks composed of different physico-chemical domains. Composed of polymeric sequences that bear permeable molecular crosslinking junctions, these materials function as a swellable matrix permitting the uptake and encapsulation of water or organic solvents. Polymeric hydrogels are a particularly interesting class of mimetic matrices due to their biological relevance. They are composed of hydrophilic regions which are capable of entrapping high concentrations of water with an interconnected polymeric network analogous to that of the extracellular matrix, rendering them suitable as augmented biomaterials.[1, 2] Macromolecular modelling of native protein interactions has led to synthetic polypeptide based hydrogels that can be modulated by optimising the chemistry of amino acid side groups. The inherent self-assembly of polypeptide amphiphiles has been explored by many groups as a basis for gelation. Native amino acids have been utilised as polymeric blocks in these supramolecular gelators, contributing to material with tailored mechanical properties due to control of conformational assemblies.[3,4] The physical bonding contributing to gelation usually emanates from the polypeptide chain composition via electrostatic interactions,[5] hydrophobic interactions,[6] hydrogen bonding,[7] stacking[8], and van der Waals forces.[9] The resulting hydrogels possess relatively moderate mechanical strength in addition to unique properties as a consequence of their reversible non-covalent bonding character. In chemically crosslinked hydrogels, the framework consists of covalent networks formed through stepwise orthogonal chemical reactions. A number of reactions have been used in the generation of polypeptide organogels/hydrogels such as thiol-ene click,[10] schiff-base[11] enzyme induced crosslinking,[12] radical polymerisation[13] and the recently utilised triazolinedione (TAD) click reaction.[14]

Covalent crosslinks evident in nature are limited to the spontaneously occurring disulphide bond of native cysteine residues.[15] Cystine, the endogenous dimerised version of oxidised cysteine, is the only naturally occurring difunctional amino acid. To the best of our knowledge, there has only been one difunctional amino acid monomer synthesised and used in NCA ROP, namely cystine NCA.[16, 17] For the development of core

crosslinked star (CCS) polypeptides cystine NCA has been successfully used as a crosslinker using arm first approaches. Chen and coworkers have reported the use of a PEG-NH_2 initiated copolymerisation of benzyl-L-glutamate (BLG) NCA or carbobenzyloxy-L-lysine (ZLL) NCA with L-cystine NCA, which formed nanogels post-deprotection.[18] The nanogels demonstrated a promising release profile of doxorubicin (DOX) molecular cargo in both reductive and acidic conditio

material design was reported by Jing et al.[19] A novel near infrared (NIR) cyanine dye was loaded into a cystine containing copolypeptide nanogel, with a reduction stimulus inducing the disassembly of the nanogel and promoting the release of the hydrophobic cyanine dye inside HepG2 carcinoma cells.

Herein, we propose a one-pot approach to synthesise organogels based on a core crosslinked copolypeptide and its conversion to mechanically robust hydrogels. Using a novel difunctional NCA (*N*-carboxyanhydride), stiff organogels were synthesised through -helical PZLL (poly-Z-L-lysine) chains. Acid hydrolysis of Z protecting groups was conducted to assess the uptake in aqueous conditions, which afforded strong hydrogels. To the best of our knowledge, this is the first reported case of the synthesis and use of the difunctional DAPA (diaminopimelic acid) NCA monomer in the development of polymeric materials.

5.2 Experimental

5.2.1 Materials

All chemicals were obtained from Sigma-Aldrich unless otherwise stated. Diaminopimelic -carbobenzyloxy-L-lysine and sarcosine were synthesised following a standard NCA literature procedure.[20]

5.2.2 Methods

^{1}H-NMR spectra were recorded on a Bruker Avance 400 (400 MHz) spectrometer at room temperature with TFA-d as a solvent. Attenuated total reflection (ATR) FTIR was recorded using a Thermo Scientific iS10 spectrometer in the region of 4000 400 cm^{-1}. A

background measurement was initially performed before analysing the sample. Sixteen scans were completed using a resolution of 2 cm^{-1}. Size exclusion chromatography (SEC)

was conducted in hexafluoroisopropanol (HFIP) using an PSS SECurity GPC system equipped with a PFG 7 µm 8 × 50 mm pre-column, a PSS 100 Å, 7µm 8 × 300 mm and a PSS 1000 Å, 7µm 8 × 300 mm column in series and a differential refractive index (RI) detector at a flow rate of 1.0 mL min^{-1}. The systems were calibrated against Agilent Easi-Vial linear poly(methyl methacrylate) (PMMA) standards and analysed by the software package PSS winGPC UniChrom. Rheological measurements were completed on a MCR 301 digital rheometer (Anton Paar). All experiments were conducted at room temperature using a conical plate (CP50-1, Anton Paar) consisting of a 50 mm diameter geometry and a gap length of 0.1 mm. The use of a protective hood was employed to prevent evaporation.

5.2.3 Preparation of diaminopimelic acid NCA

-pinene (5.73 g, 42.06 mmol) were suspended in 130 mL of anhydrous THF in a three neck flask and heated to reflux. Then triphosgene (4.99 g, 16.82 mmol) dissolved in 50 mL anhydrous THF was added dropwise. The mixture was allowed to stir for 24 hours at which point a clear solution was observed. The solution was bubbled with nitrogen for one hour then filtered and reduced under vacuum to yield an oil. After multiple precipitations in hexane an off yellow oil was obtained (yield: 45%).

5.2.4 Synthesis of poly-Z-L-lysine-*b*-poly-diaminopimelic acid

The NCA of -carbobenzyloxy-L-lysine (430 mg, 1.40 mmol) was dissolved in a 25 mL mixture of anhydrous $CHCl_3$ and DMF (5:1) in a Schlenk flask under a N_2 atmosphere. The flask was then placed in a thermostatically controlled water bath containing 5M NaCl at 0°C. Allylamine (1.34 mg, 2.34×10^{-2} mmol) was solubilised in 2.5 mL of anhydrous $CHCl_3$ and added via syringe to the Schlenk flask. The flask was evacuated under vacuum to liberate the CO_2 generated, with stirring allowed for 18 hours at 0°C. FTIR was used to confirm total consumption of the ZLL NCA monomer. The NCA of diaminopimelic acid

(85.01 mg, 3.51×10^{-1} mmol) was dissolved in 2.5 mL of DMF and quickly added via syringe to the Schlenk flask. The solution was allowed to stir at 0°C until full conversion of the DAPA NCA monomer was confirmed by FTIR. The gelled polymer was then precipitated into excess diethyl ether thrice and dried in a vacuum oven to afford the polymer (yield 82 %). *poly-sarcosine-*b*-poly-diaminopimelic was prepared by substituting ZLL NCA for sarcosine NCA while in the copolymer both NCAs were mixed before adding in the allylamine initiator.

5.2.5 Deprotection of poly-Z-L-lysine-*b*-poly-diaminopimelic acid

The dried polymer (350 mg) was then dissolved in 10 mL trifluoroacetic acid and allowed to stir until fully dissolved. Then, 2 mL of HBr (33% wt. in acetic acid) was added drop wise to the solution in a six-fold molar excess (with respect to -carbobenzyloxy-L-lysine protecting groups) and the solution was allowed to stir for 18 hours. The polymer was precipitated thrice into diethyl ether (40 mL) and centrifuged. After a final wash with diethyl ether, the material was dried under vacuum in a desiccator. The dried polymer was then immersed in deionised water at which point swelling was observed. The pH was brought to 7.0 and dialysis was performed against deionised water for 3 days using a 10kDa MWCO membrane. The polymer was then lyophilised (yield 70%).

5.3 Results and Discussion

5.3.1 Preparation and characterisation

In this work, -helical forming polypeptide block, poly(Z-L-lysine) (PZLL) was core crosslinked through the ROP of a new difunctional NCA monomer. The material provided swells in both organic and aqueous conditions, owing to it versatility as a stabilise -helix (in organic solvents) and a chain stabilised random coil (in aqueous media). The non-ionic polymer poly(sarcosine) (PSar) was used as a reference to investigate the differing macroscopic properties respectively. As shown is Scheme 5.1, allylamine initiated ROP of NCA ZLL at 0 °C (same for NCA Sar) was carried out to generate the corresponding homopolypeptides in a mixture of chloroform and DMF (5:1).

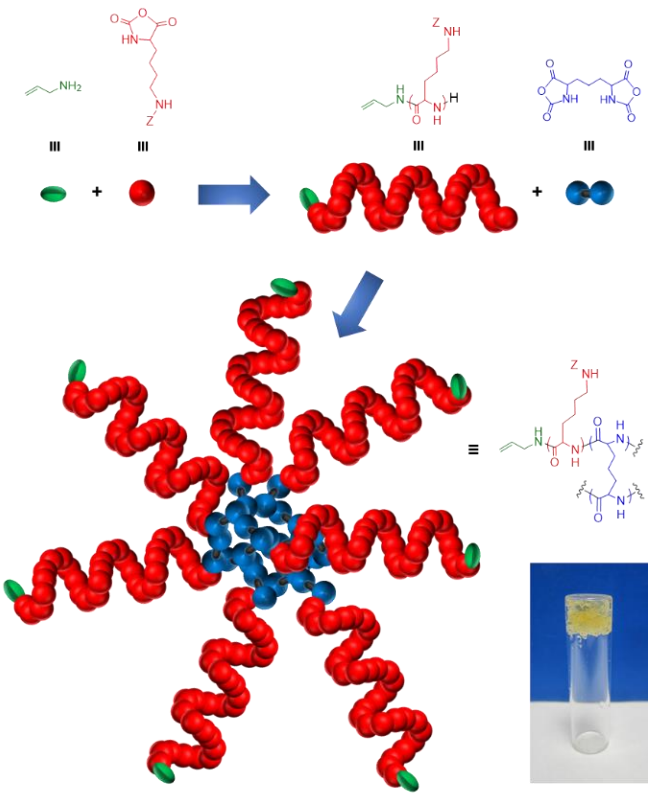

Scheme 5.1: Illustration of sequential ROP of ZLL NCA and DAPA NCA forming intercrosslinked network.

For the preparation of DAPA NCA, a modified method was used.[17] The monomer was then purified by multiple precipitations yielding an off white oily residue. The molecular structure was characterised and its purity confirmed with multiple methods, including FTIR, ^{1}H and ^{13}C NMR spectroscopies. Characteristic anhydride stretching bands from the NCA ring were present at 1841 and 1775 cm^{-1} in the FTIR spectra (Figure 5.1). The amide protons from the NCA rings can be seen in the ^{1}H NMR spectra with a signal at 9.25 ppm (Figure 5.2A). The ^{13}C NMR spectra confirms the presence of equivalent NCA anhydride carbonyls, which could be assigned to the peaks at 152 and 172 ppm respectively (Figure 5.2B).

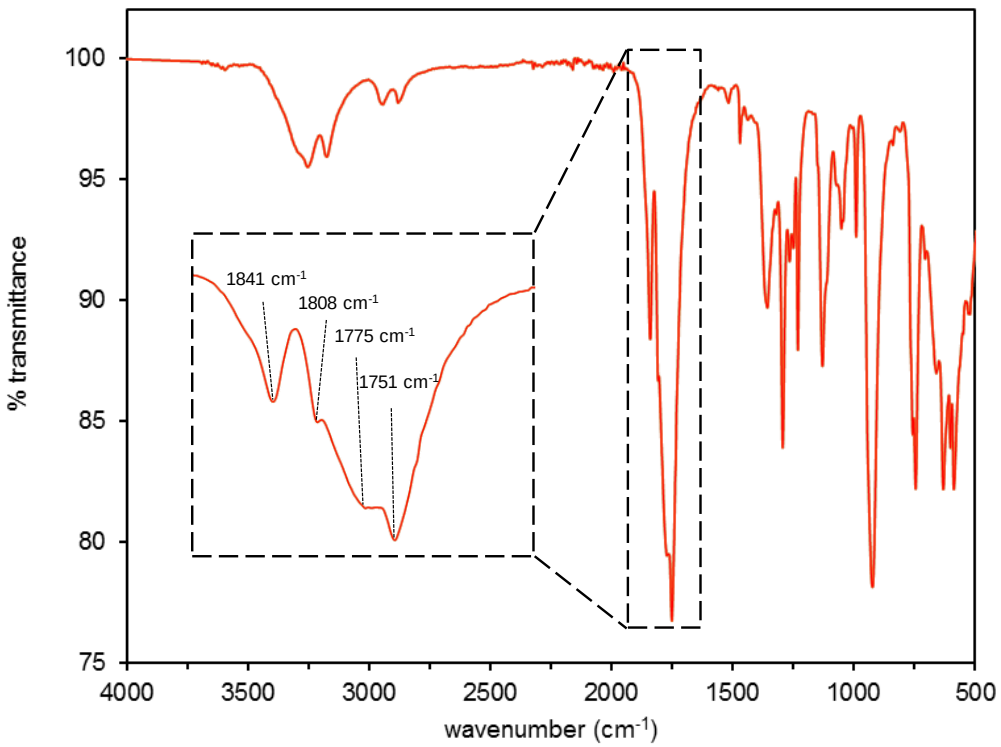

Figure 5.1: FTIR spectrum of diaminopimelic acid NCA highlighting anhydride band.

The initial PZLL and PSar structures were confirmed by the complete consumption of each respective NCA as deduced by FTIR. Acquisition of the homopolymer samples for SEC (Figure 5.3) were possible, however SEC traces for the diblock copolymers were not attainable as the diblocks swelled in HFIP. The addition of the DAPA NCA to the PZLL homopolypeptide in solution had no immediate effect on polymer solvation. However, after 2 days the entire solution was immobilised and would no longer stir (Figure 5.4).

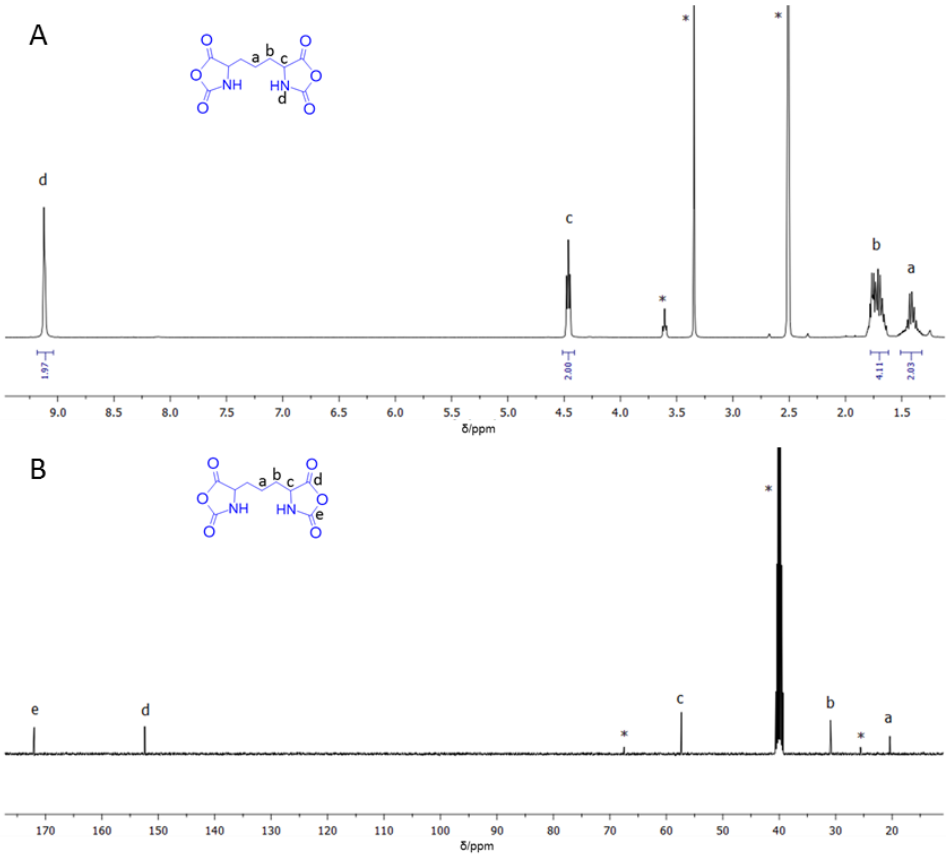

Figure 5.2: A) ^{1}H-NMR and B) ^{13}C-NMR spectrum of DAPA NCA (in DMSO-d^6).

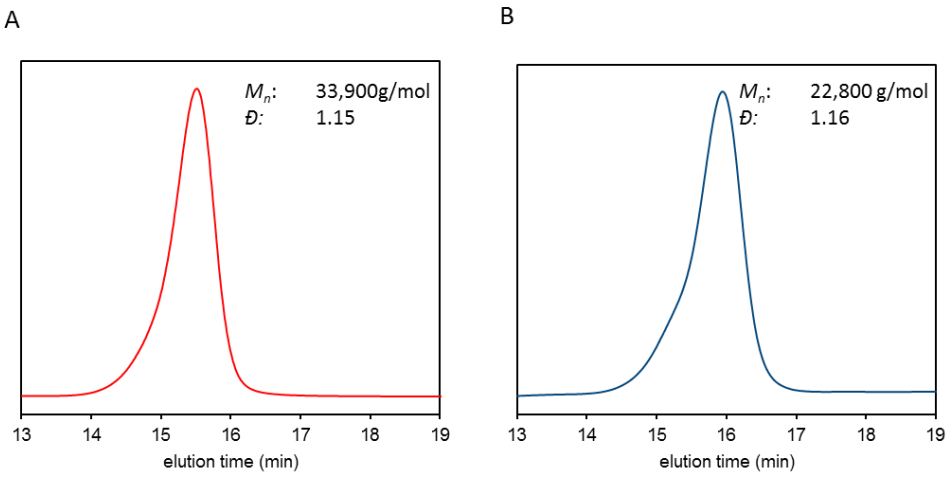

Figure 5.3: SEC traces with molecular weight and dispersities for initial blocks consisting of A) $PZLL_{80}$ (P1)and B) $PSar_{80}$ (P2).

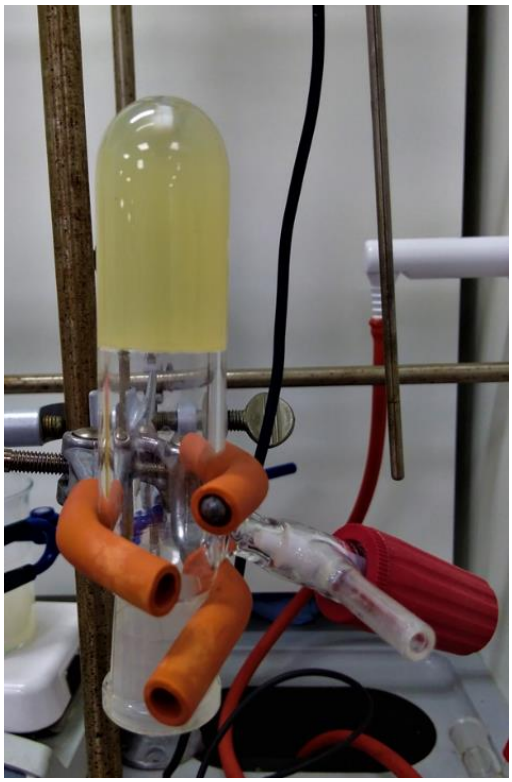

Figure 5.4: Organogel (1.9 wt%) in $CHCl_3$/DMF (5:1) mixture formed in schlenk flask.

It was difficult to obtain a well resolved ^1H NMR spectra for the copolypeptide as it gelled in all commonly used NMR solvent. Initial attempts resulted in spectra with suppressed proton signals from the characteristic PZLL highly crosslinked DAPA core (Figure 5.5). This is caused by the restricted movement of protons in the highly crosslinked polypeptide core, which leads to reduced mobility when subject to the NMR field and thus yielding a poor signal intensity.[21]

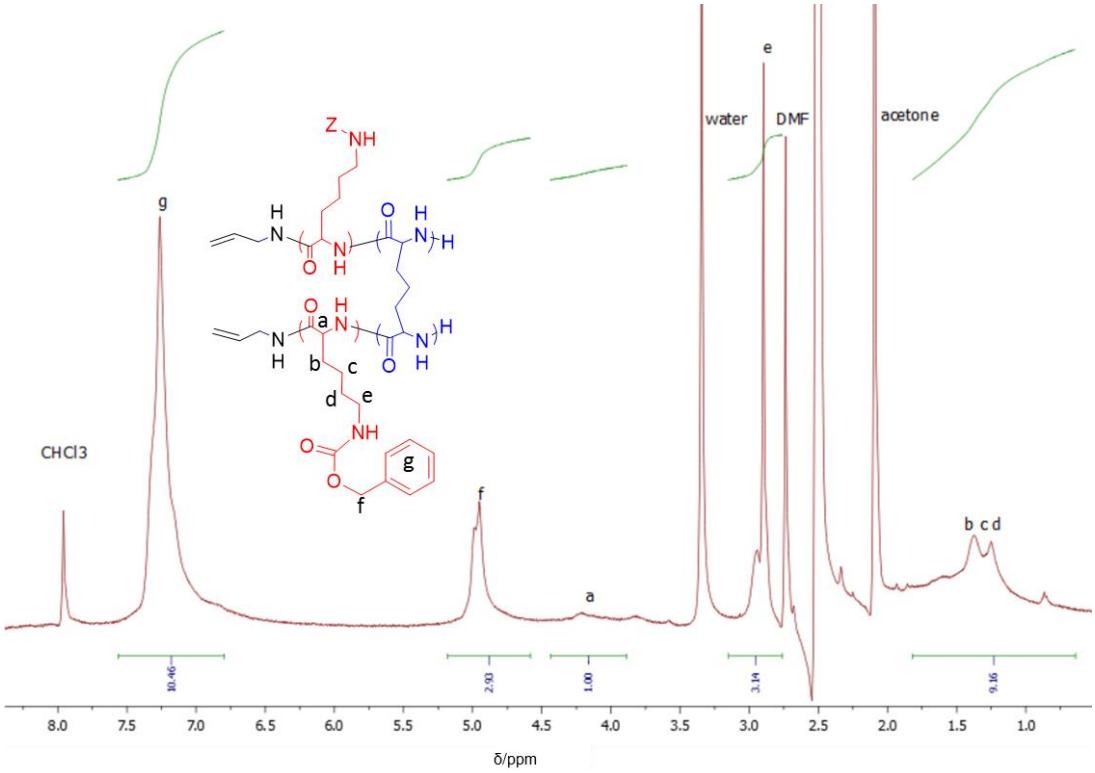

Figure 5.5: ^{1}H-NMR spectrum of PZLL-b-PDPA organogel (measured in DMSO-d^{6}).

stoichiometric control, switching the initial PZLL sequence for a PSar sequence failed to induce any *in situ* organogelation, rather the solution turned opaque and slight precipitation was observed. Since PSar is a predominately random coil forming sequence, it is devoid of the structural organisation of -helical forming PZLL, which is a conformation known to facilitate solvent gelation at sufficiently high concentrations.[22] Thus, for *in situ* gelation, maintaining the PZLL as the initial sequence was necessary in order to promote organogelation through subsequent macroinitiation of the difunctional NCA monomer. After precipitation of PSar-PDAPA polypeptide, it was found at higher polymer concentrations in both DMF and water.

5.3.2 Gel properties

After removing the entrapped solvent from each of the copolypeptides, they were trialed for uptake of a range of different organic solvents showing a particularly high efficacy for each of the polar aprotic solvents. They formed stable organogels in toluene, chloroform, dichloromethane, tetrahydrofuran (THF), ethyl acetate, dimethyl sulphoxide (DMSO), dimethylformaide (DMF), hexafluoroisopropanol (HFIP) and acetonitrile; while ethanol, methanol, isopropanol, hexane, petroleum ether and diethyl ether has no solubilising or swelling effect on the materials. Improvement in the gelation efficacy in DMF could be promoted by its hydrogen bonding breaking effect, resulting in a reduction of the helical self-assembly of the PZLL sequences and swelling due to the highly hydrophobic crosslinked core, similar to random coiling of the P2 PSar copolymer. To corroborate this, P1 was found to have a three-fold swelling ratio in comparison to P2 (Table 5.1). A similar uptake was also observed in P3 poly(L-lysine-co-diaminopimelic acid) copolymer.

Table 5.1: Swelling ratio of polymers in organic solvents and water

entry	polymer	swelling ratio[a]	swelling ratio[b]
P1	PZLL-b-PDAPA	12.8	32.8
P2	PSar-b-PDAPA	3.6	5.6
P3	PZLL-co-PDAPA	9.5	-

(a) The swelling ratio for DMF was determined from the equation (W_S W_D) / W_D, where W_D is the mass of the polymer in dry state and W_S is the organogel mass in the swollen state. (b) The swelling ratio for water was determined from the equation (W_S W_D) / W_D, where W_D is the mass of the polymer in dry state and W_S is the hydrogel mass in the swollen state.

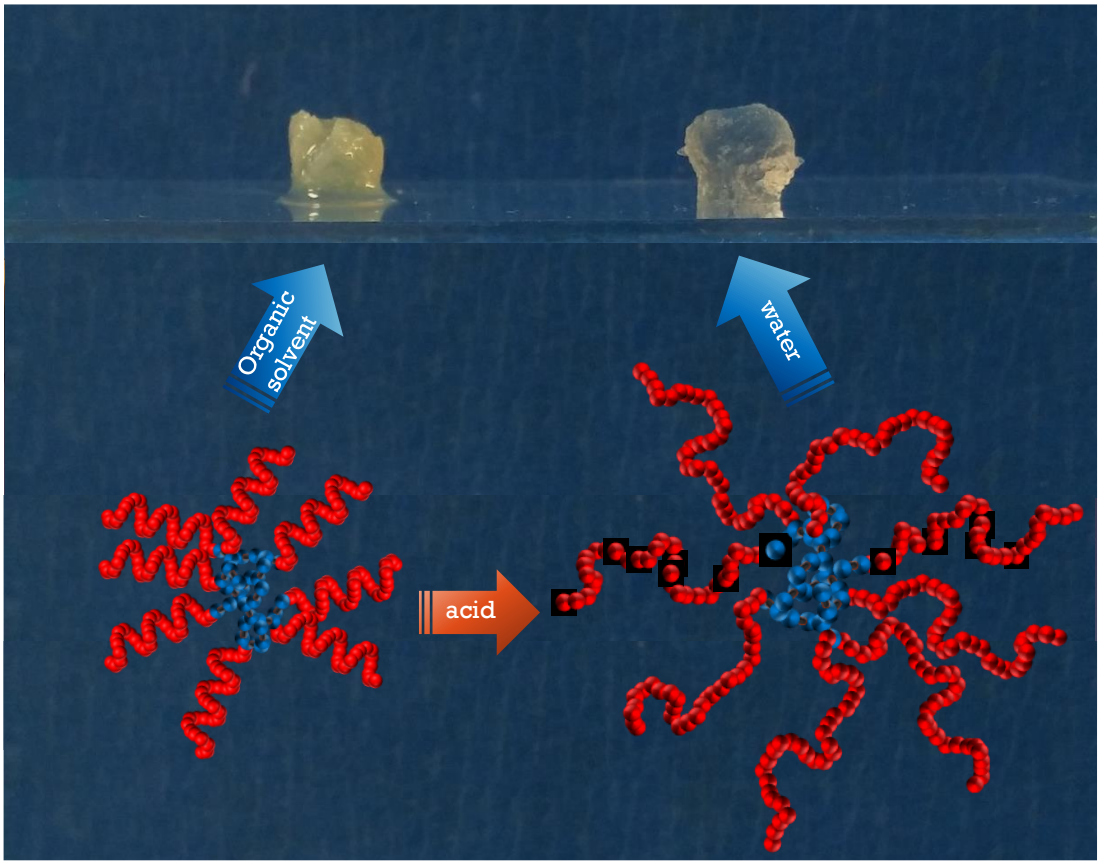

Scheme 5.2: Illustration denoting the organogel to hydrogel transition.

For P1 and P3, the Z protection group was removed by acidic treatment (TFA/HBr 33%) revealing the pendant ionised ammonium groups, promoting water solubility within the polymer architecture (Scheme 5.2). After removal of the excess acid with dialysis followed by lyophilisation of the materials, the hydrogelation ability of the now amphiphilic copolypeptides was examined using the vial Figure 5.6).

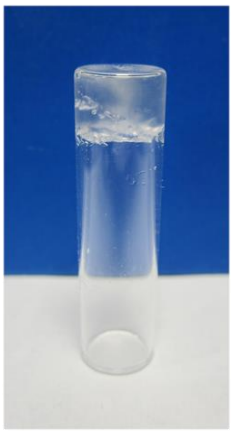

Figure 5.6: The core crosslinked copolypeptide hydrogel (P1) at 3.0 wt% in deionised water.

There was uptake of water for P1, forming a transparent hydrogel while interestingly P3 did not appear to uptake any water. For the sarcosine containing copolymer, P2, swelling in water was evident although at higher polymer concentration. The gels formed from P2 had a swelling ratio of 5.62 after an incubation period of 2 hours in water. Prompting this, only P1 was screened for its spectroscopic and rheological properties.

5.3.3 Structural conformation

FTIR spectroscopy was used to deduce backbone arrangements of the dried and swollen P1 organogel and hydrogel samples. Based on the orientation of the DAPA monomer after ROP, a multitude of turning and twisting conformation of this crosslinked peptide core could possibly be observable using FTIR -conformers in small peptides.[23] The homopolypeptide composed purely of PZLL is known to conveys characteristic bands in the amide I region (1650 cm^{-1}) correlating to the C=O, with the -amide Z protecting group stretch appearing above 1700 cm^{-1}. Interestingly, the dried P1 sample shows the split of this band into a multitude of peaks (Figure 5.7A).

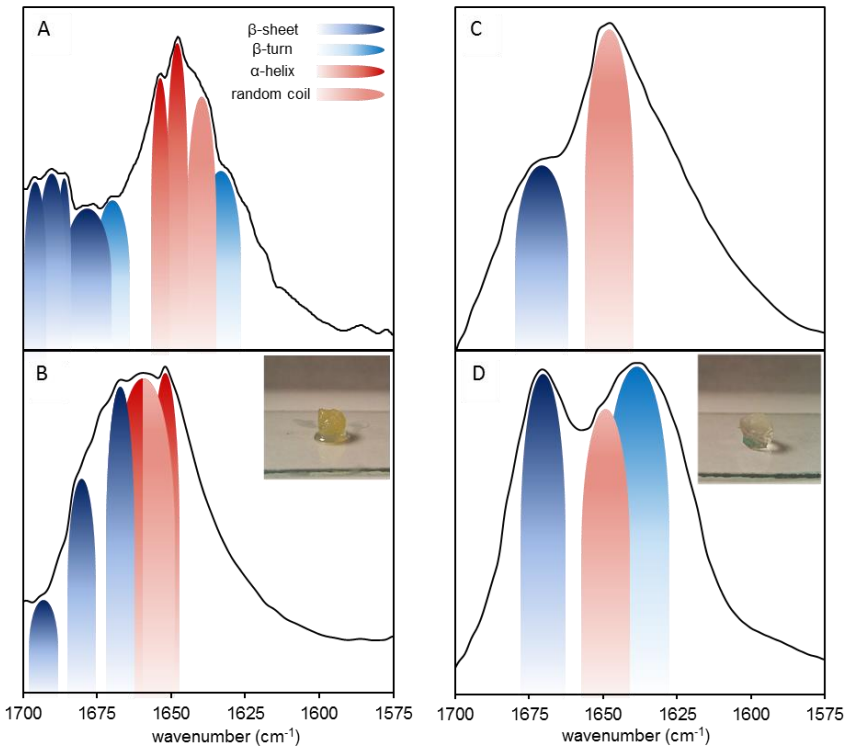

Figure 5.7: FTIR spectra of A) P1 dried organogel, B) P1 swollen organogel (in DMSO), C) lyophilised hydrogel and D) swollen hydrogel (in D_2O).

The bands at 1649/1652 cm^{-1} denote the helix, with random coiling observed at 1642 cm^{-1} and -motifs at 1632 and above 1660 cm^{-1}, probable cause of PDAPA core crosslinking. After P1 was swollen in a small volume of DMF, FTIR spectra of the resulting organogels displayed a broadened signal in the amide I region (Figure 5.7B). A strong band at 1658 cm^{-1} appeared -helix/random coil conformation, denoting the disruption of the hydrogen bonding associated with helix stabilisation. The -motif bands had receded, although peak shouldering was evident. For the deprotected P1 copolypeptide, the spectra displays two absorptions at 1647 and 1672 cm^{-1}, signifying -turn amide stretch. This correlates since the nature of the DAPA crosslink could cause the peptide backbone to orientate into multiple patterns (Figure 5.7C), with turning and twisting being a likely outcome.

Importantly, after swelling P1 in D_2O, the gel exhibited a significant shift in intensity of the -sheet and the -turn bands, with reduction of the random coil peak (Figure 5.7D). This potentially confirms the conformational state of DAPA crosslinking in the core since no intermolecular H-bonding contributes to the gelation.

5.3.4 Rheological properties

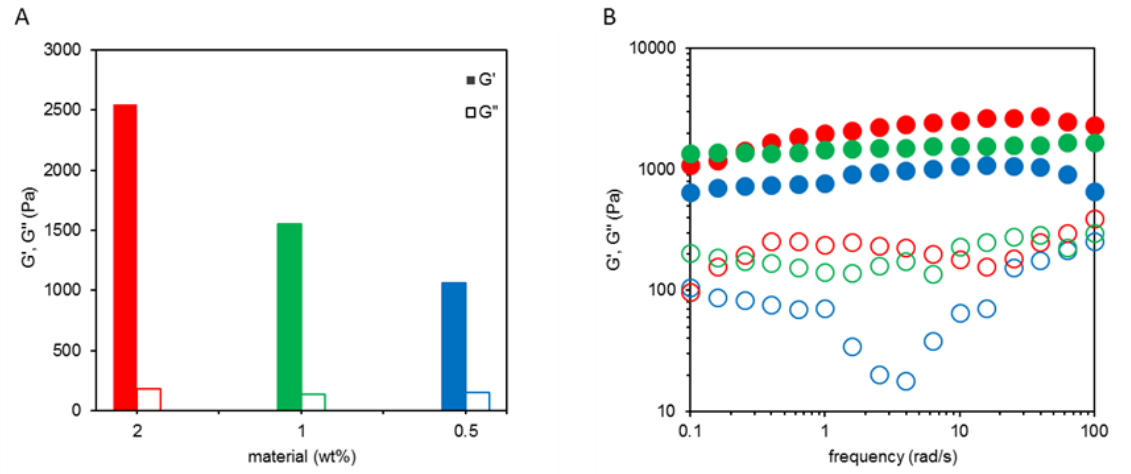

Figure 5.8: A) Compilation of rheological properties of P1 hydrogel at different concentrations. B) Frequency sweeps of at different concentrations (denoted by colour in A).

The influence of difunctional peptide crosslink on the stability of the hydrogel network was ascertained by evaluating the mechanical properties. Rheological amplitude, frequency and time sweeps were conducted to directly elucidate the m under different shear/strain parameters. At 2.0 wt%, P1 appears to take on a stiff gel state with an unusually high of 2680 Pa, comparative to 80 Pa for commonly used gelatin hydrogels used in tissue engineering.[24]

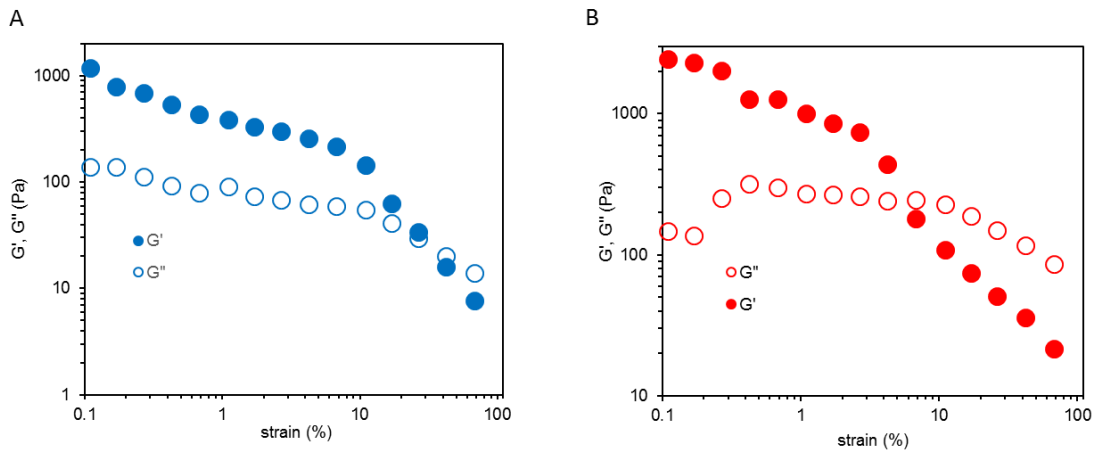

Figure 5.9: Rheological amplitude sweep of P1 hydrogel A) at 0.5 wt% and B) at 2.0 wt%.

Incrementally decreasing polymer concentrations were trialed to evaluate the impact on rheological properties. The crosslinked copolypeptide could maintain a gel network at very low material concentrations in a range below 2.0 wt% (Figure 4.8A and B).

An interesting concentration dependent property was observed in the amplitude sweep at 0.5 wt% (Figure 5.9). The reduction in material concentration appeared to constitute a more robust gel network as it appears to have a higher strain induced breaking point (29.3 %) than for the 2.0 wt% gel (5.2 %) under the same conditions (Figure 5.9B).

5.4 Conclusion

In conclusion, organogels were formed from *in situ* ring opening -helical polypeptide with a novel difunctional NCA monomer, immobilising the solvent through core crosslinking. The monomer could also core crosslink random coiling forming poly-sarcosine, forming hydrogels and organogels after an intermittent workup. The materials were able to gelate a multitude of common organic solvents showing high uptake affinity for polar aprotic solvents in particular. Ensuing cleavage of Z protecting groups of PZLL segments afforded hydrogels with high mechanical stability. The hydrogels remained intact at aqueous concentrations as high as 98.5 % and were mechanical strong as determined by rheological measurements.

5.5 References

1 D. Seliktar, *Science*, 2012, 336, 1124.

2 M. W. Tibbitt, K. S. Anseth, *Biotechnol. Bioeng*., 2009, 103, 655.

3 A. P. Nowak, J. Sato, V. Breedveld, T. J. Deming, *Supramol. Chem*., 2006, 18, 423.

4 Z. Li, T. J. Deming, *Soft Matter*, 2010, 6, 2546.

5 G. Ma, W. Lin, Z. Yuan, J. Wu, H. Qian, L. Xua, S. Chen, *J. Mater. Chem. B*, 2017, 5, 935.

6 A. P. Nowak, V. Breedveld, L. Pakstis, B. Ozbas, D. J. Pine, D. Pochan, T. J. Deming, *Nature*, 2002, 417, 424.

7 C. Vacogne, S. Brosnan, A. Masic, H. Schlaad, *Polym. Chem*., 2015, 6, 5040.

8 R. Murphy, T. Borase, C. Payne, J. S. A. Cryan, A. Heise, *RSC Adv*., 2016, 6, 23370.

9 K. N. Sill, B. Sullivan, A. Carie, J. E. Semple, *Biomacromolecules*, 2017, 18, 1874.

10 C. C. Ahrens, M. E. Welch, L. G. Griffith, P. T. Hammond, *Biomacromolecules*, 2015, 16, 3774.

11 M. T. Popescu, G. Liontos, A. Avgeropoulos, E. Voulgari, K. Avgoustakis, C. Tsitsilianis, *ACS Appl. Mater. Interfaces*, 2016, 8, 17539.

12 Y. Sun, Y. Hou, X. Zhou, J. Yuan, J. Wang, H. Lu, *ACS Macro Lett*., 2015, 4, 1000.

13 R. Murphy, D. P. Walsh, C. A. Hamilton, S. A. Cryan, M. in het Panhuis, A. Heise, Biomacromolecules, 2018, 19, 2691.

14 S. B. Hanay, B. Ritzen, D. Brougham, A. A. Dias, A. Heise, *Macromol. Biosci*., 2017, 17, 1700016.

15 R. C. Fahey, J. S. Hunt, G. C. Windham, *J. Mol. Evol*. 1977, 10, 155.

16 A. Sulistio, A. Widjaya, A. Blencowe, X. Zhang, G. G. Qiao, *Chem. Commun*. 2011, 47, 1151.

17 J. Ding, S. Fenghua, C. Xiao, L. Lin, L. Chen, C. He, X. Zhuang, X. Chen, *Polym. Chem*., 2011, 2, 2857.

18 F. Shi, J. Ding, C. Xiao, X. Zhuang, C. He, L. Chen, X. Chen, *J. Mater. Chem*. 2012, 22, 14168.

19 T. Jing, L. Fu, L. Liu, L. A. Yan, *Polym. Chem.,* 2016, *7,* 951.

20 G. J. Habraken, M. Peeters, C. H. Dietz, C. E. Koning, A. Heise, *Polym. Chem.*, 2010, 1, 514.

21 K. Y. Baek, M. Kamigaito, M. Sawamoto, *Macromolecules*, 2001, *34*, 215.

22 C. D. Vacogne, M. Schopferer, H. Schlaad. *Biomacromolecules*, 2016, 17, 2384.

23 M. Hollosi, Z. Majer, A. Z. Ronai, A. Magyar, K. Medzihradszky, S. Holly, A. Perczel, G. D. Fasman, *Biopolymers*, 1994, 34, 177.

24 N. I. zur Nieden, C. C. Turgman, X. Lang, J. M. Larsen, J. Granelli, Y. J. Hwang, J. G. Lyubovitsky, *ACS Appl. Mater. Interfaces*, 2015, 7, 10599.

CHAPTER 6

CONCLUSION AND FUTURE OUTLOOK

The improvement of synthetic polypeptides

their applicability in the field of biomedical science. They exhibit biological degradability and compatibility which holds potential in many different areas of biomedicine. well-defined -helical -motif based assemblies which provides them responsivity to stimuli based triggers is another advantageous aspect of their character. Of those materials, star shaped polypeptides represent attractive candidates for the field due to their sophisticated architecture and likeness to biomolecules.

This PhD thesis aimed to shed light on new synthetic processes that could produce hydrogelating materials from star polypeptide architectures and potentially apply them using current cargo delivery and fabrication strategies in biomedical science.

Chapter 2 investigated a series of star-shaped amphiphilic diblock copolypeptides with alternating hydrophobic residues and analysed their effect on hydrogelation. Aqueous self-assembly was noted for star diblock of L-tyrosine, L-phenylalanine and L-valine shell block but not for those with L-alanine or linear copolymers with an equivalent polypeptide arm length. Particularly lower polymer content was required for gelation (1.25 wt%) of phenylalanine containing star copolymers. All hydrogels exhibited self-recovery behavior and were shown to be injectable.

In chapter 3 core and shell disulphide crosslinking of star polypeptide were achieved by alternating oligo(L-cysteine) and poly(L-lysine) sequences to afford hydrogels that were stable at low material content (<0.5 wt%). Changing the sequence order on a 32-arm PPI dendrimer from core crosslinking to shell crosslinking had a significant effect on each respective hydrogel mechanical properties. Switching from core to shell crosslinking changed the modulus from 820 to 4530 Pa. Moreover, after increasing the degree of branching from 32-arm to 64-arm architecture, there was a proportional increase in the mechanical properties. Spectroscopic analysis revealed that both core and shell crosslinked copolypeptides exhibited -motif assemblies. Using DTT mediated disulphide cleavage, acceleration of the release of doxorubicin was observed from hydrogel depots.

In chapter 4, shear thinning hydrogels based on amphiphilic star block copolypeptides were developed using poly(L-glutamate) and oligo(L-valine). To achieve a material capable of fabricating microstructures, the star physical star copolypeptides were synthetically modified with UV reactive groups. The composition of hydrogel ink was found to be suitable for 3D extrusion printing as scaffolds were afforded which maintained structural cohesion, which was in agreement with rheological analysis. The constructs were also found to be degradable and exhibited favorable release of encapsulated molecular cargo. Additionally, leachates of the constructs did not affect the metabolic health of the Balb/3T3 fibroblast cells.

Chapter 5 explored the newly synthesised difunctional NCA monomer which was subsequently used for crosslinking both ionic polypeptide and non-ionic polypeptoide sequences. Organogels were formed after addition of the diaminopimelic acid (DAPA) NCA monomer to a helical poly(Z-L-lysine), which in turn could form hydrogels after removal of the protecting groups. The hydrogels were also found to be rheologically stable at high aqueous concentrations (98.75 %). Poly(sarcosine) was also found to swell, although at higher polymer content, in both organic solvents and water after an intermittent workup.

The future potential of the star shaped polypeptide materials in the field is very exciting. They offer structurally more than their linear counterparts in terms of controlled self-assembly and cargo loading capability, and also can be more finely tuned with shorter sequences required which are sometimes unattainable with linear analogues. Functionality can be easily built in with the range of synthetic tools available, which could allow for the modulation of their properties to be tailored toward specific biomedical applications. They possess interesting potential for the development of sustainable biological or chemical delivery matrices which have applicability in the field of regenerative medicine, in particular gene delivery. They also have significant potential in the field of additive manufacturing as they can be chemically derivatised to meet the curing needs of ink or resin based 3D deposition processes and also represent a viable polymeric material feedstock which is degradable and inherently biocompatible. Overall,

polypeptides represent materials which have potential to be used at the forefront of biomedicine in the near future.

Appendix A

Supporting Information

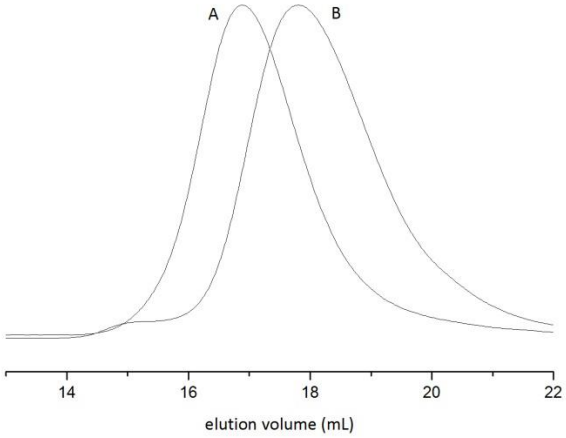

Figure A1: SEC trace of; 8-PZLL$_{40}$-b-PLA$_5$ (A) and 8-PZLL$_{40}$ (B).

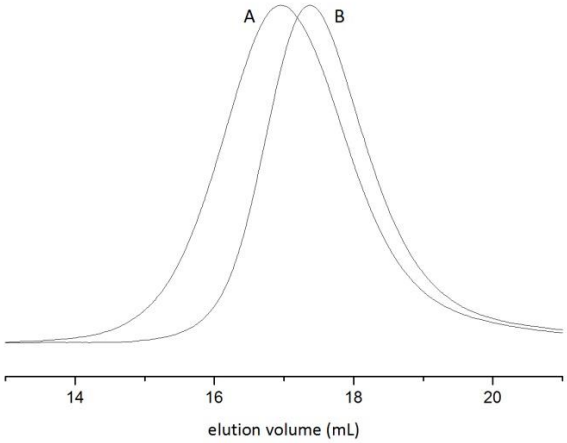

Figure A2: SEC trace of; 8-PZLL$_{40}$-b-PLT$_5$ (A) and 8-PZLL$_{40}$ (B).

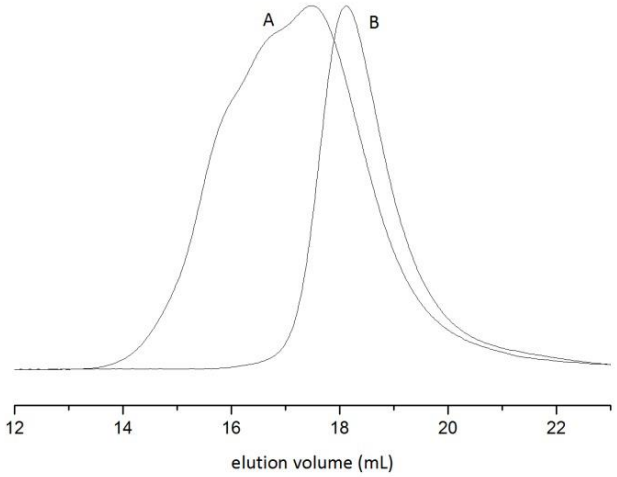

Figure A3: SEC trace of; 1-PZLL$_{148}$-b-PBLT$_{30}$ (A) and 1-PZLL$_{148}$ (B).

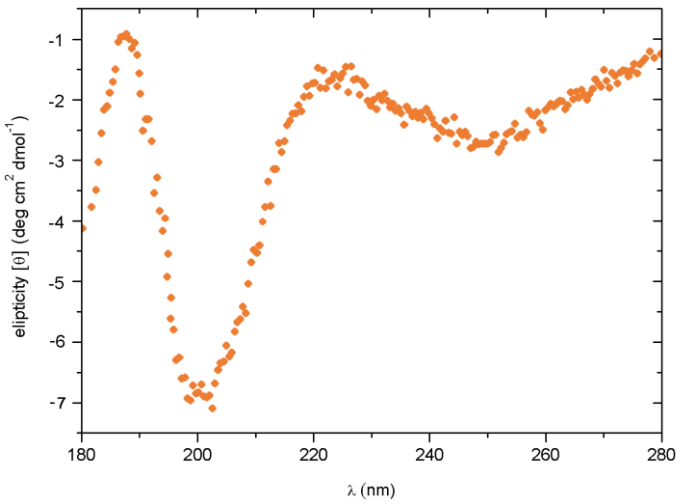

Figure A4: Circular dichroism (CD) spectrum of 8-PLL$_{40}$ in water.

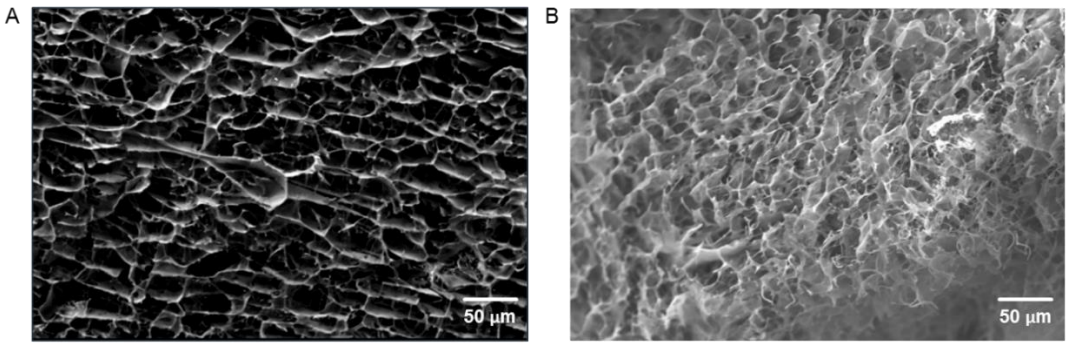

Figure A5: Scanning electron microscope (SEM) micrograph from cross section of (A) 32-OLC_5-b-PLL_{40} hydrogel and (B) 32-PLL_{40}-b-OLC_5.

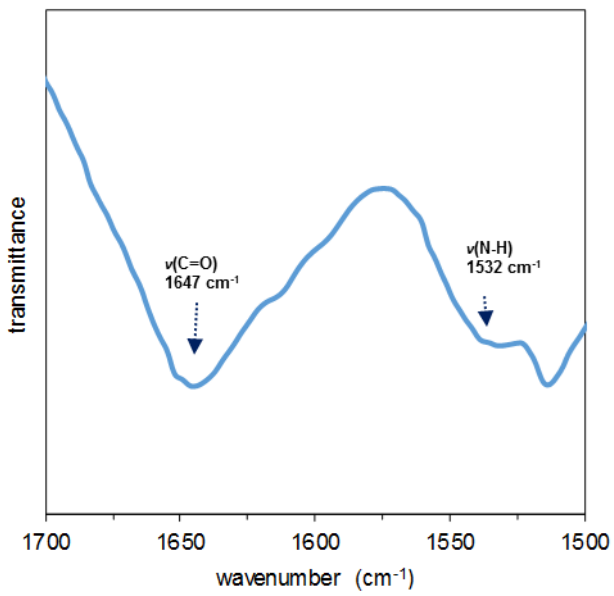

Figure A6: FTIR spectra of lyophilised 64-PLL_{40} star polypeptide.

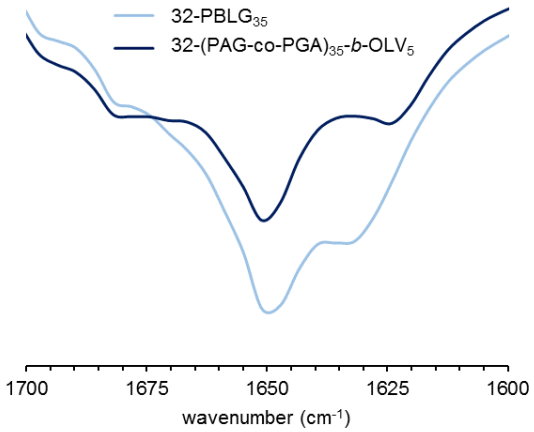

Figure A7: FTIR spectra of star diblock copolypeptide with amide band before and after allyl functionalisation.

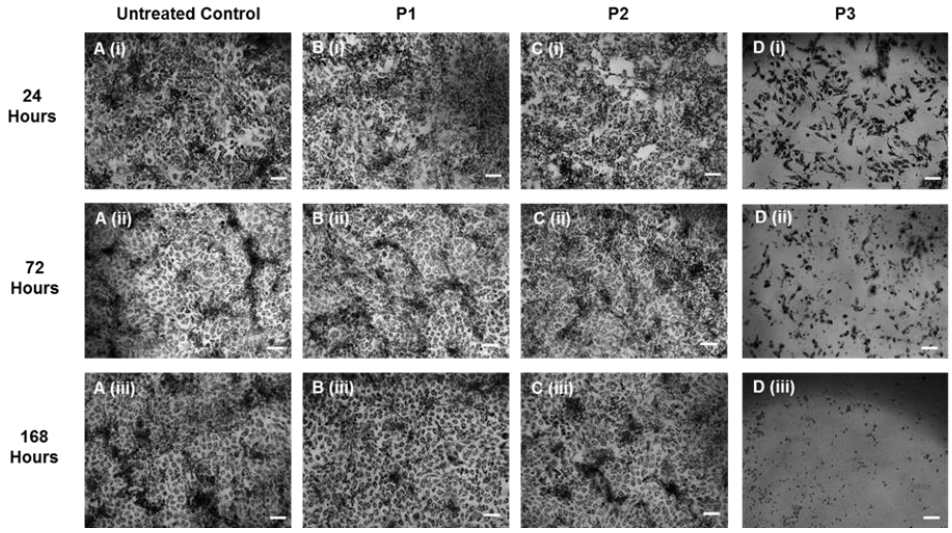

Figure A8: Visual assessment of the viability of Balb/3T3 cells following incubation with extracted ring construct leachates. Illustrated above are representative phase contrast images of formazan crystals produced by untreated control cells (A) and cells incubated in the presence of extracted leachates from each of P1 (B), P2 (C) and P3 (D) at 24 hours (i), 72 hours (ii) and 168 hours (iii). Viable cells cleave MTT substrate to form formazan crystals which are visually evident as black crystal deposits. A lack of crystal production indicates a reduction in cell viability. Scale bar = 100µm.

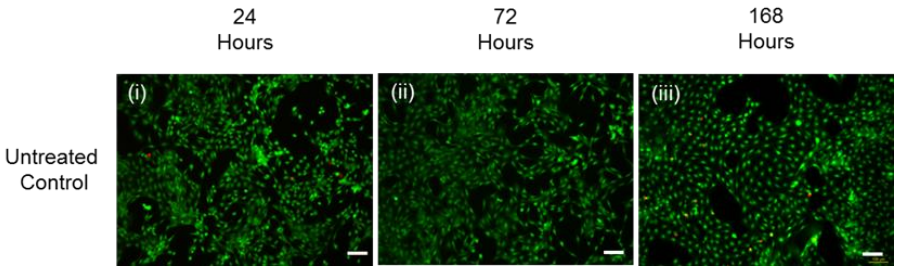

Figure A9: Live/Dead fluorescence microscopy images of Balb/3T3 cells which been incubated in control media at 24 hours (i), 72 hours (ii) and 168 hours (iii). Scale bar = 100µm.